MICROCOPY RESOLUTION TEST CHART

NATIONAL BUREAU OF STANDARDS 1963 A

Department of Mechanical and Aerospace Engineering

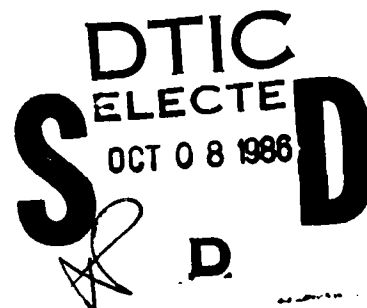Rutgers University

New Brunswick, New Jersey 08903

DTIC
ELECTE
OCT 0 8 1986
D

Report RU-TR-163-MAE-F

THEORETICAL INVESTIGATION OF

THREE-DIMENSIONAL SHOCK WAVE-

TURBULENT BOUNDARY LAYER

INTERACTIONS

Part IV

Approved for public release;
distribution unlimited.

Doyle D. Knight

Interim Report for Period 1 October 1984 to 30 September 1985

Approved for Public Release - Distribution Unlimited

Air Force Office of Scientific Research

Building 410

Bolling AFB

Washington, DC 20332

January 1986

86 10 8 080

SECURITY CLASSIFICATION OF THIS PAGE *(When Data Entered)* *ADA172826*

REPORT DOCUMENTATION PAGE	READ INSTRUCTIONS BEFORE COMPLETING FORM	
1. **AFOSR·TR·** 86 - 0893 RU TR 163 MAE F	2. GOVT ACCESSION NO.	3. RECIPIENT'S CATALOG NUMBER
4. TITLE *(and Subtitle)* THEORETICAL INVESTIGATION OF THREE-DIMENSIONAL SHOCK WAVE-TURBULENT BOUNDARY LAYER INTERACTIONS Part IV	5. TYPE OF REPORT & PERIOD COVERED Interim Oct. 1, 1984 - Sept. 30, 1985	
	6. PERFORMING ORG. REPORT NUMBER	
7. AUTHOR(s) Professor Doyle D. Knight	8. CONTRACT OR GRANT NUMBER(s) AFOSR-82-0040	
9. PERFORMING ORGANIZATION NAME AND ADDRESS Dept. of Mechanical and Aerospace Engineering Rutgers University New Brunswick, New Jersey 08903	10. PROGRAM ELEMENT, PROJECT, TASK AREA & WORK UNIT NUMBERS 61102F- 2307/A1	
11. CONTROLLING OFFICE NAME AND ADDRESS Air Force Office of Scientific Research Building 410 Bolling AFB, DC 20332	12. REPORT DATE January 1986	
	13. NUMBER OF PAGES	
14. MONITORING AGENCY NAME & ADDRESS*(if different from Controlling Office)* Same as 11	15. SECURITY CLASS. *(of this report)* UNCLASSIFIED	
	15a. DECLASSIFICATION/DOWNGRADING SCHEDULE	

16. DISTRIBUTION STATEMENT *(of this Report)*

Approved for Public Release; Distribution Unlimited

17. DISTRIBUTION STATEMENT *(of the abstract entered in Block 20, if different from Report)*

18. SUPPLEMENTARY NOTES

19. KEY WORDS *(Continue on reverse side if necessary and identify by block number)*

High Speed Flows; Viscous-Inviscid Interactions; Shock-Boundary Layer Interactions; Computational Fluid Dynamics; Navier-Stokes Equations; Turbulence

20. ABSTRACT *(Continue on reverse side if necessary and identify by block number)*

ABSTRACT
The principal focus of the research effort is the understanding of 3-D shock wave-turbulent boundary layer interactions ('3-D turbulent interactions'). The theoretical model consists of the Reynolds-averaged 3-D compressible Navier-Stokes equations, with turbulence incorporated using the algebraic turbulent eddy viscosity model of Baldwin and Lomax. During the fourth year, research efforts focused on both 2-D and 3-D turbulent interactions.

DD FORM 1473 JAN 73 EDITION OF 1 NOV 65 IS OBSOLETE
 S/N 0102-LF-014-6601

In former category, the theoretical model was examined for a series of separated 2-D compression corner flows at Mach 2 and 3. Calculations were performed for four separate compression corners using a 2-D compressible Navier-Stokes code, employing MacCormack's hybrid algorithm. The results were compared to earlier computations using the Beam-Warming algorithm, and recent experiment data for turbulent Reynolds stresses. It was observed that the calculated Reynolds stresses differed significantly from the experimental measurements due to the inability of the turbulence model to incorporate the multiple scale effects of the turbulence structure downstream of reattachment. The computed results using the MacCormack hybrid algorithm were observed to be insensitive to the Courant number. In the category of 3-D turbulence interactions, research efforts were concentrated on two configurations, namely 1) the 3-D sharp fin, and 2) the 3-D swept compression corner. In the former case, the computed flowfield for the 20 deg sharp fin at Mach 3 and a Reynolds number of 9.3 x 10 was compared with the calculated results of Horstman (who employed the Jones-Launder turbulence model) and experimental data of the Princeton Gas Dynamics Laboratory. The overall comparison with experiment was very good. The two separate calculations were observed to be in close agreement. The overall flowfield structure, consisting of a large vortical structure, was identified. In the case of the 3-D swept compression corner, three separate computations were performed for the (α, λ) = (24, 60) deg configuration, and the results compared with experiment. Further examination of these results is in progress.

PREFACE

This report presents the research accomplishments for the fourth year (1 October 1984 to 30 September 1985) of the research investigation entitled "Theoretical Investigation of Three-Dimensional Shock-Wave Turbulent Boundary Layer Interactions."

Table of Contents

"A Comparative Study of the Hybrid MacCormack and
Implicit Beam-Warming Algorithms for a Two-Dimen-
sional Supersonic Compression Corner" by C. Ong
and D. Knight (AIAA Paper No. 86-0204)

"The Flowfield Structure of the 3-D Shock Wave-
Boundary Layer Interaction Generated by a 20 deg
Sharp Fin at Mach 3" by D. Knight, C. Horstman, B.
Shapey and S. Bogdonoff (AIAA Paper No. 86-0343)

6

List of Illustrations

List of Tables

Section I.   Introduction

In the original proposal (Knight 1981), the general goals of the theo-
retical research program were described.   Although specific programmatic
changes have naturally occurred during the past four years, the fundamental
objectives remain the same, namely :

o   To determine the accuracy of a theoretical model of 3-D shock wave-
     turbulent boundary layer interactions ("3-D turbulent interac-
     tions"), where the theoretical model consists of the 3-D mean com-
     pressible Navier-Stokes equations with a turbulent eddy viscosity

o   To investigate the flow structure of 3-D turbulent interactions in
     simplified geometries through a close cooperative research effort
     between theory and experiment

o   To evaluate the hypothesized physical structure of the 3-D turbulent
     interactions at a variety of conditions outside the range of experi-
     ments

These goals represent a chronological sequence of objectives.   A major
portion of the first three years focused on the first objective (Knight 1982,
1983, 1984a) through a close collaboration with the Princeton Gas Dynamics
Laboratory.   The overall evaluations have been strongly favorable, and provide
the impetus for achievement of the second goal.   During the fourth year, the
research program has made significant progress in achieving the second objec-
tive.   In the following sections, the research accomplishments for the fourth
year and research program for the fifth year are presented.

Section II. Research Accomplishments for the Third Year
and Research Program for Fourth Year

A. 2-D Turbulent Interactions

Although the principal focus of the research effort is the understanding
of 3-D turbulent interactions, a modest effort has been directed towards 2-D
turbulent interactions over the past four years. The same theoretical model
has been employed for both the 2-D and 3-D research, namely, the Reynolds-
averaged compressible Navier-Stokes equations with the Baldwin-Lomax turbulent
eddy viscosity model.

During the first two years (Knight 1982, 1983), the objective of the 2-D
turbulent interaction effort was the examination of the efficacy of the theo-
retical model through comparison of the computed flowfields with the mean
flowfield measurements of Settles (Settles, Gilbert and Bogdonoff 1980) for
the 2-D supersonic compression ramp. Calculations were performed (see Table
1) for the entire experimental matrix of Settles at a nominal Mach number of
3, ramp angles from 8 deg to 24 deg, and Reynolds numbers $Re_{\delta\infty} = 0.76 \times 10^6$ to
7.7×10^6. The experimental data, consisting of surface pressure, skin fric-
tion, surface oil flow visualization, and boundary layer profiles of pitot and
static pressure, provided an extensive database for examination of the effi-
cacy of the theoretical model. The numerical algorithm of Beam and Warming
(1978) was employed for solution of the theoretical equations. The con-
clusions of the research effort, summarized in Visbal (1983) and Visbal and
Knight (1984), are the following :

a. The determination of the length and velocity scales of the Baldwin-
    Lomax turbulent eddy viscosity in the outer region is unsuitable in
    the vicinity of separation. The model predicts a sudden, unphysical
    decrease in the turbulence length scale of approximately an order of
    magnitude, resulting in an corresponding unphysical reduction in the
    magnitude of the eddy viscosity.

Table 1. Theoretical Research

2-D Shock Wave Turbulent Boundary Layer Interactions

Computations of 2-D Compression Ramp
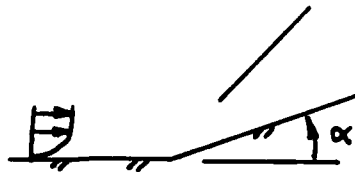
Year	Code	Mach No. (nominal)	Ramp Angle (α, deg)	Reynolds No. ($Re_{\delta\infty}$)	Data Comparison
81-82	B-W	3	8 deg	1.6×10^6	p_w, c_f, U, M, p
			16 deg		p_w, c_f, U, M, p
			20 deg		p_w, c_f, x_s, x_r, U, M, p
			24 deg		p_w, c_f, x_s, x_r, U, M, p
82-83	B-W	3	20 deg	0.76×10^6	p_w, x_s, x_r
				3.4×10^6	p_w, x_s, x_r
				5.6×10^6	p_w, x_s, x_r
				7.7×10^6	p_w, x_s, x_r
	B-W	2	16 deg	0.25×10^6	p_w, x_s, x_r
83-84	Development of 2-D Navier-Stokes code using MacCormack's hybrid method (MacCormack 1982)				
84-85	MH	3	8 deg	1.6×10^6	p_w, c_f, τ, U, M, p
			16 deg		p_w, c_f, τ, U, M, p
			20 deg		p_w, c_f, τ, x_s, x_r, U, M, p
	MH	2	16 deg	0.25×10^6	p_w, x_s, x_r

Note : There are typically two or more computations for each case

Legend for Numerical Algorithm :

B-W   Beam and Warming's Method (Beam and Warming 1978)
MH   MacCormack's Hybrid Method (MacCormack 1982)

Legend for Data Comparison with Experiment :

p_w Wall static pressure
c_f Wall skin friction coefficient
x_s, xr   Separation and Reattachment points
U   Velocity
M   Mach No. Profiles
p   Static pressure profiles

11

b.   The Baldwin-Lomax model exhibits an insufficient upstream propoga-
     tion of the corner interaction

c.   The incorporation of a 'relaxation model' into the turbulent eddy
     viscosity model improves the prediction of the upstream propogation.
     The relaxation model introduces an additional length scale, which is
     observed to be Reynolds number dependent.

d.   The Baldwin-Lomax model, with or without the relaxation model, fails
     to accurately predict the rapid recovery of the boundary layer
     downstream of reattachment.   This deficiency was attributed to the
     inability of the theoretical model to simulate the observed rapid
     amplification of the turbulent fluctuations (Settles, Baca, Williams
     and Bogdonoff 1980, Delery 1983) across a shock-boundary layer
     interaction.   The effect of the inclusion of the relaxation model is
     to diminish the turbulent eddy viscosity, thereby increasing the
     upstream propogation as noted in c.) above.   While improving the
     flowfield prediction upstream of the corner, the empirical relaxa-
     tion model therefore produces the wrong behavior downstream of
     reattachment.

   On the basis of these results, a second effort in 2-D turbulent interac-
tions was initiated during the second year, and completed in the fourth year.
The objectives of this effort are:

a.   Examination of the sensitivity of the computed flows to the numeri-
     cal algorithm   .

     The understanding of the characteristics of a numerical algor-
     ithm is crucial to the evaluation of the theoretical equations which
     it solves.   It was deemed important, therefore, to develop a second
     2-D compressible Navier-Stokes code using the popular MacCormack
     hybrid algorithm (MacCormack 1982), and to recompute many of the
     same cases which Visbal had computed using the Beam-Warming algor-
     ithm.   In addition, effort was focused on determining whether the

12

steady-state numerical solutions obtained using the MacCormack hybrid algorithm displayed any sensitivity to the time step employed (i.e., Courant number).

b. Direct comparison of computed and measured Reynolds shear stress for the 2-D compression ramp

Subsequent to the theoretical investigation of Visbal and Knight, a series of experiments (Muck et al 1983, 1984a,b) were performed at the Princeton Gas Dynamics Laboratory to measure the Reynolds shear stress for the 2-D supersonic compression ramp at Mach 3 for ramp angles of 8, 16 and 20 deg at $Re_{\delta\infty} = 1.6 \times 10^6$. This experimental database provided the opportunity for direct comparison with the computed Reynolds shear stress. The objective, therefore, is to understand the reasons for the failure of the Baldwin-Lomax turbulent eddy viscosity model to predict the rapid recovery of the boundary layer downstream of reattachment.

A series of computations were performed using the Reynolds-averaged compressible Navier-Stokes equations and the same Baldwin-Lomax turbulence model (see Table 1). Calculations were performed for a Mach 2 compression corner at 16 deg and $Re_{\delta\infty} = 0.25 \times 10^6$, and for a Mach 3 compression corner at 8, 16 and 20 deg and $Re_{\delta\infty} = 1.6 \times 10^6$. The computations at Mach 3 employed the same grid spacing, turbulence model parameters and upstream profile as employed by Visbal and Knight. The calculations differed only in the numerical algorithm utilized (MacCormack hybrid vs. Beam-Warming).

The conclusions of the research are (see Appendix I) :

a. The computed Reynolds shear stress profiles are observed to be significantly different from the experimental data. The height of the computed peak shear stress is typically a factor of two to four too small. The magnitude of the computed peak shear stress is in approximate agreement with the experimental data for the 16 deg corner, and displays a modest decrease with downstream distance. For the 20 deg corner, the computed peak shear stress shows a rapid

13

decrease with downstream distance, in disagreement with the experimental results.

b. The Baldwin-Lomax model, based upon the mixing length concept, is incapable of accurately predicting the recovery of a separated 2-D compression corner flow. The mixing length model is formulated on the concept of an equilibrium turbulent boundary layer exhibiting a single characteristic velocity scale (Tennekes and Lumley 1972). Downstream of reattachment, there are two characteristic velocity scales of the turbulence, namely, 1) an outer velocity scale associated with the turbulence fluctuations in the outer portion of the reattaching shear layer, and 2) an inner velocity scale $u_* = \sqrt{\tau_w(x)/\rho_w(x)}$ associated with the imposition of the no-slip boundary condition downstream of reattachment, which creates an 'inside layer' within the boundary layer. A more physically realistic turbulence model is required for 2-D separated compression corner flows, which incorporates the effect of the upstream history on the turbulence and the oscillatory motion of the shock wave structure (Dolling and Murphy 1982, Dolling and Or 1983).

c. The computed flowfields utilizing the Beam-Warming and MacCormack Hybrid algorithms are overall in excellent agreement. This implies, therefore, that the effect of numerical damping, which was incorporated differently in the two methods, is negligible on the flowfield elements examined (e.g., surface pressure, skin friction, and boundary layer profiles of velocity, temperature, density and Reynolds shear stress).

d. The steady-state solutions using MacCormack's hybrid algorithm are observed to be insensitive to the Courant number.

It is evident, therefore, that further research is needed to provide an adequate qualitative and quantitative understanding of the separarated 2-D supersonic compression ramp flows. Firstly, a 'new look' at theoretical modelling for these flows is required. It is clearly evident, on the basis of the results cited above, that the present theoretical model (i.e., the Rey-

nolds-averaged compressible Navier-Stokes equations with the Baldwin-Lomax turbulent eddy viscosity model) does not embody the correct physics for 2-D separated compression corners. Current efforts are directed towards reviewing these issues, and developing alternative approaches. Secondly, the recent experimental measurements of Reynolds shear stress for the 2-D compression corner by Kuntz, Amatucci and Addy (1986) using an LDV differ significantly from the earlier measurements of Muck et al; typically, the maximum values of the kinematic Reynolds shear stress differ by a factor of two to four depending on ramp angle. Additional detailed experimental investigation of these flows is clearly needed.

B.   3-D Turbulent Interactions

The principal focus of the overall research program is the understanding of 3-D turbulent interactions. During the first three years of the research effort, the principal objective was the determination of the efficacy of the theoretical model, namely, the 3-D Reynolds-averaged compressible Navier-Stokes equations with turbulence incorporated using the Baldwin-Lomax algebraic turbulent eddy viscosity model. The 3-D sharp fin configuration (Fig. 1) at Mach 3 was selected for the initial investigations. It was observed that the theoretical model provided good agreement with the experimental data (see Table 2). Consequently, in the fourth year a major effort focused on the development of the mean flowfield model for the 3-D sharp fin configuration. In addition, a new configuration, the 3-D swept compression corner, was computed during the fourth year. In the following sections, the results of the fourth year are described.

1.   3-D Sharp Fin at 20 deg

The configurations computed during the first three years (Table 2) involve a range of fin angles from 4 deg to 20 deg and Reynolds numbers from 2.8 $\times 10^5$ to 9.3 x 10^5. Overall, the agreement between the computed and experimental results is very good (Knight 1984b, 1985a, 1985b; Knight et al 1986) for both the algebraic turbulent eddy viscosity of Baldwin and Lomax (Knight 1984b, 1985a, 1985b; Knight et al 1986) and the two-equation Jones-Launder

15

Table 2. Theoretical Research

3-D Shock Wave Turbulent Boundary Layer Interactions

Computations of 3-D Sharp Fin
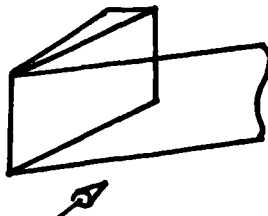
Year	Mach No. (nominal)	Fin Angle (α, deg)	Reynolds No. ($Re_{\delta\infty}$)	Data Comparison
81-82	3	4	9.3×10^5	p_w, sfc visual p_p, yaw c_h, p, pitch
	3	10	9.3×10^5	p_w, sfc visual p_p, yaw c_h, p, pitch
82-83	3	10	2.8×10^5	p_w, sfc visual p_p, yaw
83-84	3	20	9.3×10^5	p_w, sfc visual p_p, yaw

NOTE :   Each configuration typically represents two or more computations. The purpose of multiple calculations is to investigate the effects of grid resolution.

Legend for Data Comparison with Experiment :

p_w	Wall static pressure
sfc visual	Surface flow visualization (oil flow or kerosene-lampblack)
p_p	Pitot Pressure
yaw	Yaw Angle
c_h	Wall heat transfer coefficient (Stanton No.)
p	Static pressure profiles
pitch	Pitch Angle

(1972) turbulence model (Knight 1985b, Knight et al 1986), for which the computations were performed by Dr. C. C. Horstman of NASA Ames. On the basis of this verification of the efficacy of the theoretical model for this configuration, the computed flowfields using both theoretical models were employed to determine the structure of the mean flowfield. The principal conclusions of the investigation for the 20 deg sharp fin are (Appendix II) :

o   The three-dimensional velocity fields computed by both theoretical models are in close agreement, except within the immediate vicinity of the surface (specifically, within the lower approximate 20% of the boundary layer), where differences of the order of 10% to 20% exist in the yaw angle.

o   The computed turbulent Reynolds shear stress profiles differ by an order of magnitude and more within the 3-D interaction region

o   The similarity of the computed velocity fields and significant difference in computed turbulent Reynolds shear stresses imply that the 3-D sharp fin interaction is principally an inviscid, rotational flow except within the immediate vicinity of the surface.

o   The computed flowfields display a prominent vortical structure associated with the shock-boundary layer interaction. This large structure agrees with the flowfield models of Token (1974) and Kubota and Stollery (1982). The calculated flow reveals two significant surfaces, namely, 1) a three-dimensional surface of separation which originates from the line of coalescence (separation) and spirals into the center of the vortical structure, and 2) an upper surface, extending upstream into the undisturbed portion of the flow, which defines the extent of the flowfield which is entrained into the vortical structure.

An important element of this research has been the close collaboration between Dr. C. C. Horstman (NASA Ames), Prof. S. Bogdonoff and his colleagues (Princeton Gas Dynamics Laboratory), and the present author. The most recent 3-D sharp fin configuration (α_g = 20 deg, δ_∞ = 0.5 inch) exemplifies this

17

productive interaction. As indicated in Section III.B and III.C, the specific configuration was selected after detailed discussion, and the computations for both the Baldwin-Lomax model (Knight) and Jones-Launder model (Horstman) were performed prior to the experiment.

2. 3-D Swept Compression Corner

The second major focus for the 3-D turbulent interaction research in the fourth year was the computation of a selected configuration for the 3-D swept compression corner. This specific geometry, described in terms of the compression corner angle α (measured in the streamwise direction) and sweepback angle λ (Fig. 2), represents an important family of 3-D turbulent interactions. The 3-D sharp fin and 2-D compression ramp may be considered specific cases of the 3-D swept compression corner family corresponding to (α,λ) equal to $(90,\alpha_g)$ and $(\alpha,0)$ deg, respectively. Extensive experimental data has been obtained for a large number of configurations of the 3-D swept compression corner at Mach 3 at the Princeton Gas Dynamics Laboratory (Settles, Perkins and Bogdonoff 1980; Settles and Bogdonoff 1982; McKenzie 1983; Settles and Teng 1984). The data includes surface pressure and kerosene-lampblack surface flow visualization for more than forty different (α,λ) configurations at values of α and λ up to 24 deg and 70 deg, respectively (Settles 1983). Detailed flowfield surveys of pitot pressure and yaw angle have been obtained for $(\alpha,\lambda) = (24,40)$ deg at two different Reynolds numbers.

A series of 3-D swept compression corner configurations have been calculated by Horstman (Settles, McKenzie and Horstman 1984; Horstman 1984) using the 3-D mean compressible Navier-Stokes equations. The $(\alpha,\lambda) = (24,40)$ deg configuration was computed using the algebraic eddy viscosity model of Cebeci-Smith (1974) and the two-equation $k - \epsilon$ model of Jones-Launder (1972) for two Reynolds numbers. The computed results were found to be in reasonable agreement with experiment, although discrepancies were noted in the surface pressure distribution. In addition, a total of thirty-five (35) different configurations were calculated by Horstman at various (α,λ) using the Jones-Launder $(k-\epsilon)$ turbulence model with the wall function model of Viegas and Rubesin. The numerical results displayed close agreement with the measured boundary in the (α,λ) plane between cylindrical and conical flow. Recently,

however, a debate has arisen concerning the existence of the cylindrical-conical boundary (Wang and Bogdonoff 1986). These computations displayed good agreement with experimental data for surface pressure for a number of (α, λ) configurations. The model, however, failed to accurately predict the surface pressure distribution for high sweepback angles for which the flow exhibited a large separation region inferred from the surface streamlines. In particular, the disagreement for the $(\alpha, \lambda) = (24, 60)$ deg configuration is most notice-able (Fig. 3). Subsequent computations by Horstman (unpublished) utilizing finer streamwise grid spacing improved the prediction of the surface pressure within and downstream of the corner region; however, the pressure distribution upstream of the corner remained essentially unaffected.

The marginal performance of the Jones-Launder turbulence model (using the Viegas-Rubesin wall function model) for the $(\alpha, \lambda) = (24, 60)$ deg configuration motivated a reexamination of this flowfield using the theoretical model of the present author, which utilizes the Baldwin-Lomax turbulence model. The objec-tives of this research effort are the following :

o   To examine the accuracy of the Baldwin-Lomax model for the class of 3-D swept compression corner interactions

o   To examine the sensitivity of the computed flowfield to the turbu-lence model employed

o   To provide a theoretical data base for detailed analysis of the flowfield structure

A total of three separate computations were performed for the $(\alpha, \lambda) = (24, 60)$ deg configuration. In all cases, the freestream Mach number $M_\infty = 2.95$, and the freestream total pressure $p_{t\infty} = 100$ psia.

Case 1 :   Grid System and Upstream Boundary Layer Profile
             Equivalent to Horstman

The first computation of the $(\alpha, \lambda) = (24, 60)$ deg configuration employed approximately the same grid spacing as Horstman (1984). A total

19

of forty (40) streamwise grid planes were incorporated. Within each plane, a total of 729 ordinary grid points were utilized (27 x 27), with an additional 162 points within the computational sublayer. The total number of grid points was 35,640. The spanwise grid spacing (z-direction) was uniform. The grid in the y-direction was stretched geometrically to resolve the boundary layer on the surface.

The upstream boundary layer profile was the same as employed by Horstman. It is important to note that the upstream boundary of the computational domain was parallel to the corner line (Fig. 4) for both Horstman and the present author. Horstman utilized the same boundary layer profile at all points on the upstream boundary with $\delta_\infty = 0.38$ cm), effectively simulating a boundary layer which had developed from a swept leading edge. In the experiment, however, the leading edge of the flat plate (to which the swept compression corner was affixed), was perpendicular to the oncoming flow, thereby implying a boundary layer whose thickness varied on the upstream boundary of the computational domain. This effect was examined later (Case 2).

The freestream total temperature $T_{t\infty}$ was 495 deg R, and the wall temperature 520 deg R in agreement with Horstman. These values are in agreement with the experiment.

Case 2 : Modified Upstream Boundary Layer Profile

The second computation utilized the same grid system as Case 1, with a total of 35,640 grid points. The upstream profile, however, was chosen to accurately represent the oncoming boundary layer in the experiment. ,A separate boundary layer code, developed through AFOSR support (Knight 1983, 1984a), was utilized to compute an upstream profile corresponding to the flat plate leading edge perpendicular to the oncoming flow. The boundary layer profile on the upstream surface was in good agreement with the experimental boundary layer which developed on the flat plate in the wind tunnel. The boundary layer thickness δ_∞ on the upstream boundary varied from 0.091 cm to 0.38 cm over the 13.2 cm width of the computational domain.

The freestream total temperature $T_{t\infty}$ was 479 deg R, in agreement with the experiment (Kimmel 1985). The wall temperature 505 deg R in agreement with the experiment and previous computational studies of the 3-D sharp fin.

Case 3 : Modified Spanwise (Z-Direction) Grid Spacing

The third computation utilized the same grid spacing in the x- and y-directions as Cases 1 and 2. The spanwise (z-direction) mesh, however, was modified. As indicated previously, the spanwise grid spacing for Cases 1 and 2 was uniform and equal to 0.508 cm. At the apex of the swept compression corner (i.e., at the intersection of the corner line and the plane of symmetry), the size of the 3-D interaction is small. It was deemed necessary, therefore, to examine the effect of refining the grid in the spanwise direction in the vicinity of the apex in order to accurately resolve the 'inception region'. Consequently, in Case 3 a highly stretched grid spacing was employed in the z-direction, with a fine spacing $\Delta z = 4.57 \times 10^{-3}$ cm near the symmetry plane ($z = 0$), and a larger spacing $\Delta z = 0.539$ cm near the right boundary. The total number of grid points in the z-direction increased from 27 (Cases 1 and 2) to 46. The overall total number of grid points was 60,720.

The upstream profile was identical to Case 2, and the boundary layer thickness δ_∞ on the upstream boundary varied from 0.091 cm to 0.38 cm over the 13.2 cm width of the computational domain.

The total temperature and surface temperature were identical to Case 2.

The results for Cases 1 to 3 are presented in Figs. 5 through 7. In Fig. 5a to 5e, the computed surface pressure is displayed at five spanwise locations, corresponding to z = 2.03 cm, 4.06 cm, 6.09 cm, 8.12 cm and 10.15 cm. As indicated above, the boundary layer thickness on the upstream surface (Fig.

21

4) is $\delta_\infty = 0.38$ cm for Case 1 (in agreement with the profile of Horstman), and varies from 0.091 cm to 0.38 cm for Cases 2 and 3. The vertical axis is the surface pressure, normalized by the upstream static pressure p_∞. The horizontal axis is the streamwise distance $x - x_{corner}$, where x_{corner} is the streamwise location of the corner line at the specified spanwise location. In Fig. 6, the computed and experimental surface pressure are displayed in conical coordinates, where the horizontal axis is $(x - x_{corner})/(z + z_{origin})$, and $z_{origin} = 1.6$ cm is the z-coordinate of the approximate virtual origin as estimated from the experimental surface flow visualization. The experimental data was obtained at $z = 7.62$ cm, 9.4 cm, 9.65 cm and 10.16 cm. The computed profiles in Fig. 6 are obtained at $z = 12.2$ cm. Additional profiles (not shown) indicate that the computed surface pressure is approximately conical outside of an initial inception region at the apex.

Several features are evident from Figs. 5 and 6 :

1. The calculated upstream propogation is insensitive to the boundary layer on the upstream surface.

    The computed surface pressure profiles for Case 1, which employed a uniform boundary layer thickness on the upstream boundary surface (thereby simulating a swept leading edge to the flat plate), is quantitatively very similar to the profiles of Cases 2 and 3, which employed a non-uniform boundary layer thickness on the upstream boundary surface (thereby simulating a straight leading edge to the flat plate, as employed in the experiment). There is a slight decrease in the upstream propogation for Cases 2 and 3 as compared with Case 1.

2. The calculated upstream propogation is in good agreement with the experimental data as indicated in Fig. 6.

3. The computed pressure profile upstream of the corner is quantitatively different from the experiment (Fig. 6). The computed profile fails to reproduce the rapid pressure rise (although the location of the beginning of the pressure rise is accurately predicted as in-

22

dicated in 1.) above). In addition, the drop in pressure immediate-
ly upstream of the corner is not observed in the computations.

4. The peak pressure at the corner is accurately predicted (Fig. 6).

5. The recovery of the surface pressure downstream of the corner is
   somewhat sensitive to the upstream boundary layer profile, with
   Cases 2 and 3 displaying a more rapid recovery than Case 1. Never-
   theless, the computed pressure downstream of the corner is too low.

6. The computed surface pressure is insensitive to the refinement in
   the grid spacing in the spanwise direction near $z = 0$, i.e., the
   calculated profiles for Cases 2 and 3 are nearly identical.

In Fig. 7a, calculated surface pressure profiles are displayed in conical
coordinates $(x - x_{corner})/(z + z_{origin})$ for the Baldwin-Lomax model (Cases 1
to 3). The spanwise location of the profiles is typically 11.9 cm, which is
within the region where the computed surface pressure profiles display approx-
imate conical similarity. In Fig. 7b, calculated surface pressure profiles
are shown for three cases using the Jones-Launder model (Cases 4 through 6) at
a spanwise location of 11.9 cm. Case 4 represents the original computation by
Horstman, with the minimum streamwise grid spacing $\Delta x = 0.38$ cm. The computa-
tions using the Baldwin-Lomax model utilized the same streamwise grid spacing.
In Case 5, the streamwise grid spacing was refined with $\Delta x_{min} = 0.25$ cm. Both
Case 4 and 5 utilized the original 3-D version of the Viegas-Rubesin wall
function model ('Viegas-Rubesin I'). In Case 6, a modification of the Viegas-
Rubesin model was employed ('Viegas-Rubesin II'). In Fig. 7c, the profiles of
Figs. 7a and 7b are incorporated in a single plot. Several observations are
evident from Figs. 7a-c, namely :

1. The computed upstream influence is relatively insensitive to the
   turbulence model.

2. The calculated profiles upstream of the corner consistently fail to
   reproduce the rapid pressure rise and subsequent drop (see Fig. 6).

23

3. The peak pressure at the corner for the Jones-Launder model is sensitive to the streamwise grid spacing and version of the wall function model (i.e., Viegas-Rubesin I or II).

4. The peak pressure at the corner for the Baldwin-Lomax model is insensitive to the streamwise grid spacing. The computed peak corner pressures for Cases 1 to 3 and 6 are essentially identical.

5. The pressure profiles downstream of the corner for the Baldwin-Lomax model (Cases 1 to 3) and the Jones-Launder model with the refined streamwise grid (Cases 5 and 6) are very similar.

At the present time, further investigation of the computed flowfields is in progress. Several possible causes for the discrepancy between the computed and measured surface pressure are under investigation, including a) effect of grid resolution, and b) inadequacies in the turbulence modelling.

C. Research Program for Fifth Year

The research program for the remainder of the fifth year focuses on two principal objectives (Knight 1985c) :

1. **Analysis of 3-D Swept Compression Corner :**
    $(\alpha, \lambda) = (24, 60)$ **deg at** $Re_{\delta\infty} = 2.5 \times 10^5$

The computed results for the 3-D swept compression corner at $(\alpha, \lambda) = (24,60)$ deg and $Re_{\delta\infty} = 2.5 \times 10^5$, obtained during the previous year, are analyzed in detail. A detailed comparison of the computed flowfields using the Baldwin-Lomax model (Knight) and Jones-Launder model (Horstman) is performed, including profiles of yaw angle, pitch angle, velocity, Mach number and static pressure. A comparison of particle pathlines is also performed to examine the predicted flowfield structure. A significant effort is focused on the examining the quality of the numerical grid to assure the fidelity of the computed solution.

24

2. **Calculation of 3-D Swept Compression Corner :**
   (α, λ) = (24, 60) deg at $Re_{\delta\infty}$ = 9.5 x 10^5

The 3-D swept compression corner at (α, λ) = (24, 60) deg and $Re_{\delta\infty}$ = 9.5 x 10^5 is computed. The choice of this configuration is based upon several factors :

a. Concurrence with Experimental Effort at Princeton Gas Dynamics Laboratory

A major investigation of the 3-D swept compression corner at (α, λ) = (24,60) deg and $Re_{\delta\infty} \cong$ 9.5 x 10^5 is planned for 1985-1986 at the Princeton Gas Dynamics Laboratory (Bogdonoff, Andreopoulos and Smits 1985, p. 66). This effort will include a detailed flowfield study near feature lines (e.g., lines of coalescence) and in the inception region. The computation of this configuration during the same period will provide opportunities for continued close interaction between the theoretical and experimental efforts. This interaction can include the utilization of the computed flowfields to suggest locations for experimental measurements.

b. Complement the Previous Calculation of the 3-D Swept Compression Corner at (α, λ) = (24, 60) deg for $Re_{\delta\infty}$ = 2.5 x 10^5

The present calculation will complement the previous computational study of the same geometry at the lower Reynolds number $Re_{\delta\infty}$ = 2.5 x 10^5. These combined studies will provide a detailed examination of the effects of Reynolds number on this complex interaction. Previous experience with the 3-D sharp fin at α_g = 10 deg indicated that certain features (e.g., the overshoot in pitot pressure upstream of the theoretical inviscid shock and outside the boundary layer) were accurately predicted at the lower Reynolds number, but not as closely at the higher Reynolds number. In addition, certain features (e.g., the overshoot in yaw angle in the same physical location) were not accurately predicted at either Reynolds number. This

experience strongly suggests the importance of performing separate computations at different Reynolds numbers for each geometrical configuration (i.e., specific values of α and λ) of the 3-D swept compression corner.

Section III.   Publications and Scientific Interactions

A.   Written Publications - Cumulative Chronological List

1.   1 October 1981 - 30 September 1982

   a.   Knight, D., "Application of Curvilinear Coordinate Generation
         Techniques to the Computation of Internal Flows", in Numerical
         Grid Generation - Proceedings of a Symposium on the Numerical
         Generation of Curvilinear Coordinates and their Use in the
         Numerical Solution of Partial Differential Equations, North-
         Holland, New York, 1982, pp. 357-384.   [*] [**]

   b.   Knight, D., "A Hybrid Explicit-Implicit Numerical Algorithm for
         the Three-Dimensional Compressible Navier-Stokes Equations",
         AIAA Paper No. 83-0223, AIAA 21st Aerospace Sciences Meeting,
         January 10-13, 1983.   Published in AIAA J., Vol. 22, Aug 1984,
         pp. 1056-1063.   [*] [**]

   c.   Visbal, M., and Knight, D., "Generation of Orthogonal and
         Nearly Orthogonal Coordinates with Grid Control Near Boun-
         daries", AIAA J., Vol. 20, No. 3, March 1982, pp. 305-206. [**]
         [***]

2.   1 October 1982 - 30 September 1983

   a.   Knight, D., "Calculation of a Simulated 3-D High Speed Inlet
        Using the Navier-Stokes Equations", AIAA Paper No. 83-1165,
        AIAA/SAE/ASME 19th Joint Propulsion Conference, Seattle, Wash-
        ington, June 27-29, 1983. [*]

   b.   Visbal, M., and Knight, D., "Evaluation of the Baldwin-Lomax
        Turbulence Model for Two-Dimensional Shock Wave Boundary Layer
        Interactions", AIAA Paper No. 83-1697, AIAA 16th Fluid and
        Plasma Dynamics Conference, Danvsers, Mass., July 12-14, 1983.
        Published in the AIAA J., Vol. 22, July 1984, pp. 921-928. [*]

3.   1 October 1983 - 30 September 1984

   a.   Knight, D., "Numerical Simulation of Three-Dimensional Shock-
        Turbulent Boundary Layer Interaction Generated by a Sharp Fin",
        AIAA Paper No. 84-1559, AIAA 17th Fluid Dynamics, Plasmady-
        namics and Lasers Conference, June 25-27, 1984. Published in
        the AIAA J., Vol. 23, December 1985, pp. 1885-1891. [*]

   b.   York, B., and Knight, D., "Calculation of Two-Dimensional Tur-
        bulent Boundary Layers Using the Baldwin-Lomax Model", AIAA
        23rd Aerospace Sciences Meeting, Jan 14-17, 1984. Published in
        the AIAA J., Vol. 23, Dec 1985, pp. 1849-1850.

4.   1 October 1984 - 30 September 1985

   a.   Knight, D., "Modelling of Three Dimensional Shock Wave Turbu-
        lent Boundary Layer Interactions", in Macroscopic Modelling of
        Turbulent Flows, Lecture Notes in Physics, Vol 230, Springer-
        Verlag, NY, 1985, pp. 177-201.

28

b. Knight, D., Horstman, C., Shapey, B., and Bogdonoff, S., "The
    Flowfield Structure of the 3-D Shock Wave - Boundary Layer
    Interaction Generated by a 20 deg Sharp Fin at Mach 3", AIAA
    Paper No. 86-0343, AIAA 24th Aerospace Sciences Meeting, Jan-
    uary 6-9, 1986. Submitted for publication in the AIAA J.

c. Ong, C., and Knight, D., "A Comparative Study of
    the Hybrid MacCormack and Implicit Beam-Warming Algorithms for
    a Two-Dimensional Supersonic Compression Corner", AIAA Paper
    No. 86-0204, AIAA 24th Aerospace Sciences Meeting, January 6-9,
    1986. Submitted for publication in the AIAA J.

B. Interactions with Research Group at Princeton Gas Dynamics Laboratory - 1 October 1984 to 1 November 1985

1. 11 October 1984 : Meeting with Princeton Gas Dynamics Lab
    Research Group

    Topics : 1) Discussion of computed results for 3-D sharp fin ($\alpha = 20$ deg and $\delta = 0.5$ inch).

    2) Discussion of planned boundary layer profile measurements for the 3-D sharp fin ($\alpha = 20$ deg, $\delta = 0.5$ inch) at Princeton Gas Dynamics Laboratory.

    3) Discussion of C. Horstman's calculations for the 3-D swept compression corner.

    4) Discussion of future collaborative computational and experimental research on 3D turbulent interactions

2. 3 December 1984 : Conversation with S. Bogdonoff

    Topics : 1) Discussion of joint paper with Princeton, Rutgers and NASA Ames on flowfield structure of 3-D sharp fin

3. 3 December 1984 : Conversation with S. Goodwin

    Topics : 1) Discussion of experimental surface pressure data for 3-D sharp fin ($\alpha = 20$ deg, $\delta = 0.5$ inch).

4. 21 December 1984 : Conversation with S. Bogdonoff

    Topics : 1) Discussion of boundary layer profile measurements for 3-D sharp fin ($\alpha = 20$ deg, $\delta = 0.5$ inch).

    2) Discussion of future experimental measurements for 3-D swept compression corner.

30

5.   20 February 1985 : Conversation with S. Bogdonoff

    Topics : 1)   Discussion of initial experimental boundary layer
                   measurements for 3-D sharp fin ($\alpha = 20$ deg, $\delta = 0.5$ inch).

              2)   Discussion of recent measurements of 3-D sharp fin ($\alpha = $
                   17.25 deg)

6.   22 April 1985 : Conversation with S. Bogdonoff

    Topics : 1)   Discussion of initial experimental boundary layer
                   measurements for 3-D sharp fin ($\alpha = 20$ deg, $\delta = 0.5$ inch).

              2)   Discussion of planned measurements for 3-D swept
                   compression corner.

7.   21 May 1985 : Conversation with S. Bogdonoff

    Topics : 1)   Discussion of planned second experimental data set for 3-D
                   sharp fin ($\alpha = 20$ deg, $\delta = 0.5$ inch).

              2)   Discussion of planned computation of 3-D swept compression
                   corner for $(\alpha, \lambda) = (24, 60)$ deg.

              3)   Discussion of experimental investigation of 17.25 deg
                   sharp fin, 25 deg semi-cone and $(\alpha, \lambda) = (30, 60)$ swept
                   compression corner.   .

8.   1 August 1985 : Conversation with S. Bogdonoff

    Topics : 1)   Discussion of structure of 3-D sharp fin flowfield.

9.   22 August 1985 : Conversation with S. Bogdonoff

    Topics : 1)   Discussion of flowfield structure for 3-D swept

compression corner.

2) Discussion of planned experimental investigation of symmetric 3-D sharp fin.

3) Discussion of future computations for 3-D swept compression corner.

10. 23 September 1985 : Conversation with S. Bogdonoff

Topics : 1) Discussion of 3-D turbulent interaction flowfield structures for sharp fin and swept compression corner.

11. 9 Oct 1985 : Meeting with Princeton Gas Dynamics Lab
Research Group

Topics : 1) Discussion of experimental surface visualization (kerosene lampblack) for 3-D sharp fin

2) Discussion of experimental schlieren photographs for 3-D sharp fin

12. 21 Oct 1985 : Meeting with Princeton Gas Dynamics Lab
Research Group, C. Horstman (NASA Ames)

Topics : 1) Discussion of computed particle pathlines for 3-D sharp fin (α = 20 deg, δ = 0.5 inch).

2) View videotape of particle pathlines

2) Development of model for mean flowfield structure for 3-D sharp fin

C. Interactions with C. C. Horstman (NASA Ames Research Center)
1 October 1984 - 1 November 1985

1. 16 Oct 1984 : Conversation with Mike Horstman

    Topics : 1) Current computations of 3-D sharp fin for fin angles of 10 to 20 deg

    2) Discussion of secondary separation line structure for 3-D sharp fin

2. 28-30 November 1984 : Conversations with Mike Horstman

    Topics : 1) Discussion of status of computations for 3-D sharp fin by Horstman and Knight

    2) Discussion of future computations

3. 4 February 1985 : Conversation with Mike Horstman

    Topics : 1) Discussion of comparison of computed results by Knight and Horstman for 3-D sharp fin (α = 20 deg, δ = 0.5 inch)

4. 14 February 1985 : Conversation with Mike Horstman

    Topics : 1) Further discussion of computed results for 3D sharp fin.

    2) Requested additional computed results from Horstman for comparison

    3) Discussion of future work

5. 28 February 1985 : Conversation with Mike Horstman

    Topics : 1) New wall function turbulence model employed by Horstman

6. 25 March 1985 : Conversation with Mike Horstman

    Topics : 1) Effect of new wall function model on predicted results for
                  swept compression corner

7. 16 April 1985 : Visit by Mike Horstman to Rutgers University

    Topics : 1) Flowfield structure for 3-D sharp fin interaction

             2) Contents of joint paper with Knight, Horstman, Bogdonoff
                 and Shapey for AIAA 24th Aerospace Sciences Meeting in Jan
                 1986

             3) Discussion of recent computated results for 3-D swept
                 compression corner

             4) Discussion of 2-D compression ramp, including calculations
                 by C. Ong (Rutgers), and Dennis Johnson (NASA Ames).

             5) Discussion of experimental fluid dynamics program at NASA
                 Ames

8. 25 April 1985 : Conversation with Mike Horstman

    Topics : 1) Contents of joint paper with Knight, Horstman, Bogdonoff
                 and Shapey for AIAA 24th Aerospace Sciences Meeting in Jan
                 1986

             2) Discussion of computational results for 3-D swept
                 compression corner $(\alpha,\lambda) = (24,60)$ deg

9. 10 and 19 June 1985 : Conversation with Mike Horstman

    Topics : 1) Discussion of new 3-D finite volume code being developed
                 by Mike Horstman

        2)   Discussion of parameters for 3-D sharp fin calculations

10. 16 July 1985 : Conversation with Mike Horstman

     Topics : 1)   Boundary conditions employed by Horstman for 3-D swept
                 compression corner calculations

11. 16 August 1985 : Communication with Mike Horstman

     Topics : 1)   Sent Mike Horstman the results of computations by Knight
                 for 3-D swept compression corner $(\alpha,\lambda) = (24,60)$ deg

12. 22 August 1985 : Communication with Mike Horstman

     Topics : 1)   Sent Mike Horstman additional results of computations for
                 3-D swept compression, with emphasis on effect of upstream
                 boundary conditions

13. 6 September 1985 : Conversation with Mike Horstman

     Topics : 1)   Discussion of comparison of computed (Knight and Horstman)
                 and experimental (Princeton Gas Dynamics Lab) data for 3-D
                 sharp fin ($\alpha = 20$ deg, $\delta = 0.5$ inch)

14. 16 Oct 1985 : Communication with Mike Horstman

     Topics : 1)   Sent comparison of experimental and computed profiles of
                 pitot pressure and yaw angle for 3-D sharp fin ($\alpha = 20$
                 deg, $\delta = 0.5$ inch). Copies also sent to Shapey and
                 Bogdonoff (Princeton).

15. 22 Oct 1985 : Visit by Mike Horstman to Rutgers University

     Topics : 1)   Discussion of particle pathlines for 3-D sharp fin

             2)   Discussion of flowfield structure for 3-D sharp fin

3) Discussion of videotape of particle pathlines to be presented at AIAA Aerospace Sciences Meeting in Jan 1986

4) Discussion of contents of paper by Knight, Horstman, Shapey and Bogdonoff to be presented at AIAA 24th Aerospace Sciences Meeting in Jan 1986

5) Discussion of new concepts in 3-D flowfield graphics

6) Discussion of flowfield structure of 3-D swept compression corner

D. Spoken Papers Presented at Technical Meetings
1 October 1984 to 1 November 1985

1. Knight, D., "Calculation of Three-Dimensional Shock Wave-Turbulent Boundary Layer Interaction Generated by a Sharp Fin", Thirty-Seventh Annual Meeting, Division of Fluid Dynamics, American Physical Society, 18-20 November 1984, Bulletin of American Physical Society, Vol. 29, No. 9, Nov 1984, p. 1569.

2. Knight, D., "Theoretical Investigation of Shock Wave - Turbulent Boundary Layer Interaction : Problems in Reconciling Computation and Experiment", Workshop on Structure of High Speed Turbulent Boundary Layers, Princeton University, 29-30 July 1985.

E. Seminars - 1 October 1984 to 1 November 1985

1. Knight, D., "Theoretical Investigation of 3-D Shock Wave-Turbulent Boundary Layer Interaction Generated by a Sharp Fin", Air Force Wright Aeronautical Laboratory, Wright-Patterson AFB, OH, 28 October 1985.

Section IV.   List of Personnel and Degrees Awarded

A.   Personnel

Principal Investigator :   Prof. Doyle Knight
                                  Dept. of Mechanical and
                                      Aerospace Engineering

Graduate Research Assistant :   Mr. Cho Ong
                                  Dept. of Mechanical and
                                      Aerospace Engineering

Section V. References

Beam, R., and Warming, R. 1978 "An Implicit Factored Scheme for the Compressible Navier-Stokes Equations", AIAA J., Vol. 16, pp. 393-402.

Bogdonoff, S., Andreopoulos, Y., and Smits, A. 1985 The Study of Shock Wave and Turbulent Boundary Layer Interactions. Proposal submitted to the Air Force Office of Scientific Research for the period beginning 1 August 1985.

Cebeci, T., and Smith, A.M.O. 1974 Analysis of Turbulent Boundary Layers. Academic Press, New York.

Delery, J. 1983 Experimental Investigation of Turbulence Properties in Transonic Shock/Boundary-Layer Interactions, AIAA J., Vol. 21, No. 2, 1983, pp. 180-185.

Dolling, D., and Murphy, M. 1982 Wall Pressure Fluctuations in a Supersonic Separated Compression Ramp Flowfield, AIAA Paper No. 82-0986.

Dolling, D., and Or, C. 1983 Unsteadiness of the Shock Wave Structure in Attached and Separated Compression Ramp Flow Fields, AIAA Paper No. 83-1715.

Jones, W., and Launder, B. 1972 The Prediction of Laminarization with a Two-Equation Model of Turbulence. Int. J. Heat and Mass Transfer, Vol. 15, pp. 301-304.

Horstman, C. 1984 A Computational Study of Complex Three-Dimensional Compressible Turbulent Flow Fields. AIAA Paper No. 84-1556, AIAA 17th Fluid Dynamics, Plasma Dynamics and Lasers Conference.

Kimmel, R. 1985 Private Communication.

Knight, D. 1981 Theoretical Investigation of Three-Dimensional Shock Wave-Turbulent Boundary Layer Interactions. Research Proposal Submitted to the Air Force Office of Scientific Research.

Knight, D. 1982 Theoretical Investigation of Three-Dimensional Shock Wave-Turbulent Boundary Layer Interactions. Interim Report for Period 1 Oct 81 to 30 Sept 82; also Report RU-TR-157-MAE-F.

Knight, D. 1983 Theoretical Investigation of Three-Dimensional Shock Wave-Turbulent Boundary Layer Interactions - Part II. Interim Report for Period 1 Oct 82 to 30 Sept 83; also Report RU-TR-160-MAE-F.

Knight, D. 1984a Theoretical Investigation of Three-Dimensional Shock Wave-Turbulent Boundary Layer Interactions - Part III. Interim Report for Period 1 Oct 83 to 30 Sept 84; also Report RU-TR-162-MAE-F.

Knight, D. 1984b A Hybrid Explicit-Implicit Numerical Algorithm for the Three-Dimensional Compressible Navier-Stokes Equations. AIAA J., Vol.

22, pp. 1056-1063.

Knight, D. 1985a Calculation of Three-Dimensional Shock/Turbulent Boundary-
       Layer Interaction Generated by a Sharp Fin. AIAA J., Vol. 23, pp. 1885-
       1891.

Knight, D. 1985b Modelling of Three-Dimensional Shock Wave Turbulent
       Boundary Layer Interactions. Conf. on Macroscopic Modelling of Turbulent
       Flows and Fluid Mixtures. INRIA, France. Lecture Notes in Physics, Vol.
       230, pp. 177-201.

Knight, D. 1985c Theoretical Investigation of Three-Dimensional Shock Wave -
       Turbulent Boundary Layer Interactions. A Three Year Proposal for the
       Period Beginning 1 October 1985. Submitted to Air Force Office of
       Scientific Research, 1 May 1985.

Knight, D., Horstman, C., Shapey, B., and Bogdonoff, S. 1986 The Flowfield
       Structure of the 3-D Shock Wave - Boundary Layer Interaction Generated by
       a Sharp Fin at Mach 3. AIAA Paper 86-0343, AIAA 24th Aerospace Sciences
       Meeting, Jan 6-9, 1985.

Kubota, H., and Stollery, J. 1982 An Experimental Study of the Interaction
       Between a Glancing Shock Wave and a Turbulent Boundary Layer J. Fluid
       Mech., Vol. 116, pp. 431-458.

Kuntz, D., Amatucci, V., and Addy, A. 1986 The Turbulent Boundary Layer
       Properties Downstream of the Shock Wave-Boundary Layer Interaction, AIAA
       Paper No. 86-0348.

MacCormack, R. 1982 A Numerical Method for Solving the Equations of
       Compressible Viscous Flow. AIAA J., Vol. 20, pp. 1275-1281.

McKenzie, T. 1983 A Flow Field Scaling of the Three-Dimensional
       Shock/Boundary Layer Interaction of the Swept Compression Corner. M.S.E.
       Thesis, Dept. of Mechanical and Aerospace Engineering, Princeton U.

Muck, K., Hayakawa, K., and Smits, A. 1983 Compilation of Turbulence Data
       for a 20° Compression Corner at Mach 2.9. MAE Report 1620, Dept. of
       Mech. and Aero. Engr., Princeton Univ.

Muck, K., Hayakawa, K., and Smits, A. 1984a Compilation of Turbulence Data
       for a 16° Compression Corner at Mach 2.9. MAE Report 1619, Dept. of
       Mech. and Aero. Engr., Princeton Univ.

Muck, K., Spina, E., and Smits, A. 1984b Compilation of Turbulence Data for
       an 8° Compression Corner at Mach 2.9. MAE Report 1642, Dept. of Mech.
       and Aero. Engr., Princeton Univ.

Settles, G., Baca, B., Williams, D., and Bogdonoff, S. 1980 A Study of
       Reattachment of a Free Shear Layer in Compressible Turbulent Flow, AIAA
       Paper No. 80-1408.

Settles, G., Gilbert, R., and Bogdonoff, S. 1980 "Data Compilation for Shock
       Wave/Turbulent Boundary Layer Interaction Experiments on Two-Dimensional
       Compression Corners", Report MAE-1489, Dept. of Mech. and Aero. Engr.,

Princeton Univ.

Settles, G., Perkins, J., and Bogdonoff, S. 1980 Investigation of Three-Dimensional Shock/Boundary Layer Interaction at Swept Compression Corners. AIAA J., Vol. 18, pp. 779-785.

Settles, G., and Bogdonoff, S. 1982 Scaling of Two- and Three-Dimensional Shock/Turbulent Boundary Layer Interactions at Compression Corners", AIAA J., Vol. 20, pp. 782-789.

Settles, G. 1983 Private Communication (24 May 1983).

Settles, G., and Teng, H. 1984 Cylindrical and Conical Upstream Influence Regimes of Three-Dimensional Shock/Turbulent Boundary Layer Interactions. AIAA J., Vol. 22, 1984, pp. 194-200.

Settles, G., McKenzie, T., and Horstman, C. 1984 Flow Field Scaling of a Swept Compression Corner - A Comparison of Experiment and Computation. AIAA Paper 84-0096.

Tennekes, H., and Lumley, J. 1972 A First Course in Turbulence, The MIT Press, Cambridge, MA.

Token, K. 1974 Heat Transfer Due to Shock Wave/Turbulent Boundary Layer Interactions on High Speed Weapons Systems. AFFDL-TR-74-77.

Visbal, M. 1983 Numerical Simulation of Shock/Turbulent Boundary Layer Interactions Over 2-D Compression Corners. Ph.D. Thesis, Dept. of Mech. and Aero. Engr., Rutgers Univ.

Visbal, M., and Knight, D. 1984 The Baldwin-Lomax Turbulence Model for Two-Dimensional Shock-Wave/Boundary Layer Interactions. AIAA J., Vol. 22, pp. 921-928.

Wang, S., and Bogdonoff, S. 1986 A Re-Examination of the Upstream Influence Scaling and Similarity Laws for 3-D Shock Wave/Turbulent Boundary Layer Interaction. AIAA Paper No. 86-0347, AIAA 24th Aerospace Sciences Meeting.
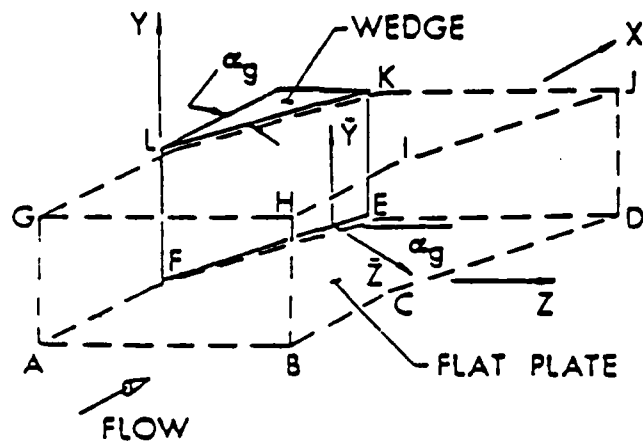
Fig. 1   3-D Sharp Fin
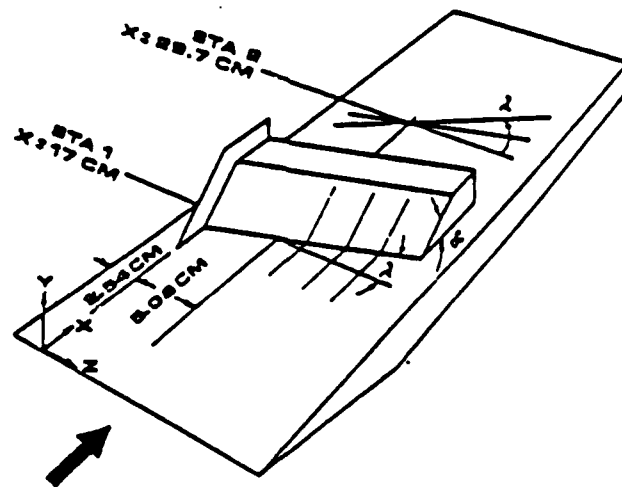
Fig. 2   3-D Swept Compression Corner

42
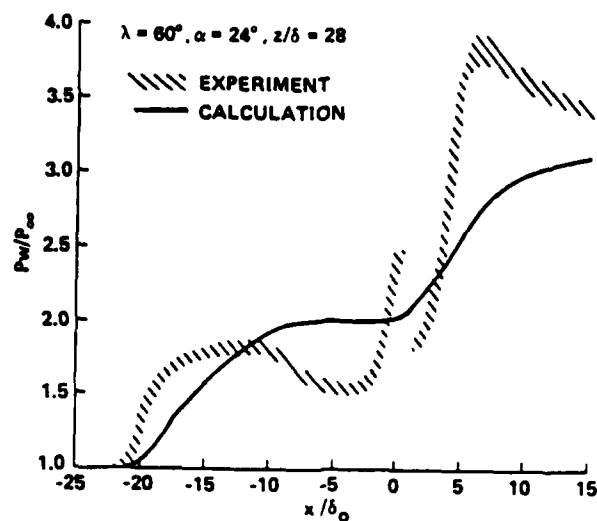
Fig. 3   Comparison of Computed and Experimental Surface Pressure
for 3-D Swept Compression Corner $(\alpha,\lambda) = (24, 60)$ deg
(Horstman 1984)
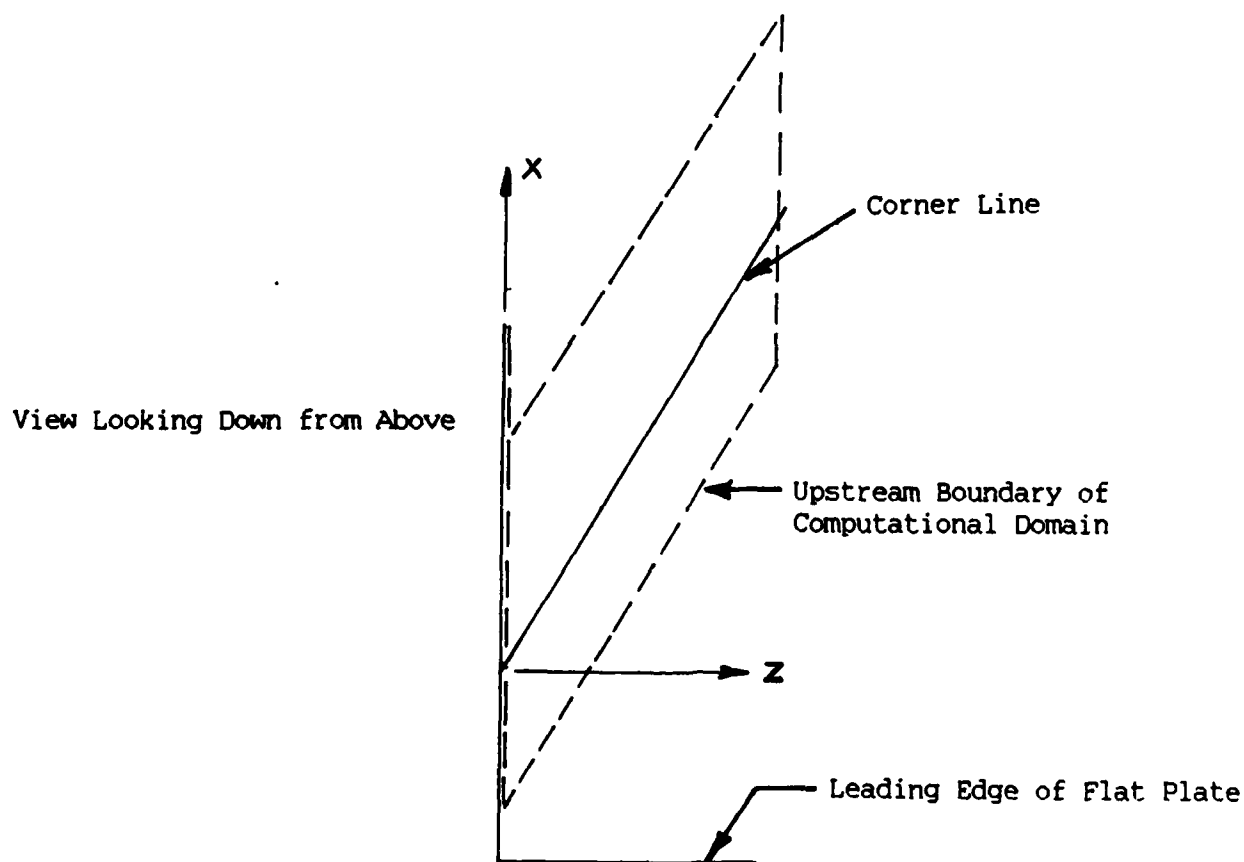
Fig. 4   Computational Region for 3-D Swept Compression Corner

43

P/PINF VS X-Xcorner
Pinf=422.63 (psf)
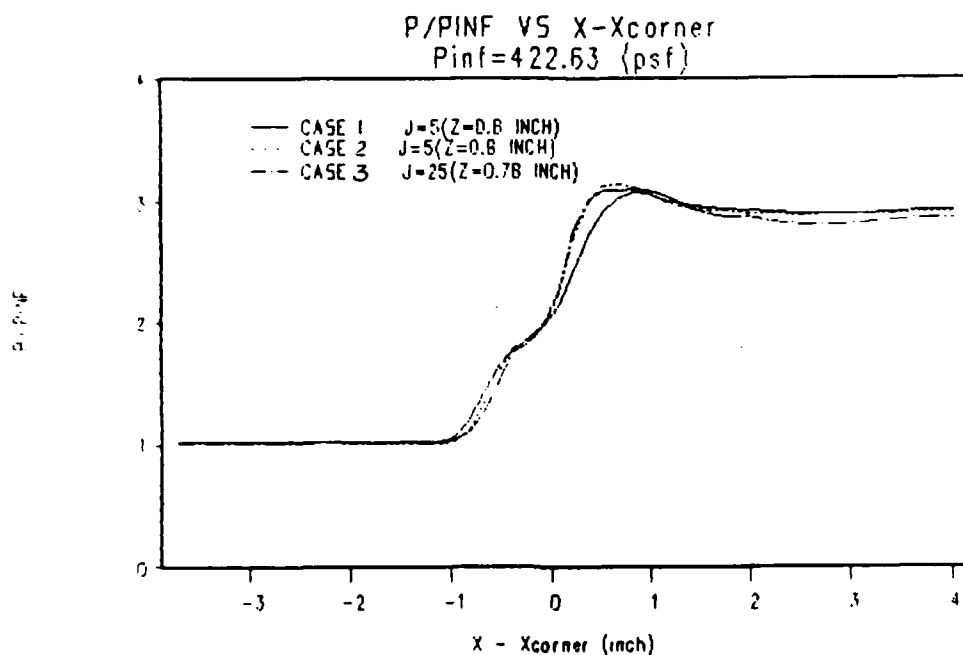
Fig. 5a   Computed Surface Pressure (Knight) for 3-D Swept
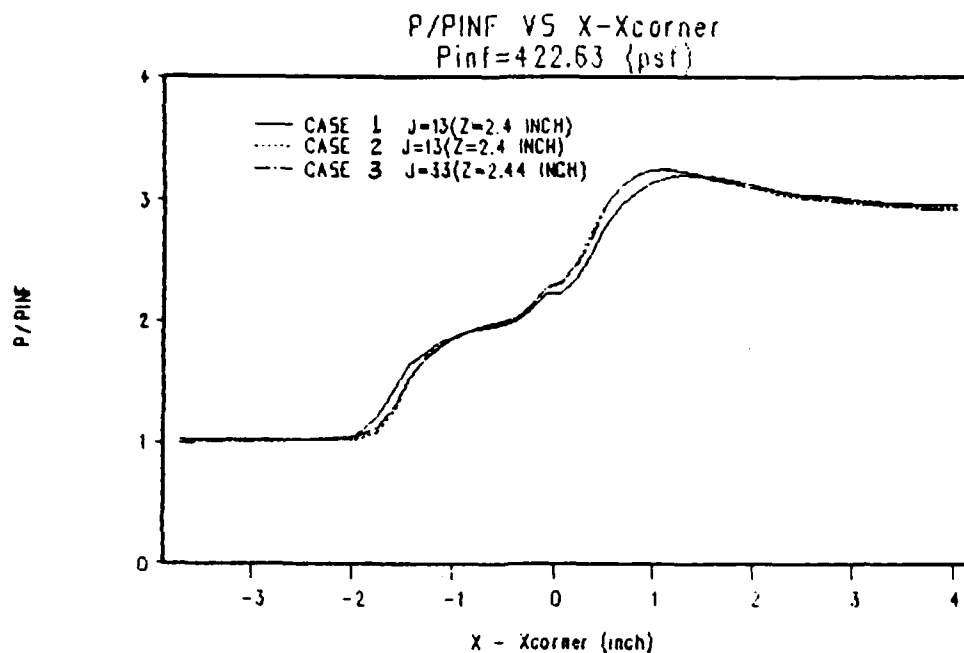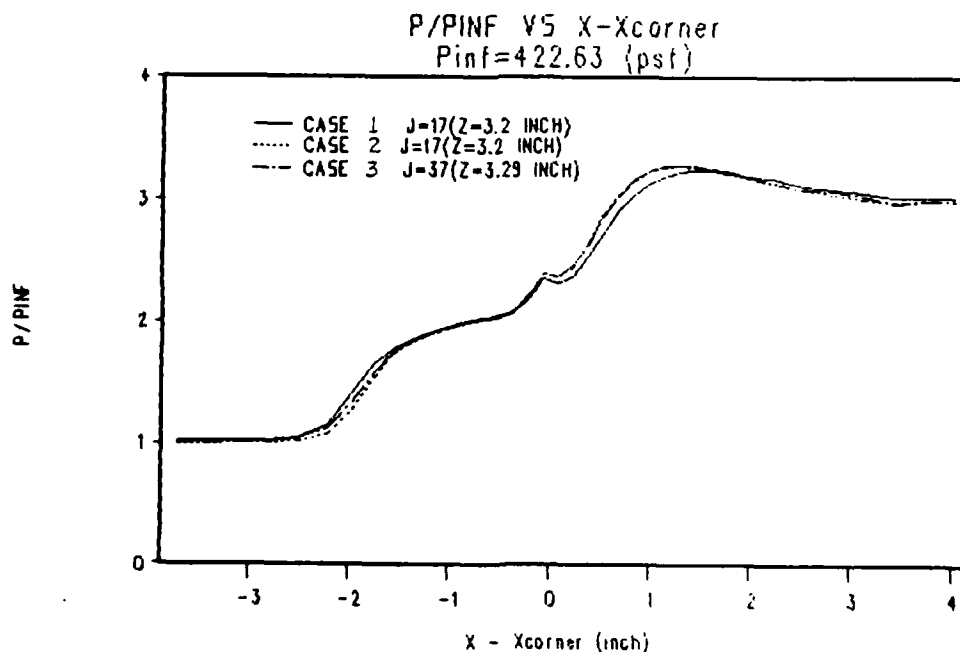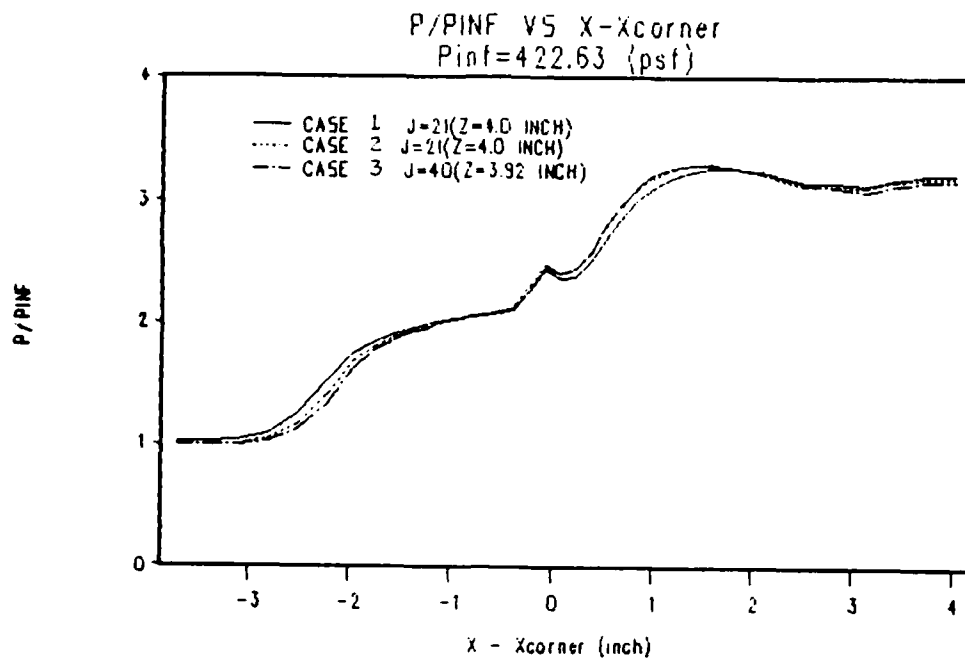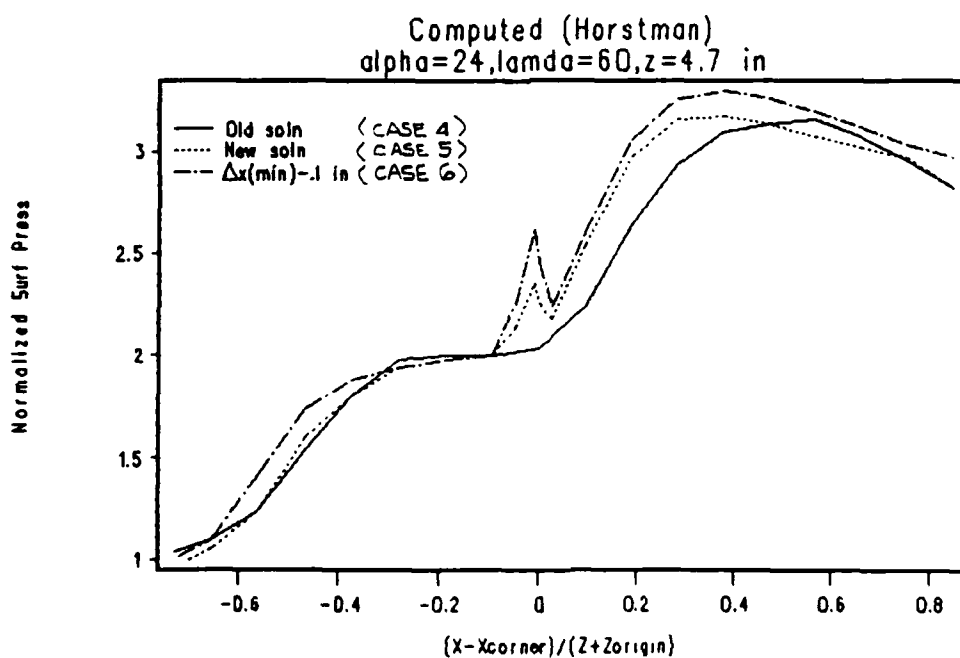   Compression Corner $(\alpha,\lambda) = (24,60)$ deg at $z = 2.03$ cm

P/PINF VS X-Xcorner
Pinf=422.63 (psf)
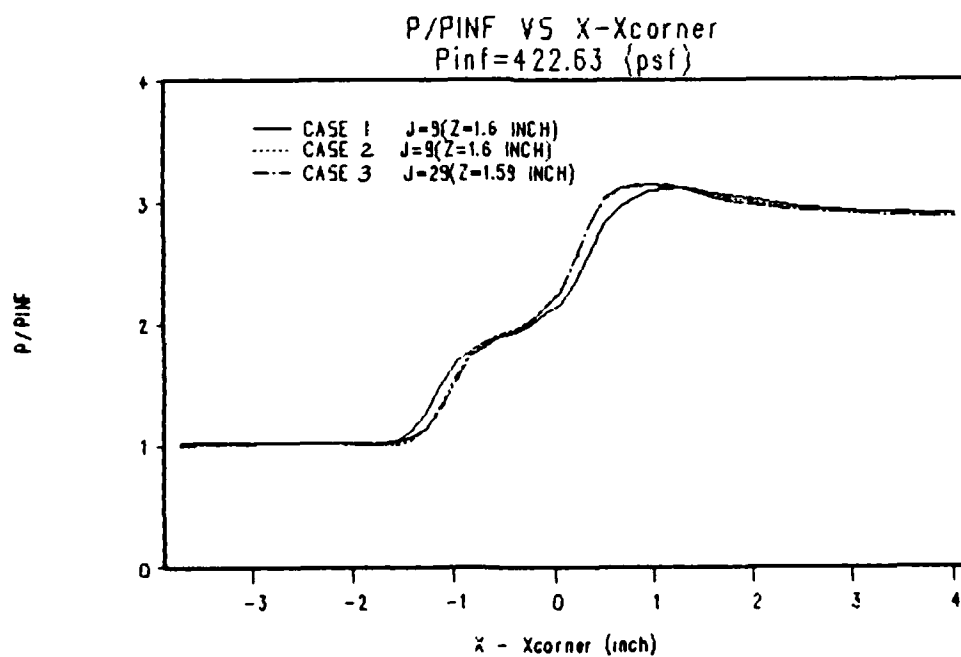
Fig. 5b   Computed Surface Pressure (Knight) for 3-D Swept
           Compression Corner $(\alpha,\lambda) = (24,60)$ deg at $z = 4.06$ cm

P/PINF VS X-Xcorner
Pinf=422.63 (psf)

Fig. 5c   Computed Surface Pressure (Knight) for 3-D Swept
           Compression Corner (α, λ) = (24,60) deg at z = 6.09 cm

P/PINF VS X-Xcorner
Pinf=422.63 (psf)

Fig. 5d   Computed Surface Pressure (Knight) for 3-D Swept
           Compression Corner (α, λ) = (24,60) deg at z = 8.12 cm

45

P/PINF VS X-Xcorner
Pinf=422.63 (psf)

Fig. 5e   Computed Surface Pressure (Knight) for 3-D Swept
          Compression Corner $(\alpha,\lambda) = (24,60)$ deg at z = 10.16 cm

EXPT AND THEORY
ZORIGIN=0.63 IN,P=422.63 LB/FT2
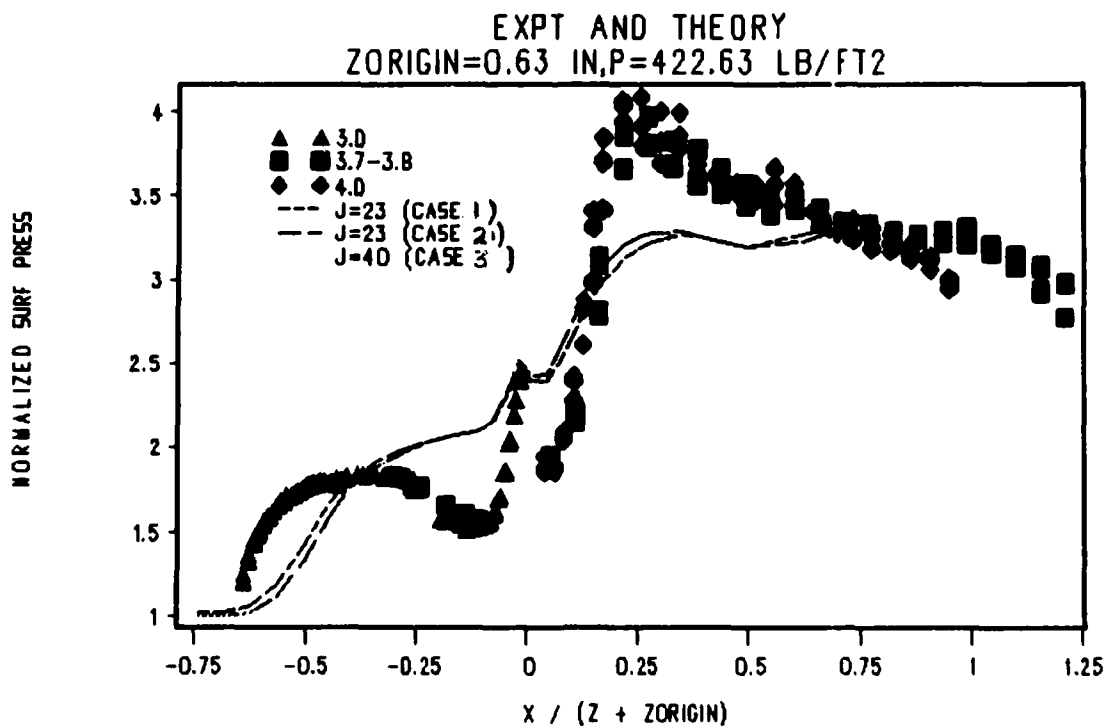
Fig. 6   Computed (Knight) and Experimental Surface Pressure for
          3-D Swept Compression Corner at $(\alpha,\lambda) = (24,60)$ deg

46
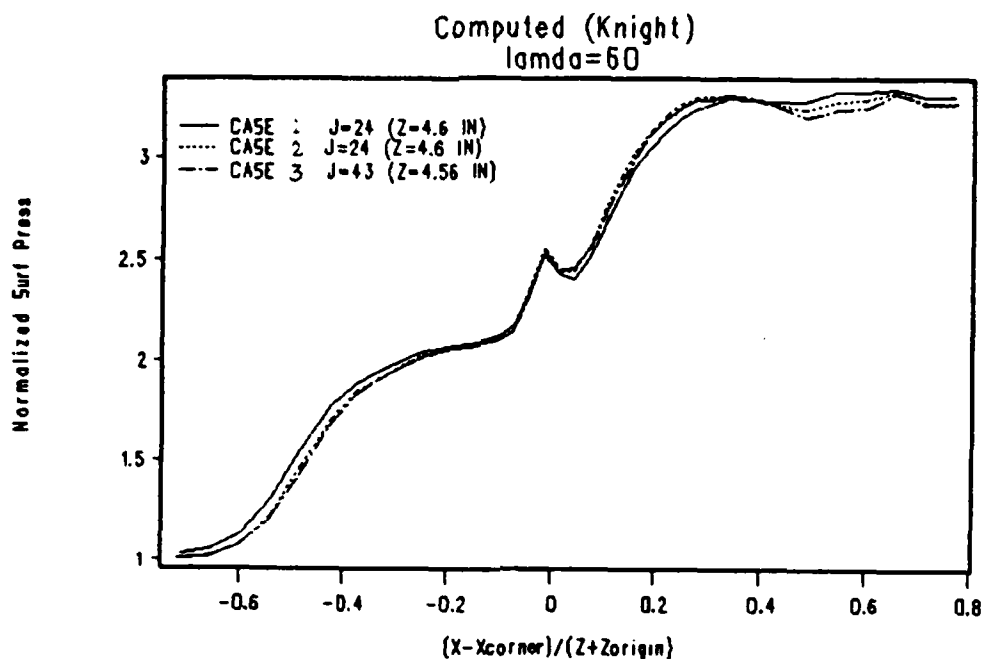
Fig. 7a   Computed Surface Pressure (Knight) for 3-D Swept
           Compression Corner (α,λ) = (24,60) deg in
           conical coordinates

Fig. 7b   Computed Surface Pressure (Horstman) for 3-D Swept
           Compression Corner (α,λ) = (24,60) deg in
           conical coordinates

Comparison (Horstman & Knight)
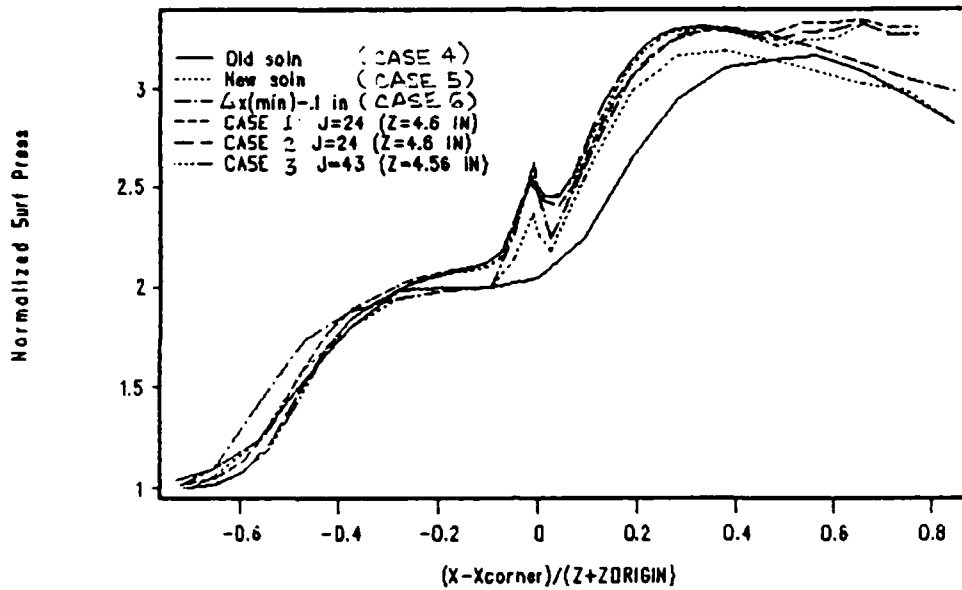
Fig. 7c   Computed Surface Pressure (Knight and Horstman) for 3-D
Swept Compression Corner $(\alpha,\lambda) = (24,60)$ deg in
conical coordinates

VII.   Appendix I

"A Comparative Study of the Hybrid MacCormack and
Implicit Beam-Warming Algorithms for a Two-Dimen-
sional Supersonic Compression Corner"

by C. Ong and D. Knight

AIAA Paper No. 86-0204

Presented at the AIAA 24th Aerospace Sciences Meeting
January 6-9, 1986
Reno, NV

A COMPARATIVE STUDY OF THE HYBRID MACCORMACK
AND IMPLICIT BEAM-WARMING ALGORITHMS FOR A
TWO-DIMENSIONAL SUPERSONIC COMPRESSION CORNER

C. Ong* and D. Knight**
Department of Mechanical and Aerospace Engineering
Rutgers-The State University of New Jersey
New Brunswick, New Jersey 08903

Abstract

A comparative study is made between the MacCormack explicit-implicit predictor-corrector and the Beam-Warming fully implicit algorithms for solving compressible viscous flow. The mass-averaged two-dimensional compressible Navier-Stokes equations in strong conservation law form and general curvilinear coordinates are solved numerically by marching forth in time on a body-fitted curvilinear grid for a shock wave-turbulent boundary layer interaction over a two-dimensional compression corner. Along the surface of the corner the boundary condition for the implicit part of the hybrid MacCormack algorithm is formulated using an approximation involving a lag in time of one-half time step. Turbulence is simulated by means of the Baldwin-Lomax algebraic turbulent eddy viscosity model. Computations are performed for a Mach number of 1.96 with a Reynolds number Re_{δ_∞} (based on the incoming boundary layer thickness δ_∞) of 0.25×10^6, and for a Mach number of 2.83 with a Reynolds number of 1.8×10^6. The primary objectives of the study are, 1) to determine the extent to which the steady state solution obtained by the hybrid MacCormack algorithm is dependent upon the size of the time step employed in marching the calculation toward the steady state solution, 2) to compare the two algorithms regarding accuracy and efficiency, and 3) to further examine the efficacy of the Baldwin-Lomax algebraic turbulent eddy viscosity model through comparison with recent experimental measurements of the Reynolds shear stress.

I. Introduction

Until the mid 1970's most numerical schemes used to solve the Navier-Stokes equations were explicit algorithms such as MacCormack's explicit method[1]. The restriction placed on the size of the maximum allowable time step by the CFL (Courant, Lewy, and Friedrichs) condition severely limited the usefulness of explicit procedures in the solution of high Reynolds number, viscous, compressible flow. By the mid 1970's this CFL restriction was removed by the fully explicit numerical schemes of Briley and McDonald[2], and Beam and Warming[3] which became very widely used. In particular, the Beam-Warming[3] method has been used to compute flows around airfoils[4], nosetips[5], boattail afterbodies[6], cascades[7], and inside 2-D inlets[8] and nonaxisymmetric nozzles[9]. However, these implicit methods require linearization of terms in the governing equations in order to form

desirable block matrix structures. The resulting block pentadiagonal or septadiagonal matrices need to be approximately factored into block tridiagonal matrices before an efficient matrix inversion procedure can be applied. Both these approximations result in limitations to the size of the maximum allowable time step[10].

In 1981 MacCormack[11] presented an explicit-implicit predictor-corrector method which involved the simple inversion of block bidiagonal matrices in an effort to further reduce demand on computer time. Since its introduction the hybrid scheme has been used by numerous investigators to compute a large variety of compressible viscous flows. In calculating a separated shock wave-laminar boundary layer interaction over a flat plate MacCormack was able to reduce the required computer time by a factor of 17.5 relative to his fully explicit method while maintaining comparable accuracy. Shang and MacCormack[12] evaluated the new method against its fully explicit predecessor for a Mach 8 flow over an axisymmetric biconic body and achieved computer time reduction by a factor of 13.

Accuracy and efficiency are but two features desirable in a numerical method. Independence of the steady state solution from the size of the chosen time step is another. Before asking whether the steady state solution of a given numerical algorithm is accurate it seems logical to first inquire if it yields the same steady state solution irregardless of the time step size selected. MacCormack advocated[11,13] a successive reduction of the time step size near the end of the calculation of high Reynolds number flows in order to avoid any possible dependence of the steady state solution on the time step size. This concern about time step dependence was underscored by Kumar[14] who reported finding considerable time step dependence of his steady state solution near the immediate neighborhood of a separation region induced by shock impingement upon the turbulent boundary layer in a duct whose inflow Mach number was 5. However, no significant CFL dependence was found by Gupta, Gnoffo, and MacCormack[15] who computed an unseparated laminar flow over an axisymmetric Mach number 44 with a detached bow shock.

Other investigators who used MacCormack's explicit-implicit scheme included Kordulla and MacCormack[16]; White and Anderson[17]; Hung and Kordulla[18]; and Imlay, Kao, McMaster, and MacCormack[19]. Despite the indication of possible significant CFL dependence of the steady state solution by MacCormack and Kumar, few investigators have addressed this issue and some have stated without further substantiation that "the implicit MacCormack method is unreliable such that the steady state solutions depend on time increments"[20]. Nevertheless, it is obviously important to ascertain the severity of any such dependence, particularly in the presence of

---

*Graduate Student, Dept of Mechanical and Aero-
space Engineering; Member, AIAA. Presently at
Continuum Dynamics Inc., Princeton, NJ.
**Professor, Dept. of Mechanical and Aero-
space Engineering; Associate Fellow, AIAA.

separated regions. Hence, the first objective of the present study is to determine whether the steady state solution obtained by the MacCormack explicit-implicit method depends on the time step size.

Since the Beam-Warming method has become very popular and the explicit-implicit hybrid method appears to be accurate and efficient, the question regarding their relative accuracy and efficiency is clearly a relevant and important one. Lawrence, Tannehill, and Chausee[21] discussed this issue in the case of the Mach 2 laminar flow over a flat plate. They used both algorithms to solve the parabolized Navier-Stokes equations by marching in space rather than in time for the Beam-Warming and MacCormack hybrid methods. They observed that the computer time requirements for the Beam-Warming and MacCormack hybrid were approximately equal. Iyer and von Lavante[22] attempted a comparison for a viscous transonic flow in turbomachinery cascasdes. However, a more extensive study for a time-marching solution of the full two-dimensional Navier-Stokes equations over a realistic grid appears necessary. Hence, the second objective of the present study is an accuracy and efficiency comparison between the MacCormack explicit-implicit and the Beam-Warming fully implicit algorithms.

The configuration selected for this comparative study is supersonic turbulent flow past a 2-D compression corner (Fig. 1). Related flows are common in many engineering applications including turbomachinery and high speed aircraft[23]. In view of the practical importance of shock wave-turbulent boundary layer interactions, it is not surprising therefore that this configuration has been extensively investigated both experimentally and theoretically. Several reviews have been published, including Green[24], Korkegi[23], and Hankey and Holden[25]. In particular, extensive experimental measurements have been performed by Settles[26] for the specific case of a Mach 2.83 turbulent flow past a 2-D compression corner at a series of corner angles α = 8 to 24 deg, and for a range of Reynolds numbers Re_{δ_∞} = 0.76 x 10^6 to 7.7 x 10^6. Settles' measurements include surface properties (pressure, skin friction and surface oil flow visualization), and boundary layer profiles of velocity, static pressure and Mach number. Visbal[27,28] computed the entire set of flows corresponding to the experimental configurations of Settles, utilizing the algebraic turbulent eddy viscosity model of Baldwin and Lomax. Visbal observed 1) the Baldwin-Lomax outer function was unsuitable for determination of the length scale of the turbulence in the separation region, 2) incorporation of the relaxation model of Shang and Hankey[29] improved the prediction of the extent of upstream propagation of the disturbance associated with the corner, and 3) the computed boundary layer recovery, downstream of reattachment, was significantly less than observed experimentally.

Recently, measurements of turbulent Reynolds stresses have been performed for the same configuration by Hayakawa, Muck, Smits and Spina[30,31,32]. These measurements, therefore, provide the opportunity for direct examination of the efficacy of the Baldwin-Lomax turbulence model. Hence, the third objective of the present study is to directly compare the computed and measured Reynolds shear stress for the 2-D compression

corner at Mach 2.83 for several corner angles, and to attempt to elucidate the deficiencies in the Baldwin-Lomax model. In addition, computations have been performed for 2-D compression corner at Mach 1.96 and Re_{δ_∞} = 0.25 x 10^6 for α = 16 deg, and the results compared with the experimental data of Dolling[33] for surface pressure.

II. Method of Solution

Governing Equations

The flow was assumed to be described by the two-dimensional, mass-averaged compressible Navier-Stokes equations. The equations were written in strong conservation law form and general curvilinear coordinates[34,35]. The fluid was assumed to be a perfect gas with a molecular dynamic viscosity given by Sutherland's law and a constant molecular Prandtl number of 0.72.

Turbulence was simulated by the Baldwin-Lomax[36] algebraic eddy viscosity model with r = 0.40, A^+ = 26, C_{Kleb} = 0.3 and k = 0.0168. The value of C_{cp} was obtained from the investigation of York and Knight[37] and Visbal[27], which detailed the dependence of C_{cp} on Mach number. In particular, C_{cp} varies from 1.8 at Mach 2 to 2.1 at Mach 3. The relaxation model of Shang and Hankey[29] was employed in all cases except the 8 deg compression ramp at Mach 2.83, with the relaxation length scale set equal to the upstream boundary layer thickness. The turbulent Prandtl number is 0.9.

Computational Domain and Boundary Conditions

Nearly orthogonal, body-fitted grids were generated using the method of Visbal and Knight[38]. Typically, 30 grid points were contained within the incoming boundary layer, and the distance between the wall and the nearest line of grid points had a Y^+ value smaller than 2.5, where Y^+ is the distance normal to the wall nondimensionalized by the local friction velocity and the wall value of the kinematic viscosity. For each flow configuration, the same grid was employed for the calculations using the Beam-Warming and MacCormack hybrid algorithm.

The inflow boundary was positioned in the undisturbed turbulent flat plate boundary layer where the computed momentum thickness matched the experimental value. In both the Beam-Warming and hybrid MacCormack computations, the flow variables on the inflow boundary were held fixed at the given values. The inflow boundary condition for the implicit step of the Hybrid MacCormack was prescribed by setting the temporal change in the solution[11], δU, to zero. The outflow boundary was located far enough downstream of the corner to be in a region of small streamwise flow gradients. Along the outflow boundary the extrapolation condition was assumed. For this boundary, both the Beam-Warming and the explicit step of the hybrid MacCormack represented $\partial U/\partial\xi$ = 0 by a first order accurate differencing, where ξ is the transformed coordinate in the general streamwise direction and U is the vector of dependent variables[3,11]. The implicit part of MacCormack's method set the temporal change δU at the downstream boundary equal to its value at the adjacent constant-ξ line.

2

At the lower boundary, the velocity and normal derivative of the static pressure were set to zero. For the Mach 1.96 compression corner flow, adiabatic boundary conditions were used for both schemes, while a constant (near adiabatic) temperature was specified for the Mach 2.83 corner. The lower boundary condition for the implicit portion of MacCormack's hybrid was formulated by allowing a one-half time step lag in the value of the temporal change δU. The upper boundary was placed sufficiently far from the lower so that freestream conditions prevailed all along its length. For the Beam-Warming scheme, a non-reflection condition[27] was applied there. For the hybrid MacCormack, however, the flow variables along the upper boundary were simply held at the freestream value and δU was set to zero. The shock emerges through the outflow boundary.

Numerical Procedure

The fully implicit scheme studied was the approximate factorization algorithm of Beam-Warming[3], formulated using Euler implicit time-differencing and second-order accurate, centered differencing for the spatial derivatives. Fourth order explicit damping terms were included in the manner shown by Thomas[39].

The explicit-implicit algorithm was that of MacCormack[11], extended to 2-D general coordinates by von Lavante and Thompkins[34]. The algorithm is second order accurate in space and time. While marching in time the order of finite differencing in the explicit predictor and corrector steps was cycled from one step to the next while that in the implicit steps was kept as forward differencing in the predictor and backward in the corrector. At all times opposite orders of differencing were employed in the predictor and corrector. The usual fourth order damping expressed in terms of the pressure is used for the explicit part. Implicit damping was also incorporated, in the manner suggested by MacCormack[11].

Both the explicit-implicit[40] and fully implicit[27] computer codes were carefully validated with excellent accuracy for a variety of flows, including laminar and turbulent boundary layers, and shock-laminar boundary layer interaction.

III. Results and Discussion

Courant Number Dependence of the Hybrid MacCormack

As indicated above, the first objective of the research is to examine the possible Courant number dependence of the steady state solution computed by the hybrid MacCormack algorithm. During this examination it will be convenient to also examine the accuracy of the solution in comparison with Beam-Warming results and the experimental measurements of Dolling[33] and Settles et al.[26].

Mach 1.96 flow over 16 deg compression corner

The computed and measured surface pressure distributions for the Mach 1.96 compression corner are displayed in Fig. 2. The Reynolds number $Re_{\delta_\infty} = 0.25 \times 10^6$ and $\alpha = 16$ deg. In this and all subsequent figures, X denotes the distance from the corner measured along the

surface. Calculated profiles shown are for the MacCormack hybrid method at Courant numbers of 0.9 (fully explicit) and 45 (hybrid), and the Beam-Warming algorithm, where the Courant number is defined by Shang[41]. The experimental data of Dolling[33] are also shown. The results clearly indicate that the steady state solution for the surface pressure using the MacCormack explicit-implicit algorithm is insensitive to the Courant number and very close to the Beam-Warming results. The computed upstream propagation of the surface pressure, measured from the corner (X = 0), is approximately 30% below the experimental value. Since the extent of the upstream propagation is directly related to the magnitude of the length scale employed in the relaxation model, the length scale δ_∞ is too small for this case. The present results at Mach 2 for $Re_{\delta_\infty} = 0.25 \times 10^6$, together with previous results of Visbal[28] at Mach 3 for $Re_{\delta_\infty} = 0.76 \times 10^6$ to 7.7×10^6, imply that the relaxation length is a moderate function of Re_{δ_∞} (i.e., the relaxation length[27] increases with decreasing Re_{δ_∞}). This observation is consistent with the results of Shang and Hankey[29], who employed a relaxation length of $10\delta_\infty$ for their studies of the 2-D compression corner at Mach 3 for $Re_{\delta_\infty} = 0.14 \times 10^6$.

The calculated skin friction coefficient c_f distribution for the same flow is shown in Fig. 3. The computed results using the MacCormack hybrid algorithm are again observed to have no marked dependence on the Courant number despite the fact that the two Courant numbers differ by a factor of 50. The computed results are in good agreement with the computation using Beam-Warming's fully implicit algorithm. The results using MacCormack's method manifest a small streamwise oscillation in c_f downstream of reattachment. The cause of this oscillation is currently under investigation.

In Fig. 4, the computed velocity parallel to the wall, normalized by the upstream freestream velocity U_∞, is displayed at $X/\delta_\infty = 0.16$ (downstream of the corner) for the Beam-Warming and MacCormack hybrid algorithms. In the latter case, results are displayed for Courant numbers of 0.9 and 45. In this and all subsequent figures, the distance normal to the surface is denoted by Y. The results indicate that the computed solution using the MacCormack hybrid algorithm is insensitive to the Courant number, and in close agreement with the results obtained using the Beam-Warming algorithm. Similar conclusions were obtained by examination of static temperature, Baldwin-Lomax outer function, static pressure and eddy viscosity[40].

Mach 2.83 flow over 16 deg compression corner

The surface pressure distributions for a Mach 2.83 flow at $Re_{\delta_\infty} = 1.6 \times 10^6$ and $\alpha = 16$ deg are shown in Fig. 5 for computations using the methods of MacCormack and Beam-Warming. The experimental measurements of Settles et al.[26] are also displayed. A high Courant number of 85 and a low of 30 used by the hybrid algorithm give no discernable difference in the computed surface pressure. There is also good agreement with the pressure calculated using the Beam-Warming scheme as well as with experiment.

In Fig. 6 the corresponding skin friction distributions are exhibited. As before, the skin

3

friction computed by the hybrid method is insensitive to the time step size. There is a slight tendency for the higher CFL case to predict a marginally lower skin friction further downstream from reattachment. The hybrid method predicts a modestly higher skin friction than the Beam-Warming method further downstream from reattachment but agrees closely with the latter practically everywhere else.

In Fig. 7, the computed and experimental horizontal velocity profiles along a vertical line are displayed at the corner. Again, the results clearly display no Courant number dependence for the MacCormack hybrid algorithm, and are in close agreement with the profile calculated using the Beam-Warming algorithm. The computed profiles are in good agreement with experiment[27,28] except in the immediate vicinity of the surface.

Mach 2.83 flow over 20 deg compression corner

The surface pressure for the Mach 2.83 flow at $Re_{\delta_\infty} = 1.6 \times 10^6$ and $\alpha = 20$ deg is detailed in Fig. 8. This ramp angle is the largest studied in this investigation. The Courant numbers used for the MacCormack scheme are 30 and 70. The Beam-Warming and experimental results[26] are also plotted. As in the previous cases, the computed surface pressure exhibits no Courant number dependence for the MacCormack algorithm. Also, the results obtained from the Beam-Warming and MacCormack hybrid algorithms are in close agreement.

In Fig. 9, the skin friction for the same flow is shown for both the MacCormack method, the Beam-Warming method, and the experiment. The results indicate that, even in the presence of such a strong adverse pressure gradient and large separation region, the computed skin friction is insensitive to time step size. The hybrid method predicts a slightly higher skin friction than the Beam-Warming scheme downstream of reattachment.

Efficiency of the Hybrid MacCormack Algorithm

In addition to Courant number dependence and accuracy, the efficiency of the hybrid MacCormack algorithm was also examined for the Mach 1.96 flow over a 16 deg ramp. Computations using the hybrid scheme were made at Courant numbers of 0.9 (fully explicit), 5., 10., 21., 40., and 45. One computation using the Beam-Warming scheme was performed which employed a maximum Courant number of 33. In order to avoid numerical instability, it was necessary to start the Beam-Warming calculation at a smaller time step and progressively increase it to a maximum consistent with numerical stability. Both numerical codes were written in FORTRAN, and executed on an NAS AS/9000 mainframe computer. A uniform set of convergence criteria was employed for all calculations. It was observed that convergence to steady state required approximately the same physical time of integration in all cases.

The computer time requirements for these computations are tabulated in Table 1. It is observed for this case that the hybrid scheme requires one-third of the computer time used by the Beam-Warming method, and up to a factor of 36 less than the fully-explicit MacCormack algorithm.

Table 1. Computer Time Comparison, Mach 1.96 Flow Over 16 deg Ramp

Algorithm	Courant Number[41]	Computer Time in hours (NAS AS/9000)
Beam-Warming	33.	8.7
MacCormack Explicit-Implicit Hybrid	45.	2.9
	40.	3.2
	21.	6.0
	10.	11.8
	5.	12.4
	0.9 (explicit)	104.1

Reynolds Shear Stress Comparison

Reynolds shear stress

In the present section, the computed and experimental profiles for the Reynolds shear stress, defined as $-\bar{\rho}\,\overline{u'v'}$, are displayed. The quantities u' and v' are the temporal fluctuating velocity components parallel and normal to the wall, respectively. The overbar represents the time average. The experimental Reynolds shear stress is obtained from the measurements[30,32] of $-\overline{(\rho u)'v'}$ by employing the "Strong Reynolds Analogy" (i.e., pressure fluctuations are small compared to density or temperature fluctuations) and "Very Strong Reynolds Analogy" (i.e., fluctuations in total temperature are neglected). The uncertainties (approximately ±30%) in the measurement of the Reynolds stress are discussed in Ref. 30-32. The theoretical Reynolds shear stress, modeled using the Baldwin-Lomax algebraic turbulent eddy viscosity, is $-\bar{\rho}\,\overline{u''v''}$, where u'' and v'' denote the mass-averaged fluctuating velocity components parallel and normal to the wall, respectively. With the assumption of the Strong and Very Strong Reynolds Analogies, the theoretical Reynolds shear stress is approximately equal to $-\bar{\rho}\,\overline{u'v'}$. In all plots, the experimental and theoretical Reynolds shear stress are normalized by $0.5\,\rho_\infty U_\infty^2$.

Mach 2.83 flow over 8 deg compression corner

The computed and experimental Reynolds shear stress profile at $x = -0.63\,\delta_\infty$, located upstream of the interaction region, is displayed in Fig. 11 for the Mach 2.83 flow over an 8 degree compression corner. The computed results of MacCormack's hybrid method at Courant numbers of 95 and 0.9 are plotted together with the Beam-Warming and experimental profiles of Muck et al.[30-32]. Agreement among all three computed Reynolds stress profiles is excellent. Agreement between the computed and experimental profiles is good except in the outer portion of the boundary layer where the predicted Reynolds stress is low.

In Figs. 12 and 13, computed and experimental Reynolds stress profiles are shown at $x/\delta_\infty = 0.78$ and 1.17. They indicate that the predicted peak value of the Reynolds stress profile is significantly too low, and that the predicted peak is located too near the wall.

4

Mach 2.83 flow over 16 deg compression corner

For the Mach 2.83 flow over a 16 deg compression corner, the calculated and experimental Reynolds stress profiles at stations $x/\delta_\infty = 0.49$, 2.0 and 5.4 are exhibited in Figs. 14 to 16. It is apparent that the peaks of the computed and experimental Reynolds stress profiles are comparable in magnitude. This is summarized in Fig. 17, which displays the distribution of the magnitude of the peak of the Reynolds stress profiles with distance X. It is evident, however, that the computed peak is located too close to the wall. The height of the peak Y_{peak} as a function of distance X is displayed in Fig. 18. The distance of the peak from the wall increases as the boundary layer develops downstream for both computed and experimental profiles.

Mach 2.83 flow over 20 deg compression corner

In Figs. 19 to 21, the profiles of the Reynolds shear stress at stations $X/\delta_\infty = 1.0$, 2.3 and 4.6, are shown for the Mach 2.83 flow over a 20 deg compression corner. The distribution of the peak of the Reynolds stress profile is exhibited in Fig. 22. It shows that while the experimental peak remains approximately constant the computed peak steadily diminishes. In Fig. 23, the corresponding distribution of the location of the peak Y_{peak} of the Reynolds stress profile is displayed. A pronounced underprediction of the distance of the peak from the wall is evident, similar to that observed in Fig. 18 for the 16 deg corner.

Discussion of Comparison of Reynolds Stress Profiles

In summarizing the above comparison of Reynolds shear stress, the principal discrepancy is the underprediction of the height of the peak of the Reynolds shear stress. The Baldwin-Lomax model is modestly successful in predicting the magnitude of the peak of the Reynolds shear stress, although the success is tempered for $\alpha = 20$ deg by an apparent incorrect trend in X.

Recognizing the inherent simplicity and limitations of the mixing length concept, it is interesting, nonetheless, to attempt to treat the defects of the Baldwin-Lomax model "symptomatically". It is noted in Fig. 23 that the height of the peak Y_{peak} of the computed Reynolds shear stress correlates with the magnitude of the computed outer length scale Y_{max} of the Baldwin-Lomax model for $\alpha = 20$ deg; a similar observation applies for $\alpha = 16$ deg. The location of the experimental peak Reynolds stress corresponds to the outer portion of the boundary layer (i.e., outside the point where the Baldwin-Lomax model switches from the inner to the outer formulation). This suggests, therefore, that the computed Reynolds shear stress may be improved by increasing Y_{max}. This approach was attempted by Visbal[28] for $\alpha = 16$ deg. Specifically, Y_{max} was kept constant at its upstream value; this represents an increase in Y_{max} compared to the calculations with the relaxation eddy viscosity model (Fig. 24). The effect of increasing Y_{max} is seen in Figs. 17 and 18. The magnitude of the peak Reynolds shear stress is overpredicted for $x < 2\delta_\infty$, while a slight improvement in Y_{peak} is noted. The computed Reynolds shear stress profiles[40], display

a double-peaked behavior at $x/\delta_\infty = 0.49$ and 0.98, in disagreement with experiment. It may be concluded, therefore, that no overall improvement was obtained by increasing Y_{max}.

It is evident that the simple mixing-length Baldwin-Lomax model is incapable of accurately predicting the reattachment and downstream recovery of a separated 2-D compression corner flow. The model is based upon the concept of an equilibrium turbulent boundary layer exhibiting one characteristic velocity scale[42]. Downstream of reattachment, there are two characteristic velocity scales of the turbulence, namely 1) an outer velocity scale associated with the turbulence fluctuations in the outer portion of the reattaching free shear layer, and 2) an inner velocity scale $u_* = (\tau_w(x)/\rho_w(x))^{1/2}$ associated with the imposition of the no slip boundary condition downstream of reattachment, which creates an "inside layer" within the boundary layer. The failure of the "simple" extension to the Baldwin-Lomax model described above is therefore not surprising within this framework. A more physical realistic turbulence model is required for 2-D separated compression corner flows which incorporates the effect of the upstream history on the turbulent flow and the oscillatory motion of the shock wave structure[43,44]. The assumption of an algebraic eddy viscosity model precludes the incorporation of the turbulence history, except through the crude technique of the relaxation model. With regard to the unsteady large amplitude shock wave motion, additional research is needed to elucidate its effect on the turbulence structure and on the recovery of the boundary layer downstream of reattachment.

IV. Conclusions

A comparative study has been performed for the MacCormack hybrid and the Beam-Warming fully implicit algorithms for a shock wave-turbulent boundary layer interaction over a two-dimensional corner. The computations employed identical grids and the Baldwin-Lomax algebraic turbulent eddy viscosity model. It is observed that the steady state solution of the MacCormack hybrid algorithm is remarkably insensitive to Courant number. The accuracy of the steady state solution using MacCormack's hybrid algorithm is comparable to that of the Beam-Warming method for all cases. Based on experience with the Mach 1.96 computations, the MacCormack hybrid method is observed to reduce the computing time by a factor of up to 3 relative to the Beam-Warming method.

The computed Reynolds stress profiles are compared with the experimental data of Muck et al[30-32]. It is noted that the magnitude of the peak of the computed Reynolds shear stress is in approximate agreement with the measurements, although an apparent incorrect trend is evident for $\alpha = 20$ deg. The major discrepancy is the underprediction of the location of the peak of the computed Reynolds shear stress. It is noted that a simple modification of the Baldwin-Lomax turbulence model involving an increase in the length scale Y_{max} of the outer eddy viscosity fails to demonstrate overall improvement. The Baldwin-Lomax model is based on the mixing-length concept, and is incapable of accurately predicting the recovery of

a separated 2-D compression corner flow. It is noted that several additional physical factors, omitted from the theoretical model, also affect the recovery of the boundary layer including the history effect of the turbulence structure and the large amplitude oscillatory motion of the shock structure.
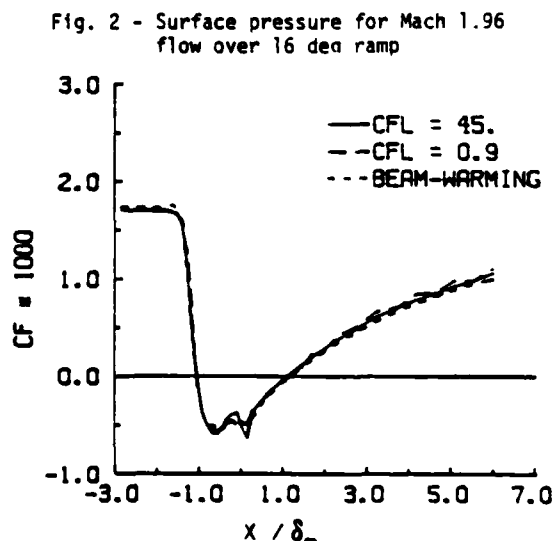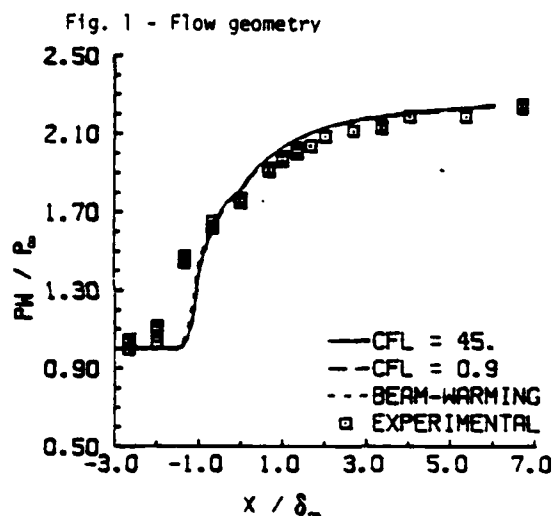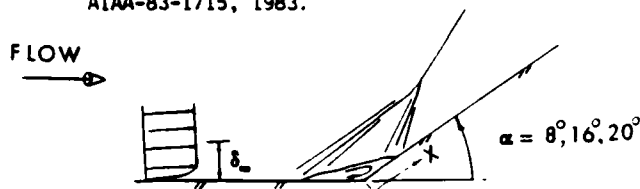
References

1. MacCormack, R.W., "The Effect of Viscosity in Hypervelocity Impact Cratering," AIAA Paper No. 69-354, 1969.

2. Briley, W.R. and McDonald, H., "An Implicit Numerical Method for the Multidimensional Compressible Navier-Stokes Equations," United Aircraft Research Lab., Report M911363-6, 1973.

3. Beam, R. and Warming, R., "An Implicit Factored Scheme for the Compressible Navier-Stokes Equations," AIAA J., Vol. 16, 1978.

4. Steger, J.L., "Implicit Finite Difference Simulation of Flow About Arbitrary Geometries with Applications to Airfoils," AIAA Paper No. 77-665, 1977.

5. Kutler, P., Pedelty, J.A., and Pulliam, T.H., "Supersonic Flow Over a 3-D Ablated Nosetips Using an Unsteady Implicit Numerical Procedure," AIAA Paper No. 80-0063, 1980.

6. Deiwert, G.S., "Numerical Simulation of 3-D Boattail Afterbody Flow Field," AIAA Paper No. 80-1347, 1980.

7. Steger, J., Pulliam, T., and Chima, R., "An Implicit Finite Difference Code for Inviscid and Viscous Flows," AIAA Paper No. 80-1427, 1980.

8. Biringen, S. and McMillan, O.J., "A Numerical Simulation of 2-D Inlet Flow Fields," AIAA Paper No. 81-0187, 1981.

9. Thomas, P.D., "Numerical Method for Predicting Flow Characteristics and Performance of Non-axisymmetric Nozzles, Part 2 - Applications," NASA CR-159173, 1980.

10. MacCormack, R.W., "Current Status of Numerical Solutions of the Navier-Stokes Equations," AIAA Paper No. 85-0032.

11. MacCormack, R.W., "A Numerical Method for Solving the Equations of Compressible Viscous Flows," AIAA Paper No. 81-0110, 1981.

12. Shang, J.S. and MacCormack, R.W., "Flow Over a Biconic Configuration with an Afterbody Compression Flap - A Comparative Numerical Study," AIAA Paper No. 83-1668, 1983.

13. MacCormack, R.W., "Numerical Solution of the Equations of Compressible Viscous Flows," Transonic, Shock, and Multidimensional Flows: Advances in Scientific Computing, Academic Press, 1982.

14. Kumar, A., "Some Observations on a New Numerical Method for Solving the Navier-Stokes Equations," NASA TP-1934, 1981.

15. Gupta, R.N., Gnoffo, P.A., and MacCormack, R.W., "A Viscous Shock-Layer Flowfield Analysis by an Explicit-Implicit Method," AIAA Paper No. 83-1423.

16. Kordulla, W. and MacCormack, R.W., "Transonic Flow Computations Using an Explicit-Implicit Method," Proceedings of the 8th International Conference on Numerical Methods, Aachen, Germany, pp. 286-295, 1982.

17. White, M.E. and Anderson, J.D., "Application of MacCormack's Implicit Method to Quasi-One-Dimensional Nozzle Flows," AIAA Paper No. 82-0992, 1982.

18. Hung, C.M. and Kordulla, W., "A Time-Split Finite-Volume Algorithm for 3-D Flow-Field Simulation," AIAA Paper No. 83-1957, 1983.

19. Imlay, S.T., Kao, T.J., McMaster, D.L., and MacCormack, R.W., "Solution of the Navier-Stokes Equations for Flow Within a 2-D Thrust Reversing Nozzle," AIAA Paper No. 84-0344, 1984.

20. Obayashi, S. and Kuwahara, K., "LU Factorization of an Implicit Scheme for the Compressible Navier-Stokes Equations," AIAA Paper NO. 84-1670, 1984.

21. Lawrence, S.L., Tannehill, J.C. and Chausee, D.S., "Application of the Implicit MacCormack Scheme to the Parabolized Navier-Stokes Equations," AIAA J., Vol. 22, No. 12, Dec. 1984.

22. Iyer, V. and von Lavante, E., "Numerical Solution of Viscous Transonic Flow in Turbo-machinery Cascades," AIAA Paper No. 85-0007, 1985.

23. Korkegi, R.H., "Survey of Viscous Interactions Associated with High Mach Number Flight," AIAA J., Vol. 9, No. 5, 771-784, 1971.

24. Green, J.E., "Interactions Between Shock Waves and Turbulent Boundary Layers," Prog. in Aerosp. Sci., Vol. 11, 235-340, 1970.

25. Hankey, W.L., Jr. and Holden, M.S., "2-D Shock Wave-Boundary Layer Interactions in High Speed Flows," AGARDograph No. 203, 1975.

26. Settles, G., Gilbert, R., and Bogdonoff, S., "Data Compilation for Shock Wave/Turbulent Boundary Layer Interaction Experiments on 2-D Compression Corners," Report MAE-1489, Dept. of Aerospace & Mechanical Eng., Princeton University, NJ, 1980.

27. Visbal, M., "Numerical Simulation of Shock/ Turbulent Boundary Layer Interactions over 2-D Compression Corners," Ph.D. Thesis, Dept. of Mechanical and Aerospace Eng., Rutgers University, NJ, 1983.

28. Visbal, M. and Knight, D., "The Baldwin-Lomax Turbulence Model for 2-D Shock-Wave/Boundary-Layer Interactions," _AIAA J._, Vol. 22, No. 7, July 1984.

29. Shang, J.S. and Hankey, W.L., "Numerical Solutions for Supersonic Turbulent Flow Over a Compression Ramp," _AIAA J._, Vol. 13, No. 10, pp. 1360-1374, 1975.

30. Muck, K.C., Hayakawa, K., and Smits, A.J., "Compilation of Turbulence Data for a 20° Compression Corner at Mach 2.9," MAE Report 1620, Dept. of Mechanical and Aerospace Eng., Princeton University, NJ, 1983.

31. Muck, K.C., Hayakawa, K., and Smits, A.J., "Compilation of Turbulence Data for a 16° Compression Corner at Mach 2.9," MAE Report 1619, Dept. of Mechanical and Aerospace Eng., Princeton University, NJ, 1984.

32. Muck, K.C., Spina, E.F., and Smits, A.J., "Compilation of Turbulence Data for an 8° Compression Corner at Mach 2.9," Report MAE-1642, Dept. of Mechanical and Aerospace Eng., Princeton University, NJ, 1984.

33. Dolling, D., Private communication, 1983.

34. von Lavante, E. and Thompkins, W.T., "An Implicit Bi-diagonal Numerical Method for Solving the Navier-Stokes Equations," AIAA Paper No 82-0063, 1982.

35. Pulliam, T. and Steger, J., "Implicit Finite-Difference Simulations of Three-Dimensional Compressible Flows," _AIAA J._, Vol. 18, pp. 159-167, 1980.

36. Baldwin, B. and Lomax, H., "Thin Layer Approximation and Algebraic Model for Separated Turbulent Flows," AIAA Paper No. 78-257, 1978.

37. York, B. and Knight, D., "Calculation of a Class of Two-Dimensional Turbulent Boundary Layer Flows Using the Baldwin-Lomax Model," AIAA Paper No. 85-0126, 1985 (to appear in _AIAA J._).

38. Visbal, M. and Knight, D., "Generation of Orthogonal and Nearly Orthogonal Coordinates with Grid Control Near Boundaries," _AIAA J._, Vol. 20, No. 3, 1982.

39. Thomas, P.D., "Boundary Conditions and Conservative Smoothing for Implicit Numerical Solutions to the Compressible Navier-Stokes Equations," LMSC-D630729, 1978.

40. Ong, C.C., "Calculation of Shock Wave-Turbulent Boundary Layer Interaction Over a Two-Dimensional Compression Corner," Ph.D. Thesis, Dept. of Mechanical and Aerospace Eng., Rutgers University, NJ, in preparation.

41. Shang, J.S., "Numerical Simulation of Wing-Fuselage Interference," AIAA Paper No. 81-0048, 1981.

42. Tennekes, H. and Lumley, J., _A First Course in Turbulence_, The MIT Press, 1972.

43. Dolling, D. and Murphy, M., "Wall Pressure Fluctuations in a Supersonic Separated Compression Ramp Flowfield," AIAA-82-0986, 1982.

44. Dolling, D. and Or, C.T., "Unsteadiness of the Shock Wave Structure in Attached and Separated Compression Ramp Flow Fields," AIAA-83-1715, 1983.

Fig. 1 - Flow geometry

Fig. 2 - Surface pressure for Mach 1.96 flow over 16 deg ramp

Fig. 3 - Skin friction for Mach 1.96 flow over 16 deg ramp
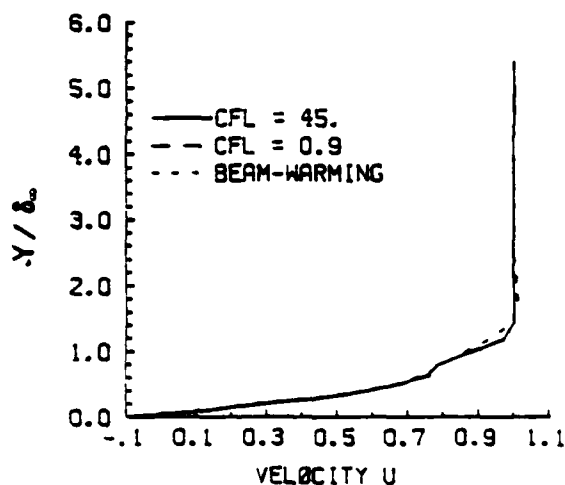
Fig. 4 - Velocity u at X/δ_∞ = 16 for Mach 1.96 flow over 16 deg ramp.
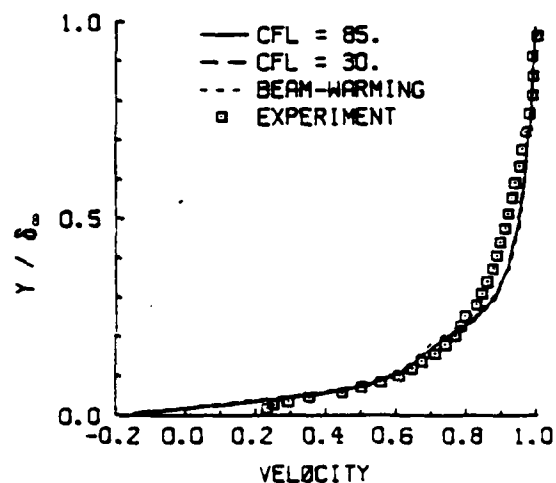
Fig. 7 - Horizontal velocity at X/δ_∞ = 0 for Mach 2.83 flow over 16 deg ramp.

Fig. 5 - Surface pressure for Mach 2.83 flow over 16 deg ramp.
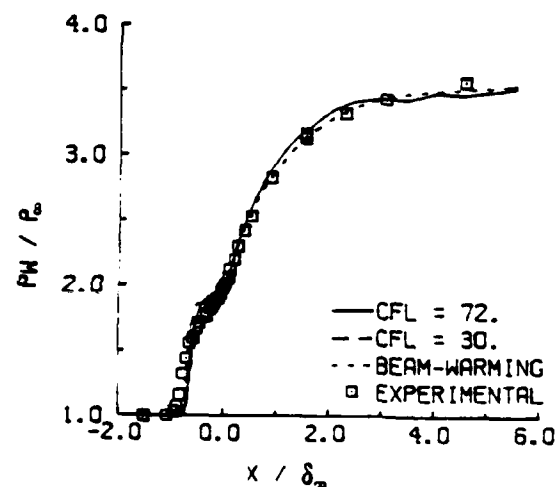
Fig. 8 - Surface pressure for Mach 2.83 flow over 20 deg ramp.
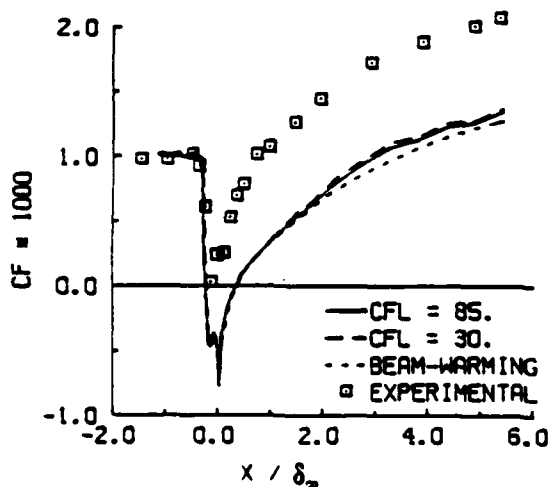
Fig. 6 - Skin friction for Mach 2.83 flow over 16 deg ramp.
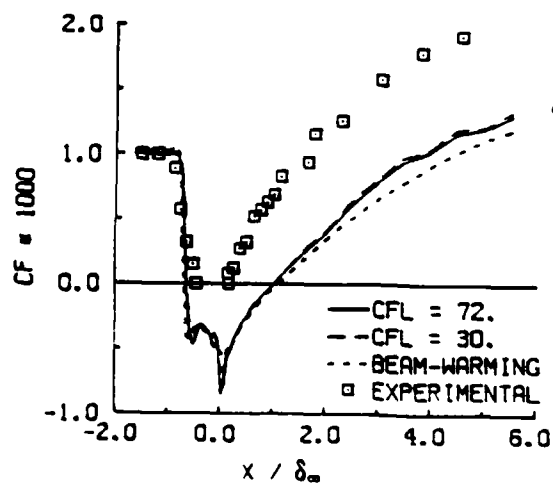
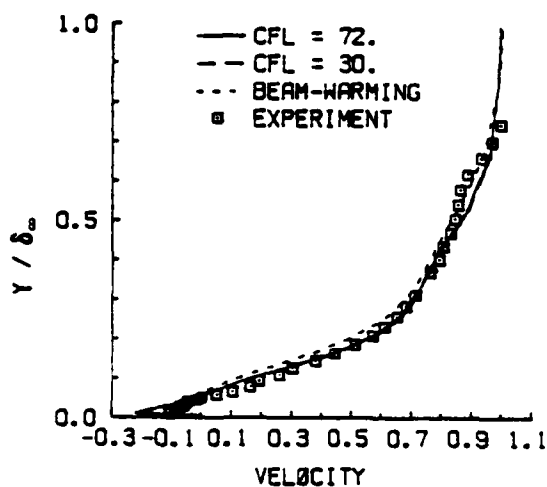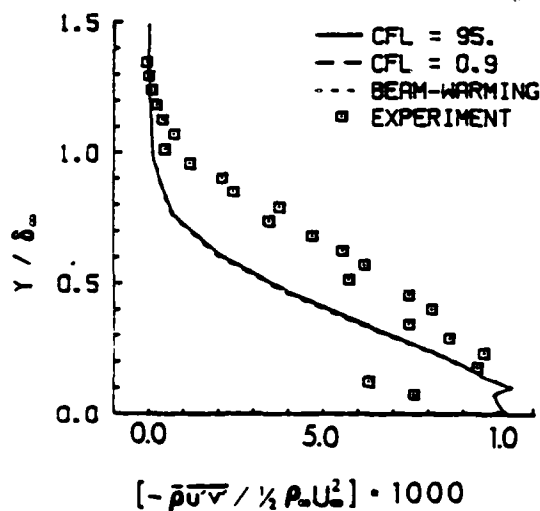Fig. 9 - Skin friction for Mach 2.83 flow over 20 deg ramp.

8

Fig. 10 - Horizontal velocity at $X/\delta_\infty = 0$ for Mach 2.83 flow over 20 deg ramp.

Fig. 13 - Reynolds shear stress at $X/\delta_\infty = 1.17$ for Mach 2.83 flow over 8 deg ramp.

Fig. 11 - Reynolds shear stress at $X/\delta_\infty = -0.63$ for Mach 2.83 flow over 8 deg ramp.
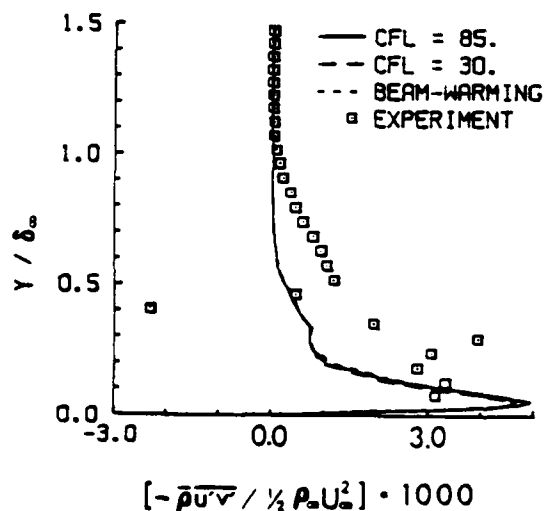
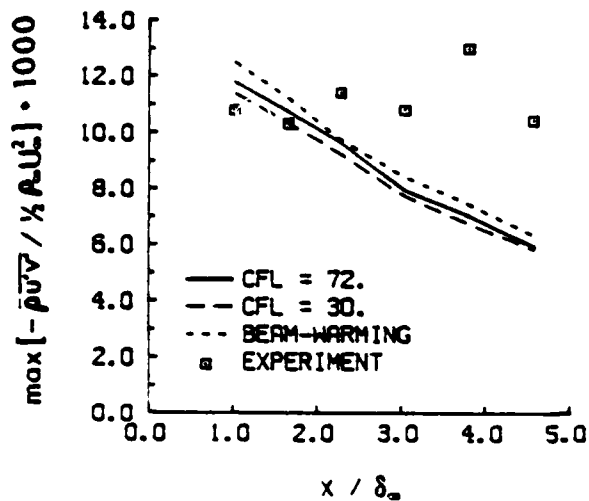Fig. 14 - Reynolds shear stress at $X/\delta_\infty = 0.49$ for Mach 2.83 over 16 deg ramp.

Fig. 12 - Reynolds shear stress at $X/\delta_\infty = 0.78$ for Mach 2.83 flow over 8 deg ramp.
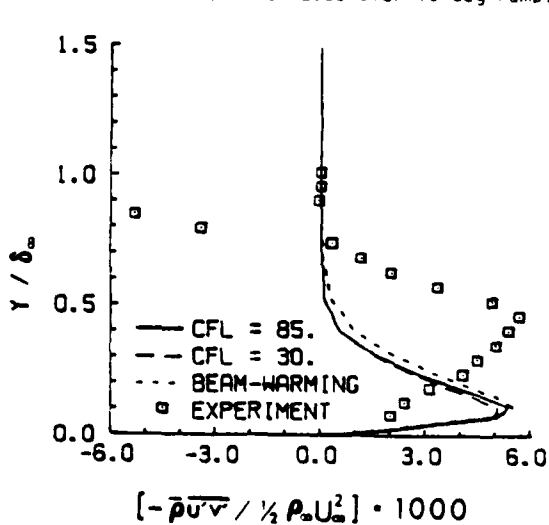
Fig. 15 - Reynolds shear stress at $X/\delta_\infty = 2.0$ for Mach 2.83 flow over 16 deg ramp.

9
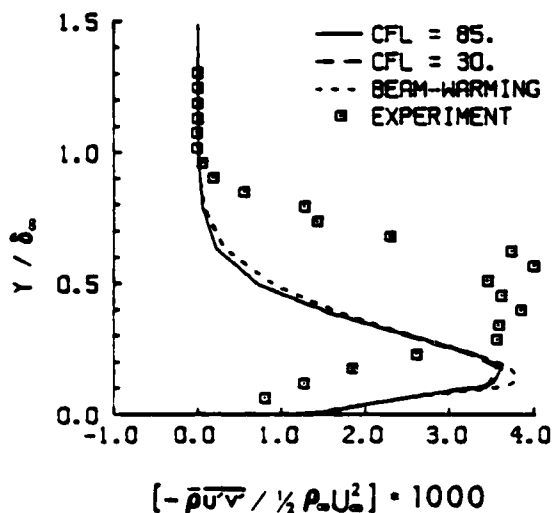
Fig. 16 - Reynolds shear stress at $X/\delta_\infty = 5.4$ for Mach 2.83 flow over 16 deg ramp.

Fig. 17 - Magnitude of peak of the Reynolds stress for Mach 2.83 flow over 16 deg ramp.

Fig. 18 - Location of peak in Reynolds shear stress profile for Mach 2.83 flow over 16 deg ramp.
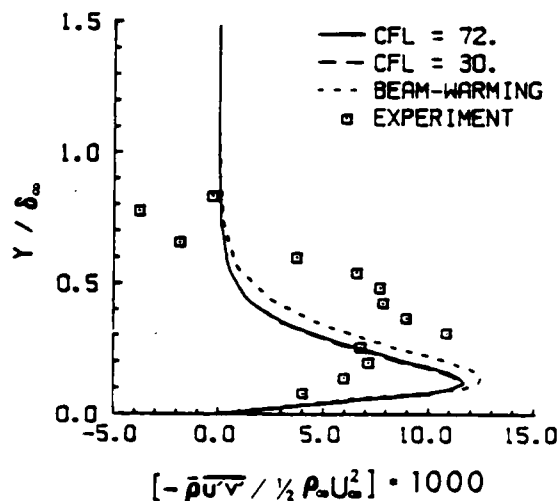
Fig. 19 - Reynolds shear stress at $X/\delta_\infty = 1.0$ for Mach 2.83 flow over 20 deg ramp.
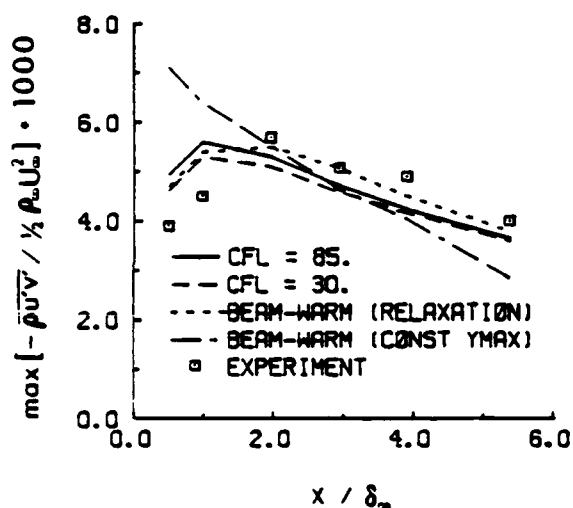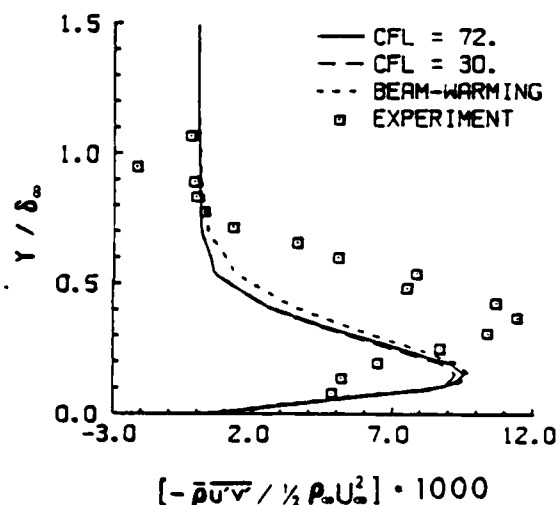
Fig. 20 - Reynolds shear stress at $X/\delta_\infty = 2.3$ for Mach 2.83 flow over 20 deg ramp.
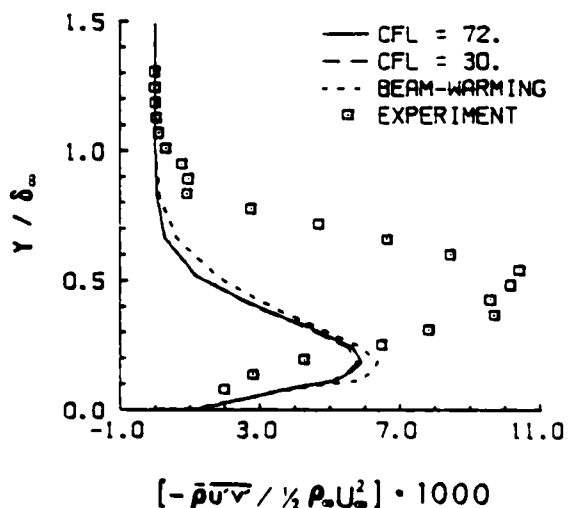
Fig. 21 - Reynolds shear stress at $X/\delta_\infty = 4.6$ for Mach 2.83 flow over 20 deg ramp.

10

Fig. 22 - Magnitude of peak of the Reynolds stress for Mach 2.83 flow over 20 deg ramp.
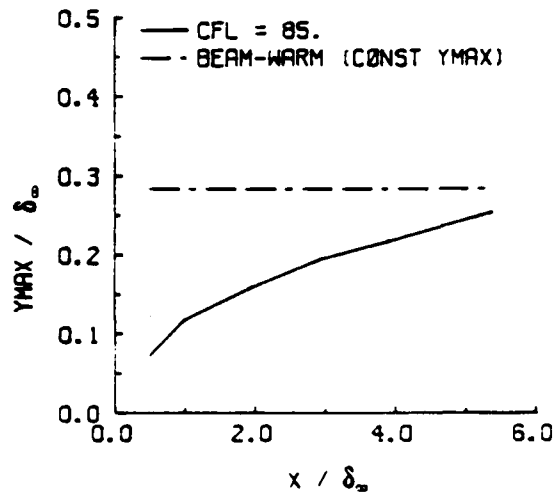
Fig. 24 - Baldwin-Lomax length scale Y_{max} for Mach 2.83 flow over 16 deg ramp.
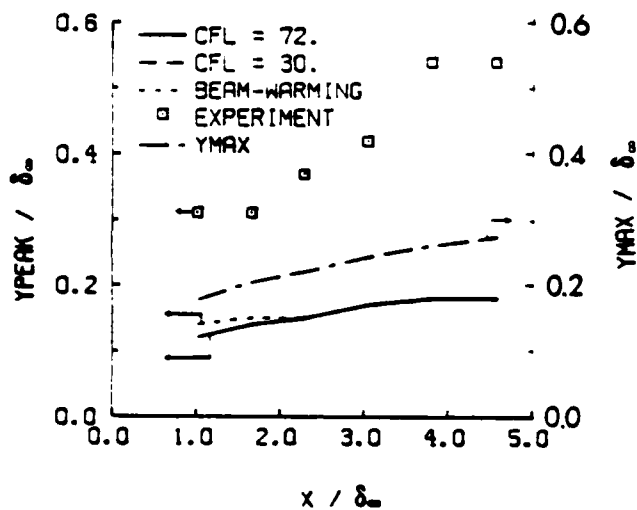
Fig. 23 - Baldwin-Lomax length scale Y_{max}, and location of the peak of the Reynolds shear stress for Mach 2.83 flow over 20 deg ramp.

11

VIII.   Appendix II

"The Flowfield Structure of the 3-D Shock Wave-
Boundary Layer Interaction Generated by a 20 deg
Sharp Fin at Mach 3"

by D. Knight, C. Horstman, B. Shapey and S. Bogdonoff

AIAA Paper No. 86-0343

Presented at the AIAA 24th Aerospace Sciences Meeting
January 6-9, 1986
Reno, NV

THE FLOWFIELD STRUCTURE OF THE
3-D SHOCK WAVE - BOUNDARY LAYER INTERACTION
GENERATED BY A 20 DEG SHARP FIN AT MACH 3

Doyle D. Knight[1]
Department of Mechanical and Aerospace Engineering
Rutgers University - The State University of New Jersey
P.O. Box 909
Piscataway, NJ 08854

C. C. Horstman[2]
NASA Ames Research Center
Moffett Field, CA 94035

Brian Shapey[3] and Seymour Bogdonoff[4]
Department of Aerospace and Mechanical Engineering
Princeton University
Princeton, NJ 08540

Abstract

The 3-D shock wave-turbulent boundary layer interaction generated by a sharp fin is examined both experimentally and theoretically at Mach 3 for a fin angle $\alpha_g = 20$ deg and Reynolds number $Re_{\delta_\infty} = 9 \times 10^5$. This study represents an extension of previous research for the sharp fin configuration to stronger interactions. The experimental data include surface pressure profiles, surface streamline patterns, and boundary layer profiles of pitot pressure and yaw angle. Two separate theoretical approaches or "models" were employed. Both models employ the 3-D compressible Navier-Stokes equations in mass-averaged variables. The theoretical approach of Knight utilizes the algebraic turbulent eddy viscosity model of Baldwin and Lomax, and the theoretical model of Horstman employs the two-equation turbulence model of Jones and Launder coupled with the wall function model of Viegas and Rubesin. The computed surface pressure, surface streamlines, pitot pressure and yaw angle profiles are in good agreement with the experimental data, thereby confirming the efficacy of the theoretical approaches which were previously validated for the 3-D sharp fin configuration at Mach 3 for smaller α_g (i.e., weaker interactions). The three dimensional velocity fields computed by both models are in close agreement, although the eddy viscosity profiles differ significantly within the 3-D interaction. This result indicates that the overall structure of this 3-D sharp fin interaction is insensitive to the turbulence model. A series of particle pathline traces were examined for each model, and found to be in close agreement. The calculated flowfields display a prominent vortical structure associated with the shock-boundary layer interaction in agreement with the flowfield models of Token, and Kubota and Stollery. The structure is characterized by two significant surfaces, namely, 1) the surface of separation which emanates from the line of coalescence (line of separation) and spirals into the vortical core, and 2) the surface of attachment which intersects the wall at the line of divergence (line of attachment) and demarcates the fluid which is entrained into the vortical structure.

I. Introduction

For nearly forty years, significant interest has been focused on the subject of two- and three-dimensional shock wave-turbulent boundary layer interactions (denoted "2-D" or "3-D turbulent interactions" for brevity). The phenomenon is widespread in aerodynamics, turbomachinery and other areas of fluid mechanics, and therefore a clear motivation exists for developing a deeper understanding. A variety of simplified geometrical configurations have been employed to investigate 3-D turbulent interactions[1]. A sample of these include, 1) sharp fin mounted perpendicular to a flat plate, 2) blunt fin mounted perpendicular to a flat plate, 3) swept compression corner, 4)semicone affixed to a flat plate, 5) cone within a circular wind tunnel, and 6) normal wall jet.

The focus of the present paper is the 3-D oblique shock wave-turbulent boundary layer interaction generated by a sharp fin attached to a flat plate (Fig. 1). The overall flowfield is determined by a small set of parameters, namely, the upstream Mach number M_∞, the Reynolds number Re_{δ_∞} based upon the boundary layer thickness δ_∞ at the streamwise station corresponding to the leading edge of the fin (where δ_∞ is measured in the absence of the fin), the nature of the thermal boundary condition on the flat plate and fin (e.g., adiabatic or fixed temperature), and the fin angle α_g. This configuration has been the subject of several experimental and theoretical investigations. Experiments have focused principally on surface measurements, and include the studies of Stanbrook[2], McCabe[3], Law[4], Kubota and Stollery[5], Zheltovodov[6], Dolling[7] and Goodwin[8]. In recent years, detailed boundary layer measurements have been obtained by Peake[9], Oskam, Vas and Bogdonoff[10-12], and McClure and Dolling[13]. Numerical simulations using the 3-D Reynolds-averaged Navier-Stokes equations have been performed principally at Mach 3, and include the studies of Horstman and Hung[14] and Knight[15-17]. These computations, detailed in Table 1, have previously considered fin angles α_g up to 10 deg. The investigations of Horstman and Hung utilized the Escudier[19] turbulence model, while the later work of Horstman[18] employed the Jones-Launder[20] model. The calculations of Knight utilize the Baldwin-Lomax[21] turbulence model. These prior calculations have been examined in comparison with experimental data for a wide variety of flow quantities including surface

---

pressure, skin friction, heat transfer, pitot pressure, yaw angle, pitch angle and static pressure. In general, good agreement was obtained with the experimental data.

The experiments were performed in the supersonic high Reynolds number wind tunnel at the

TABLE 1. Computations of 3-D Sharp Fin Configuration at Mach 3

α_g (deg)	Re_{δ_∞}	p_2/p_∞	Investigator Theoretical	Investigator Experimental
3.75	8.7×10^5	1.32	Horstman and Hung[14]	Oskam et al.[10-12]
3.75	9.3×10^5	1.32	Knight[15]	Oskam et al.[10-12]
10	2.8×10^5	2.01	Knight[16]	McClure and Dolling[13]
10	3.4×10^5	2.01	Horstman[17]	McClure and Dolling[13]
10	8.7×10^5	2.01	Horstman and Hung[14]	Oskam et al.[10-12]
10	9.3×10^5	2.01	Knight[15]	Oskam et al.[10-12]
20	8.6×10^5	3.65	Knight*	Shapey and Bogdonoff*, Goodwin[8]
20	8.6×10^5	3.65	Horstman*	Shapey and Bogdonoff*, Goodwin[8]

*Present paper
Note: Actual Mach number is 2.94 ± .01.

There are three objectives for the present paper:

1. Examine the Accuracy of the Theoretical Models for Stronger Interactions.

As indicated in Table 1, the strongest 3-D sharp fin interaction computed previously at Mach 3 corresponded to a pressure ratio $p_2/p_\infty = 2.01$ ($\alpha_g = 10$ deg), where p_∞ is the upstream static pressure and p_2 is the theoretical downstream inviscid pressure. A critical issue is the examination of the accuracy of the theoretical models for stronger interactions. In the present study, the theoretical models are examined for the 3-D sharp fin interaction at Mach 3 and $\alpha_g = 20$ deg, which exhibits a pressure rise of 3.7. This is the strongest interaction considered for these models at Mach 3.

2. Comparison of two different Theoretical Models.

An important objective of the present research is to examine the computed flowfields for the 3-D sharp fin interaction obtained using two different turbulence models. In this effort, Navier-Stokes calculations have been performed by Knight and Horstman using the Baldwin-Lomax and Jones-Launder turbulence models, respectively, for the 3-D sharp fin configuration. A principal issue is the determination of the sensitivity of the computed flowfield to the turbulence model employed.

3. Examine the Flowfield Structure of the 3-D Sharp Fin Interaction.

Provided the theoretical models yield good agreement with the experimental data for the Mach 3, $\alpha_g = 20$ deg configuration, the computed flowfields can be utilized to examine and understand the flowfield structure of this 3-D sharp fin interaction. Flowfield models have been developed, for example, by Token[22], and Kubota and Stollery[5]. These models may be examined using the computed flowfields.

Princeton University Gas Dynamics Laboratory. The facility has a 20 cm x 20 cm test section, with a nominal freestream Mach number of 2.93. The settling chamber pressure and temperature were 6.8 $\times 10^5$ Pa ±1% and 251 °K ±5%, respectively, yielding a nominal Reynolds number of 7.0×10^8 m^{-1}. The experiments were performed under near adiabatic wall conditions.

The sharp fin is 14.21 cm long and 12.7 cm high. The fin was fabricated from aluminum with a sharp unswept leading edge, and oriented at a right angle to the tunnel wall ("flat plate"). The fin was mounted in a unique variable-geometry apparatus which permitted the achievement of fin angles exceeding 20 degrees, thereby extending the range of the experiments beyond the earlier fixed-geometry configuration[10-12].

Surface pressure distributions were obtained along rows of orifices aligned with the x-direction. A kerosene-lampblack technique[23] was employed to obtain surface flow angularity. The boundary layer on the tunnel wall ("flat plate") was surveyed using a computer-controlled nulling cobra probe[13] which measured pitot pressure p_p and yaw angle β, where $\beta = \tan^{-1}(w/u)$ with (u,v,w) indicating the cartesian velocity components in the (x,y,z) coordinate system (Fig. 1). The survey locations, shown in Fig. 2, were selected to provide detailed information within the region between the line of coalescence ("3-D separation line"[9]) and shock wave, and the region downstream of the shock. The specific survey stations are indicated in Table 2, where $x_s = x - x_{shock}$ (x_{shock} is the streamwise location of the theoretical inviscid shock wave at the specified spanwise location z), z is the spanwise location, and $\delta_\infty = 1.27$ cm.

The incoming flow on the tunnel wall is an equilibrium, two-dimensional boundary layer which has been extensively surveyed[24,25] and observed to closely fit the law of the Wall and Wake[26]. The thickness of the incoming boundary layer δ_∞ is approximately 1.4 cm.

2

TABLE 2. Boundary Layer Survey Locations

Survey Location	x_s/δ_∞	z/δ_∞
1	-5.40	5.81
2	-4.40	5.81
3	-3.40	5.81
4	-2.40	5.81
5	-1.40	5.81
6	-0.40	5.81
7	0.60	5.81
8	2.60	5.81
9	-3.94	7.81
10	-0.14	4.81
11	1.13	3.81

III. Description of Computations

A. Theoretical Approach of Knight

1. Governing Equations and Numerical Algorithm

The governing equations are the full mean compressible 3-D Navier-Stokes equations using mass-averaged variables[27] and strong conservation form[28]. The molecular dynamic viscosity is given by Sutherland's law. The molecular and turbulent Prandtl numbers are 0.73 and 0.9, respectively. Turbulence is modelled through the inclusion of the two-layer algebraic turbulent eddy viscosity model of Baldwin and Lomax[21], with the mixing length specified by the formula of Buleev[29] as discussed in Gessner and Po[30]. The Baldwin-Lomax (BL) model is implemented as discussed in Ref. 15-17.

A 3-D coordinate transformation $(\xi(x,y,z), \eta(x,y,z), \zeta(x,y,z))$ is used to map the physical domain (shown as the dotted lines in Fig. 1) into a cube in the transformed domain whose simple shape facilitates the application of the numerical algorithm. Various methods have been developed for numerical generation of curvilinear coordinates[31]. For the 3-D sharp fin, however, a simple analytic transformation was employed (see below).

At the upstream boundary (ABHG in Fig. 1), the flow variables are held fixed at the values corresponding to a developed boundary layer whose properties are in close agreement with the experiment. On the solid surfaces (ABCDEF and FEKL) the velocity is zero, a fixed surface temperature (near adiabatic conditions) is applied, and the normal derivative of the static pressure is set to zero. On the plane of symmetry (AFLG), the normal component of the velocity is set to zero, and the normal derivatives of the remaining flow quantities are zero. The right boundary BCDJIH is sufficiently far from the fin to insure that the boundary layer is locally 2-D, and therefore a simple gradient boundary condition $\partial/\partial z = 0$ is employed. At the downstream boundary, the conventional $\partial/\partial \xi = 0$ condition is specified.

The governing equations are solved by an efficient hybrid explicit-implicit numerical algorithm[15]. The technique utilizes the second-order accurate explicit method of MacCormack[32,33], and the second-order accurate implicit method ("Box Scheme") of Keller[34]. The implicit algorithm of Keller is employed in a thin layer (denoted the "computational sublayer") adjacent to the solid

boundaries where the large flow gradients require exceptionally fine grid spacing for accurate resolution. The Box Scheme is applied to the asymptotic form of the Navier-Stokes equations in this region, whose height is restricted[15-17,35-37] according to the expression $z_m^+ \leq 60$, where $z_m^+ = z_m u*/\nu_w$, z_m is the local height of the computational sublayer, $u*$ is the local friction velocity ($u* = (\tau_w/\rho_w)^{1/2}$), and ν_w is the kinematic molecular viscosity evaluated at the surface. This layer is typically a few percent of the local boundary layer thickness. The explicit algorithm of MacCormack is applied to the full Navier-Stokes equations in the remainder of the flowfield (denoted the "ordinary region").

The hybrid algorithm has been successfully applied to a wide range of two- and three-dimensional flows exhibiting shock-boundary layer interaction and flow separation[15-17,35-37]. The code is written in CYBER 200 FORTRAN, and executes on the VPS 32 at NASA Langley Research Center. The VPS 32 is a vector-processing supercomputer which is architecturally similar to the CYBER 205. The explicit portion of the algorithm is highly vectorized, with typical vector lengths of 1500, and has achieved an execution rate of approximately 100 MFlops (million floating point operations per second) on the VPS 32 using a 32-bit word length.

2. Details of Computation

The upstream boundary layer profile was computed using a separate boundary layer code[38]. The flow conditions are indicated in Table 3, and are in close agreement with the experimental conditions and upstream profile of Horstman.

The finite-difference mesh was generated according to the method described in Ref. 15. A total of 32 streamwise grid planes were utilized, uniformly spaced in the x-direction with $\Delta x = \delta_\infty$. The upstream boundary was located at $5\delta_\infty$ upstream of the fin leading edge, and the downstream boundary at $x = 26\delta_\infty$. The grid spacing within each plane was a combination of geometrically-stretched and uniformly spaced points. The number of ordinary points in the y-and z-directions are 32 and 48, respectively. The computational sublayer was resolved using 8 points in the direction normal to the surface. A separate refined grid was utilized in the sublayer region in the immediate neighborhood of the corner formed by the flat plate and the fin. The total number of grid points was 64,956. The height of the first grid point adjacent to the fin or flat plate was less than 3.0 wall units at all location (i.e., $\Delta z_2^+ \leq 3.0$, where $\Delta z_2^+ = \Delta z_2 u*/\nu_w$, and Δz_2 is the distance of the first row of grid points adjacent to the surface). Two separate computations were performed to examine the sensitivity of the solution to the height z_m of the computational sublayer adjacent to the flat plate. These computations employed $z_m = 5.33 \times 10^{-3}$ cm and 7.62×10^{-3} cm. The maximum grid spacing in the y-direction for these cases was $\Delta y_\infty = 0.58\delta_\infty$ and $0.59\delta_\infty$. The height of the computational domain was $8\delta_\infty$. The width of the domain increased linearly from $13.0\delta_\infty$ at $x = 0$ to $32.6\delta_\infty$ at $x = 26\delta_\infty$. The maximum grid spacing in the z-direction varied between $0.42\delta_\infty$ and $1.07\delta_\infty$. The computed results using the two separate grids were found to be essentially identical.

3

TABLE 3. Flow Conditions for 3-D Sharp Fin at $\alpha_g = 20$ deg

Case	δ_∞ (cm)	M_∞	Re_{δ_∞}	p_{t_∞} (kPa)	T_{t_∞} (deg K)
Experiment (Shapey)	1.4	2.93	9.8×10^5	690	251
Theory (Knight)	1.3	2.93	8.8×10^5	690	256
Theory (Horstman)	1.4	2.94	8.8×10^5	690	267

B. Theoretical Model of Horstman

1. Governing Equations and Numerical Algorithm

The governing equations are the full mean compressible 3-D Navier-Stokes equations using mass-averaged variables. The molecular dynamic viscosity is specified using Sutherland's law. The molecular and turbulent Prandtl numbers are 0.72 and 0.90, respectively. The effects of turbulence are modelled using the two-equation eddy viscosity model of Jones and Launder[20] (JL). An additional element of the turbulence modelling is the incorporation of the compressible wall functions of Viegas and Rubesin[39], previously utilized in the study of the three dimensional shock boundary layer interactions for a swept compression corner configuration[40]. The other boundary conditions employed are similar to those described previously.

The governing equations are solved by the explicit numerical algorithm of MacCormack[32]. The algorithm has been widely employed for the computation of 2-D and 3-D turbulent interactions. The numerical code was executed on the CRAY X-MP/22 at NASA AMES. The code is fully vectorized using CRAY FORTRAN and utilizes the CRAY Solid State Disk.

2. Details of Computations

The upstream boundary layer profile was computed using a separate boundary layer code employing the two-equation Wilcox-Rubesin turbulence model[41]. The upstream flow conditions are indicated in Table 3, and are in close agreement with the experimental conditions and the upstream profile of Knight.

The numerical grid was generated algebraically using a combination of geometric stretching and uniform spacing. A total of 64 streamwise grid planes were employed, spaced uniformly with $\Delta x = 0.39\delta_\infty$. The upstream boundary was located $1.8\delta_\infty$ upstream of the fin leading edge, and the downstream boundary was positioned at $x = 21.9\delta_\infty$. Within each streamwise grid plane, the total number of grid points in the y- and z-directions was 32 and 44, respectively. The maximum grid spacing in the y- and z-directions was $0.39\delta_\infty$. The height of the computational domain in the y-direction was $7.2\delta_\infty$ and the width (measured from the plane of symmetry or the fin surface) was $13.0\delta_\infty$. The total number of grid points was 90,112.

IV. Results

A. Comparison with Experiment

The computed and measured pitot pressure profiles at Station 1 (not shown), located upstream of the interaction, are in close agreement. Similarly, the computed and experimental pitot profiles at Station 2 (not shown), located at the line of upstream influence (as defined by the experimental surface pressure), are in close agreement, and exhibit negligible deviation from an equilibrium 2-D profile. The computed and experimental pitot pressure profiles at Stations 3 through 8, 10 and 11 are displayed in Figs. 3 to 10. The horizontal axis is the pitot pressure p_p, normalized by the upstream freestream pitot pressure p_{p_∞}. The vertical axis is the distance measured from the flat plate, normalized by the upstream boundary layer thickness δ_∞. It is noted that the upstream boundary layer thickness is not, in general, the appropriate vertical scaling parameter for this interaction. The experimental data of McClure and Dolling[13] suggest that the appropriate vertical scaling is given by $yRe_{\delta_0}^{1/3}/\delta_0$, where δ_0 is the experimental boundary layer thickness measured immediately upstream of the shock (with the fin removed) and at the specified spanwise location. The choice of δ_∞ as the vertical scaling was motivated by the desire to clearly portray the vertical extent of the interaction relative to the height of the upstream boundary layer. Similarly, the profiles are shown at selected values of x_s/δ_∞, where $x_s = x - x_{shock}$ and x_{shock} is the location of the theoretical inviscid shock at the specified spanwise location. It is noted that the observations of Settles and Bogdonoff[42], Dolling and Bogdonoff[43], and Lu and Settles[44] indicate that the appropriate scaling is given by $x_s' = x_s Re_{\delta_0}^{1/3}/\delta_0$.

In Fig. 3, profiles of pitot pressure are shown at Station 3, which is coincident with the line of coalescence as defined by the kerosene lampblack visualization. Although displaying a slightly greater pitot pressure in the outer portion of the boundary layer, the computed results are in reasonable agreement with experiment. Similar agreement is obtained at Station 9 (not shown). In Fig. 4, the results are displayed at Station 4, located approximately one-third of the distance between the line of coalescence and the shock wave at this spanwise position. The computed and experimental profiles display a modest "overshoot" outside the boundary layer, associated with the compression system ahead of the shock wave[13,16,17]. In Fig. 5, the results are displayed at Station 5, located approximately two-thirds of the distance between the line of coalescence and the theoretical inviscid shock at this spanwise position. The experimental profile displays a slight S-shaped behavior near the wall, which is less apparent in the computed profiles. The overshoot in pitot pressure is more pronounced at this location. In both figures, the computed profiles are in reasonable agreement with the experimental data, and accurately predict the

observed overshoot in p_p. The shock capturing nature of both numerical algorithms can be seen in the smearing of the pitot pressure profile near $y = 1.5\delta_\omega$.

The calculated and experimental pitot pressure profiles at Station 6 are shown in Fig. 6. Due to the close proximity of this station to the shock wave, uncertainty exists in the measurement of pitot pressure and yaw angle outside the boundary layer, and the experimental data has therefore been denoted by a dotted line for $y > 1.5\delta_\omega$. Further experimental investigation is required to resolve this issue. Within the boundary layer, reasonable agreement is obtained between the computation and measurement. The S-shape character of the profile is again apparent, with reasonable agreement between theory and experiment. The region of high pitot pressure near the surface is associated with a local maximum in the Mach number. In Fig. 7, pitot profiles are displayed at Station 10, located immediately upstream of the shock and closer to the fin. The experimental data outside the boundary layer is again subject to uncertainty due to the proximity of the shock wave. Within the boundary layer, the agreement between the theory and experiment is good.

Pitot pressure results at Stations 7 and 11, located immediately downstream of the shock wave, are displayed in Figs. 8 and 9. Good agreement is again observed. The discrepancy in the computed pitot pressure outside the boundary layer in Fig. 8 is associated with the shock-capturing nature of the numerical algorithms, and the difference in streamwise grid spacing for the two computations, and the proximity of Station 7 to the shock ($x_s = 0.60\delta_\omega$). In Fig. 10, results are shown at Station 8, located furthest downstream of the shock. The comparison between computed and experimental results is good.

The computed and experimental yaw angle profiles at Stations 1 and 2 (not shown) display negligible values (< 3 deg). The calculated and measured yaw angle profiles at Stations 3 through 8, 10 and 11 are displayed in Figs. 11 to 18. In Fig. 3, the yaw profiles are shown at Station 3 ($x_s = -3.4\delta_\omega$, $z = 5.81\delta_\omega$), located at the experimental line of coalescence. It is observed that the computed profiles near the surface underpredict the observed yaw angle. This is attributable to the differences between computed and experimental lines of coalescence. In particular, the computed lines of coalescence for the Baldwin-Lomax (BL) model and Jones-Launder (JL) model are located at $x_s = -3.0\delta_\omega$ and $-2.4\delta_\omega$, respectively, at $z = 5.81\delta_\omega$. At Station 3, the calculated values of the surface yaw angle are 37 deg (BL) and 12 deg (JL), while the experimental surface yaw angle (based on kerosene lampblack visualization) is approximately 54 deg. A similar observation applies to Station 9 (not shown).

In Fig. 12, yaw angle profiles are shown at Station 4, located approximately one-third of the distance between the line of coalescence and shock at this spanwise position. The computed yaw angles are in reasonable agreement with experiment, except in the immediate vicinity of the surface, where the computed profiles disagree by 15-20% from the experiment. In particular, the computed surface yaw angles are 63 deg (BL) and 44 deg (JL), while the experimental value is 54 deg based upon cobra probe measurements and kerosene lampblack visualization.

Yaw angle results at Station 5, located approximately two-thirds of the distance between the line of coalescence and the shock wave at this spanwise position, are displayed in Fig. 13. The agreement between the theory and experiment is good, although the Jones-Launder model overpredicts the yaw angle in the outer portion of the boundary layer. The computed surface yaw angles are 61 deg (BL) and 53 deg (JL), in reasonable agreement with the experimental value of 60 deg.

In Figs. 14 and 15, yaw angle profiles are shown at Stations 6 and 10, immediately upstream of the shock. As discussed previously, uncertainties exist in the experimental data outside the boundary layer due to the proximity of the shock wave, and the data are consequently identified by a dotted line in that region. Overall good agreement is observed between the calculated and experimental results within the boundary layer. The calculated surface yaw angles at Station 6 are 60 deg (BL) and 57 deg (JL), in reasonable agreement with the experimental value of 64 deg. At station 10, the computed surface values are 61 deg (BL) and 58 deg (JL), in close agreement with the measured value of 58 deg.

The calculated and experimental yaw angle profiles at Stations 7 and 11, located immediately downstream of the shock, are shown in Figs. 16 and 17. The calculated results are again observed to be in close agreement with experiment, although displaying a somewhat less full profile near the surface at Station 7. The predicted surface yaw angles are 61 deg (BL) and 59 deg (JL) at Station 7, in close agreement with the experimental value of 64 deg. At Station 11, the calculated surface values are 59 deg (BL) and 51 deg (JL), and the measured value is 55 deg. In Fig. 18, yaw angle profiles are shown at Station 8, downstream of the shock. The calculated and experimental profiles are observed to be in excellent agreement. The predicted surface values of 52 deg (BL) and 50 deg (JL) are in close agreement with the experimental value of 48 deg.

The calculated surface pressure for both models has been compared with the data of Goodwin[8] for the same configuration. The models accurately predict the extent of the upstream influence, and the pressure distribution from the upstream influence location to the plateau region. Downstream of the plateau region, the computed pressures moderately underpredict the data.

8. Further Comparison of Computed Flowfield

A detailed comparison of the computed flowfields of Knight and Horstman was performed to determine the extent of similarity of the two theoretical approaches. Profiles of the computed x-component velocity, yaw angle, pitch angle $\gamma = \tan^{-1}(v/\sqrt{u^2+w^2})$, pitot pressure, Mach number and turbulent eddy viscosity were examined at a selected streamwise station $x = 11\delta_\omega$ for $z - z_{fin} = 4_\omega$ to $10\delta_\omega$ in increments of δ_ω, where z_{fin} is the width of the fin at a given x. A representative sample is displayed in Figs. 19 to 22, corresponding to $x = 11\delta_\omega$ and $z - z_{fin} = 6\delta_\omega$. The position is roughly halfway between the line of coalescence and the shock wave (as measured in the

5

streamwise direction) at this spanwise location. The x-component velocity, yaw angle and pitch angle profiles, shown in Figs. 19, 20 and 21, respectively, are observed to be in very close agreement. Differences in the computed yaw angle occur only within the region $y < 0.3\delta_\infty$. Note that it is difficult to define a "local" boundary layer thickness within the 3-D interaction region due to the non-uniformity of the inviscid flow[10,11,12]. In Fig. 20, however, the eddy viscosity profiles indicate a significant difference; in particular, the peak values of the turbulent eddy viscosity ϵ differ by a factor of fourteen. It is emphasized that this difference in eddy viscosity between the two models is typical of the profiles within the 3-D interaction region. Within the nominal 2-D portion of the boundary layer upstream of the interaction, the eddy viscosity profiles are in reasonably close agreement.

It is evident from Figs. 19 to 22 and the additional numerous profiles studied that the details (i.e., the velocity, pressure and temperature) of this 3-D turbulent interaction are relatively insensitive to the particular turbulence model employed, with the exception of a small fraction of the boundary layer adjacent to the surface where modest differences are observed in the yaw angle. This implies, therefore, that the principal elements of the flowfield structure are rotational and inviscid, except near the wall as mentioned. This represents a significant result for 3-D interactions, and is notably different from 2-D separated shock-boundary layer interactions wherein the differences between the computed flowfields obtained using algebraic and two-equation turbulence models are significant[45]. There is no reason to expect, however, that the insensitivity to turbulence model displayed in the 3-D sharp fin interaction will necessarily apply to other 3-D turbulent interactions.

C. Flowfield Structure of 3-D Sharp Fin

On the basis of the close agreement between the computed and experimental data, the computed solutions can be utilized to examine the flow structure of the 3-D sharp fin interaction. The close similarity of the computed velocity, yaw and pitch angle profiles for the Baldwin-Lomax and Jones-Launder models implies a close agreement in predicted mean streamlines, which was confirmed through detailed comparison of numerous particle traces.

In Figs. 23 and 24, the computed surface streamlines ("limiting streamlines") obtained using the Baldwin-Lomax and Jones-Launder models are shown. The lines of coalescence ("separation") and divergence ("attachment") are observed. These specific features are in general agreement with the experimental kerosene lampblack visualization as described previously, although the computed lines of coalescence appear further downstream than in the experiment. In particular, the experimental line of coalescence at $z/\delta_\infty = 10$ (the approximate spanwise limit of the experimental kerosene lampblack visualization) is $x_s = -5.7\delta_\infty$, whereas the computed lines of coalescence using the Baldwin-Lomax and Jones-Launder models occur at $x_s = -4.5\delta_\infty$ and $-3.5\delta_\infty$, respectively. It is noted that the discrepancy between the experimental and Baldwin-Lomax result, $1.2\delta_\infty$, is equal to $1.2\Delta x$. In the Jones-Launder model, the discrepancy, i.e.,

$2.2\delta_\infty$ is $5.6\Delta x$. Further investigation is needed to understand the effects of the turbulence models on the calculated lines of coalescence.

A series of calculated mean streamlines are displayed in Figs. 25 to 28, obtained from the computed solution utilizing the Baldwin-Lomax model. Three views of the streamlines are shown, corresponding to an observer looking a) towards the surface from above, b) downstream, and c) towards the fin from the side. The vertical scale has been enlarged by a factor of three for the purposes of clarity. In Fig. 25, a series of twelve stream-lines are shown. Six streamlines originate from the surface, upstream of the interaction, at equal spanwise increments of δ_∞, and serve to define the line of coalescence. Six additional streamlines originate immediately above the previous six, at a height of $0.0048\delta_\infty$. These latter streamlines clearly rise and cross the line of separation, and appear to concentrate within a core. In Fig. 26, another series of twelve streamlines are displayed. The first six again represent limiting streamlines, and define the line of coalescence. The second six originate upstream at a height of $0.52\delta_\infty$. These particles display a clear rotational motion which is counterclockwise as viewed looking downstream. In Fig. 27, the three different sets of six streamlines are shown. The streamlines display a vortical structure. Those particles originating from a higher y are swept beneath the particles originating near the surface. In Fig. 28, a final series of twelve streamlines are shown. Again, a set of six surface streamlines define the line of coalescence. A second set, originating upstream at $y = 1.1\delta_\infty$, is observed to rise in the vicinity of the line of separation, and then drop towards the surface. Unlike the particles originating at lower values of y, these particles eventually move approximately parallel to the fin surface. Additional extensive streamline patterns are consistent with the above features.

A general mean flowfield pattern, developed on the basis of the streamline patterns, is displayed in Fig. 29. As suggested by Token[22], the flowfield structure of the 3-D sharp fin at the present conditions is dominated by a large vortical structure. The line of coalescence (separation) defines the origin of the 3-D separation surface (Surface No. 1). The line of divergence (attachment) represents the intersection of a second surface (Surface No. 2) with the wall. This second surface extends upstream into the undisturbed flow. The fluid contained between the wall and the second surface is entrained into the vortical structure, while the fluid above the second surface flows towards the wall and approximately parallel to the fin. Due to the resolution of the numerical grid, the detailed mean flow structure in the immediate vicinity of the fin leading edge could not be examined. A second small vortical structure was observed within the fin boundary layer and close to the corner, in agreement with the experimental observations of Kubota and Stollery[5] at Mach 2.3 and $Re_{\delta_\infty} = 5 \times 10^4$. No experimental data was available for the immediate vicinity of the corner for this configuration, however, and consequently the computed secondary vortical structure cannot be considered verified.

6

V. Conclusions

An experimental and theoretical study is performed for the 3-D shock wave turbulent boundary layer interaction generated by a sharp fin at Mach 3 for a fin angle $\alpha_g = 20$ deg and Reynolds number $Re_{\delta_\infty} = 9 \times 10^5$. This research effort extends previous experimental and theoretical investigations of the 3-D sharp fin interaction to stronger interactions. The experimental data include surface pressure profiles, surface streamline patterns, and boundary layer profiles of pitot and yaw angle. Two separate theoretical approaches or "models" were employed, both of which utilize the 3-D compressible Navier-Stokes equations. The theoretical approach of Knight employs the algebraic turbulent eddy viscosity model of Baldwin and Lomax, and the theoretical model of Horstman employs the two-equation turbulence model of Jones and Launder coupled with the wall function model of Viegas and Rubesin. The principal conclusions are:

1. The computed surface pressure, surface streamlines, pitot pressure and yaw angle profiles are observed in good agreement with the experimental data, thereby confirming the efficacy of the theoretical approaches which were previously validated for the 3-D sharp fin configuration at Mach 3 for smaller α_g (i.e., weaker interactions).

2. The three dimensional velocity fields computed by both models are in close agreement, as indicated by a detailed evaluation of x-component velocity, pitch and yaw angle profiles. This result was confirmed by comparison of fluid particle pathlines for the theoretical models, which were found to be in close agreement. The turbulent eddy viscosity profiles, however, differ significantly within the 3-D interaction. This result implies that the overall structure of this 3-D sharp fin interaction is insensitive to the turbulence model, except within a small portion of the boundary layer adjacent to the surface. The principal elements of the flowfield structure are therefore rotational and inviscid, except near the wall as indicated.

3. The calculated flowfields display a prominent vortical structure associated with the shock-boundary layer interaction in agreement with the flowfield models of Token, and Kubota and Stollery. A three dimensional surface of separation emanates from the line of coalescence (separation), and spirals into the vortical center. A second surface, emanating from upstream, intersects the wall at the line of divergence (attachment), and defines the extent of the fluid entrained into the vortical structure.

Acknowledgements

VI. References

[1] Settles, G. and Dolling, D., "Swept Shock Wave - Boundary Layer Interactions," AIAA Progress in Astronautics and Aeronautics, to appear.

[2] Stanbrook, A., "An Experimental Study of the Glancing Interaction Between a Shock Wave and a Boundary Layer," British ARC CP-555, July 1960.

[3] McCabe, A., "The Three-Dimensional Interaction of a Shock Wave with a Turbulent Boundary Layer," The Aeronautical Quarterly, Vol. 17, 1966, p. 231-252.

[4] Law, C., "Three-Dimensional Shock Wave/Turbulent Boundary Layer Interactions at Mach 6," ARL-TR-75-0191, 1975.

[5] Kubota, H. and Stollery, J., "An Experimental Study of the Interaction Between a Glancing Shock Wave and a Turbulent Boundary Layer," J. Fluid Mechanics, Vol. 116, 1982, pp. 431-458.

[6] Zheltovodov, A., "Regimes and Properties of Three-Dimensional Separation Flows Initiated by Skewed Compression Shocks," Zhurnal Prikladnoi Mekhaniki i Tekknicheskoi Fiziki, No. 3, May-June 1982, pp. 116-123.

[7] Dolling, D., "Upstream Influence in Sharp Fin-Induced Shock Wave Turbulent Boundary-Layer Interactions," AIAA J., Vol. 21, January 1983, pp. 143-145.

[8] Goodwin, S., "An Exploratory Investigation of Sharp-Fin Induced Shock Wave/Turbulent Boundary Layer Interactions at High Shock Strengths," MS Thesis, Dept. Aero. and Mech. Engr., Princeton U., 1984.

[9] Peake, D., "Three Dimensional Swept Shock/Turbulent Boundary Layer Separations with Control by Air Injection," Aero. Report No. LR-592, National Research Council - Canada, July, 1976.

[10] Oskam, B., Vas, I., and Bogdonoff, S., "Oblique Shock Wave/Turbulent Boundary Layer Interactions at Mach 3," AFFDL-TR-76-48, Part I (1976), Part II (1978), Air Force Flight Dynamics Laboratory, Wright-Patterson AFB, Ohio.

[11] Oskam, B., Vas, I., and Bogdonoff, S., "Mach 3 Oblique Shock Wave/Turbulent Boundary Layer Interactions in Three Dimensions," AIAA Paper No. 76-336, 1976.

[12] Oskam, B., Vas, I., and Bogdonoff, S., "An Experimental Study of Three-Dimensional Flow Fields in an Axial Corner at Mach 3," AIAA Paper No. 77-689, 1977.

[13] McClure, W. and Dolling, D., "Flowfield Scaling in Sharp Fin-Induced Shock Wave Turbulent Boundary Layer Interaction," AIAA Paper No. 83-1754, 1983.

[14] Horstman, C. and Hung, C., "Computation of Three-Dimensional Turbulent Separated Flows at Supersonic Speeds," AIAA Paper No. 79-0002, 1979.

[15]Knight, D., "A Hybrid Explicit-Implicit Numerical Algorithm for the Three-Dimensional Compressible Navier-Stokes Equations," *AIAA J.*, Vol. 22, August 1984, pp. 1056-1063.

[16]Knight, D., "Numerical Simulation of 3-D Shock Turbulent Boundary Layer Interaction Generated by a Sharp Fin," *AIAA J.*, Vol. 23, December 1985, pp. 1885-1891.

[17]Knight, D., "Modelling of Three-Dimensional Shock Wave Turbulent Boundary Layer Interactions," Workshop on Macroscopic Modelling of Turbulent Flows and Fluid Mixtures, INRIA, Nice, France, December 1984; *Lecture Notes in Physics*, Vol. 230, Springer-Verlag, 1985, pp. 177-201.

[18]Horstman, C., Private communications: June 1984, July 1984, November 1984.

[19]Escudier, M., "The Distribution of the Mixing Length in Turbulent Flows Near Walls," Mech. Engr. Dept., Imperial College, London, Rept. TWF/TN/1, 1965.

[20]Jones, W. and Launder, B., "The Prediction of Laminarization with a Two-Equation Model of Turbulence," *Int. J. Heat and Mass Transfer*, Vol. 15, 1972, pp. 301-304.

[21]Baldwin, B. and Lomax, H., "Thin Layer Approximation and Algebraic Model for Separated Flows," AIAA Paper No. 78-257, 1978.

[22]Token, K., "Heat Transfer Due to Shock Wave/Turbulent Boundary Layer Interactions on High Speed Weapons Systems," AFFDL-TR-74-77, 1974.

[23]Settles, G. and Teng, H.-Y., "Flow Visualization of Separated 3-D Shock Wave/Turbulent Boundary Layer Interactions," *AIAA J.*, Vol. 21, March 1983, pp. 390-397.

[24]Settles, G., "An Experimental Study of Compressible Turbulent Boundary Layer Separation at High Reynolds Number," Ph.D. Thesis, Dept. Aero. and Mech. Engr., Princeton U., 1975.

[25]Settles, G., Perkins, J., and Bogdonoff, S., "Upstream Influence Scaling of 2D and 3D Shock/Turbulent Boundary Layer Interactions at Compression Corners," *AIAA J.*, Vol. 20, June 1982, pp. 782-789.

[26]Sun, C.-C. and Childs, M., "Wall-Wake Velocity Profile for Compressible Nonadiabatic Flows," *AIAA J.*, Vol. 14, June 1976, pp. 820-822.

[27]Rubesin, M. and Rose, W., "The Turbulent Mean-Flow, Reynolds-Stress and Heat-Flux Equations in Mass Averaged Dependent Variables," NASA TMX-62248, 1973.

[28]Pulliam, T. and Steger, J., "Implicit Finite-Difference Simulations of Three-Dimensional Compressible Flow," *AIAA J.*, Vol. 18, February 1980, pp. 159-167.

[29]Buleev, N., "Theoretical Model of the Mechanism of Turbulent Exchange in Fluid Flows," AERE Translation 957, Atomic Energy Research Estab., Hartwell, England, 1963.

[30]Gessner, F. and Po, J., "A Reynolds Stress Model for Turbulent Corner Flows - Part II: Comparison Between Theory and Experiment," *J. Fluids Engr.*, Trans. of ASME, Vol. 98, Series I, 1976, pp. 269-277.

[31]Thompson, J. and Warsi, Z., "Boundary-Fitted Coordinate Systems for Numerical Solution of Partial Differential Equations - A Review," *J. Comp. Phys.*, Vol. 47, 1982, pp. 1-108.

[32]MacCormack, R., "Numerical Solution of the Interaction of a Shock Wave with a Laminar Boundary Layer," *Lecture Notes in Physics*, Vol. 8, 1971, p. 151-163.

[33]Baldwin, B. and MacCormack, R., "A Numerical Method for Solving the Navier-Stokes Equations with Application to Shock-Boundary Layer Interactions," AIAA Paper No. 75-1, 1975.

[34]Keller, H., "Accurate Difference Methods for Nonlinear Two-Point Boundary Value Problems," *SIAM J. Numerical Analysis*, Vol. 11, 1974, pp. 305-320.

[35]Knight, D., "Improved Calculation of High Speed Inlet Flows: Part I. Numerical Algorithm," *AIAA J.*, Vol. 19, January 1981, pp. 34-41.

[36]Knight, D., "Improved Calculation of High Speed Inlet Flows: Part II. Results," *AIAA J.*, Vol. 19, February 1981, pp. 172-179

[37]Knight, D., "Calculation of High-Speed Inlet Flows Using the Navier-Stokes Equations," *J. Aircraft*, Vol. 18, September 1981, pp. 748-754.

[38]York, B. and Knight, D., "Calculation of a Class of Two-Dimensional Turbulent Boundary Layer Flows Using the Baldwin-Lomax Model," *AIAA J.*, Vol. 23, December 1985, pp. 1849-1850.

[39]Viegas, J., Rubesin, M., and Horstman, C., "On the Use of Wall Functions as Boundary Conditions for Two-Dimensional Separated Compressible Flows," AIAA Paper No. 85-0180, 1985.

[40]Horstman, C., "A Computational Study of Complex Three-Dimensional Compressible Turbulent Flow Fields," AIAA Paper No. 84-1556, 1984.

[41]Wilcox, D. and Rubesin, M., "Progress in Turbulence Modelling for Complex Flow Fields Including the Effects of Compressibility," NASA TP-1517, 1980.

[42]Settles, G. and Bogdonoff, S., "Scaling of Two- and Three-Dimensional Shock/Turbulent Boundary-Layer Interactions at Compression Corners," *AIAA J.*, Vol. 20, 1982, pp. 782-789.

[43]Dolling, D. and Bogdonoff, S., "Upstream Influence Scaling of Sharp Fin-Induced Shock Wave Turbulent Boundary Layer Interactions," AIAA Paper 81-0336, 1981.

[44]Lu, F. and Settles, G., "Conical Similarity of Shock/Boundary Layer Interactions Generated by Swept Fins," AIAA Paper No. 83-1756, 1983.

[45]Coakley, T., Viegas, J. and Horstman, C., "Evaluation of Turbulence Models for Three Primary Types of Shock Separated Boundary Layers," AIAA Paper No. 77-692, 1977.
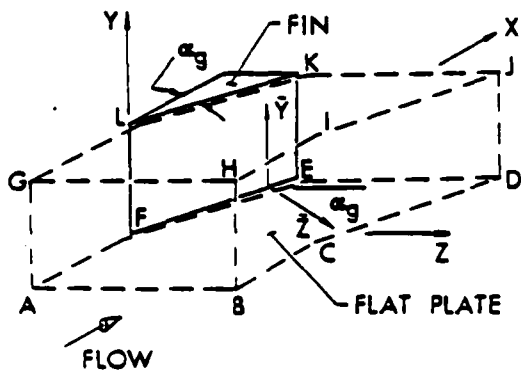
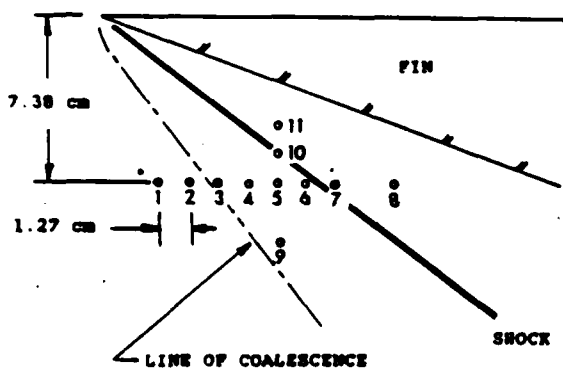Fig. 1   Physical Region for 3-D Sharp Fin
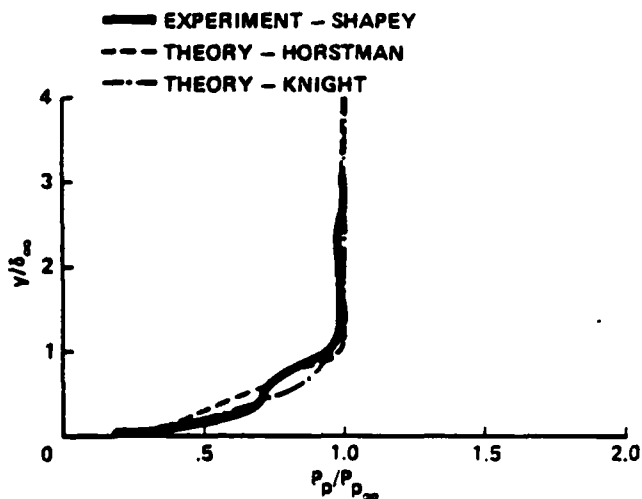

Fig. 2   Location of Experimental Surveys

Fig. 3   Pitot Pressure at Station 3
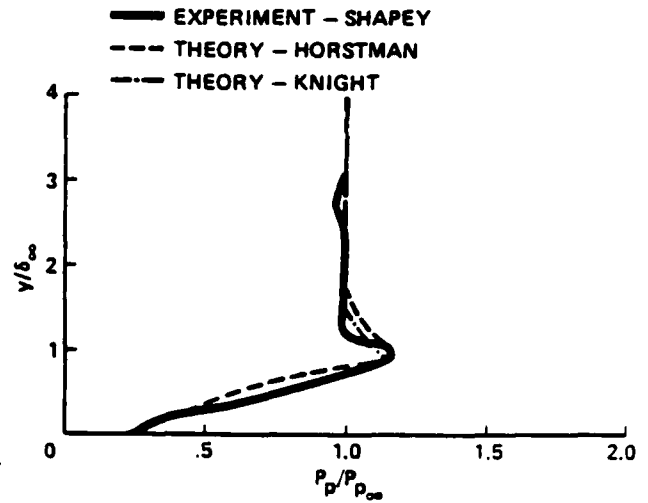
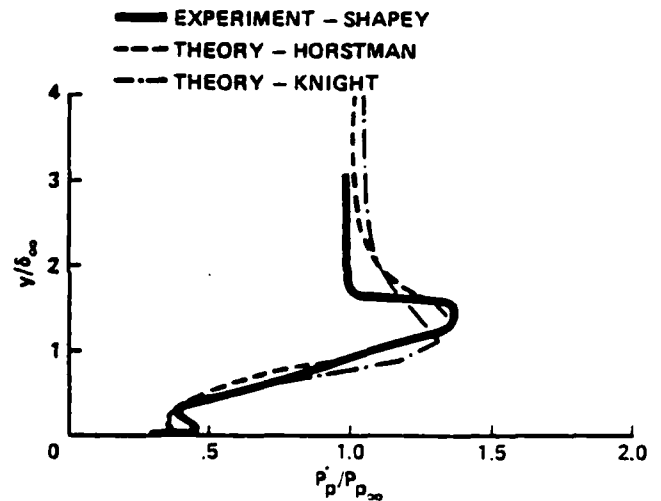

Fig. 4   Pitot Pressure at Station 4
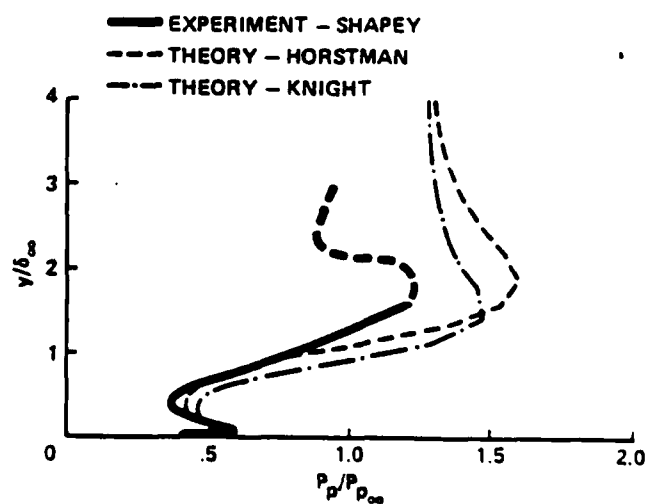

Fig. 5   Pitot Pressure at Station 5

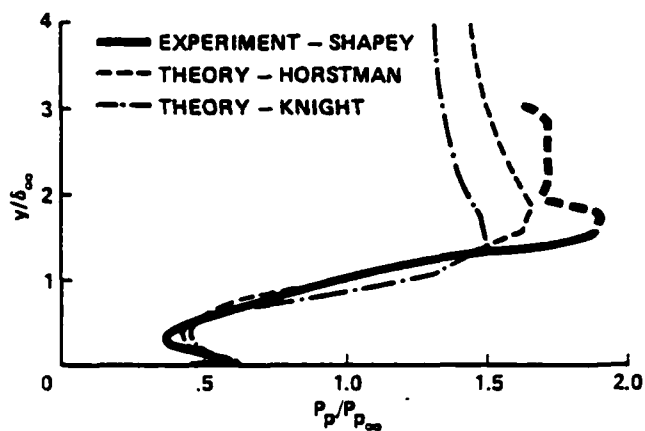

Fig. 6   Pitot Pressure at Station 6
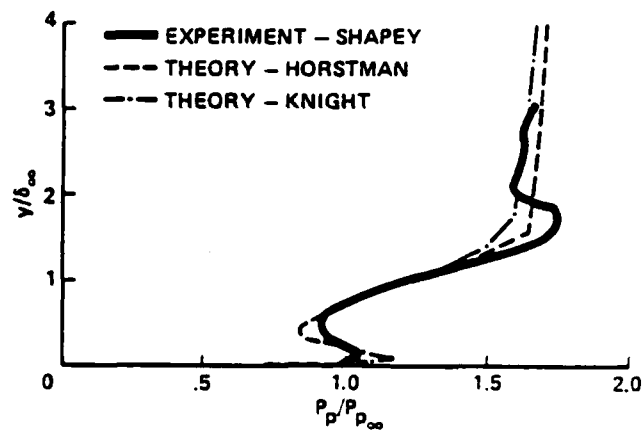
9

Fig. 7   Pitot Pressure at Station 10

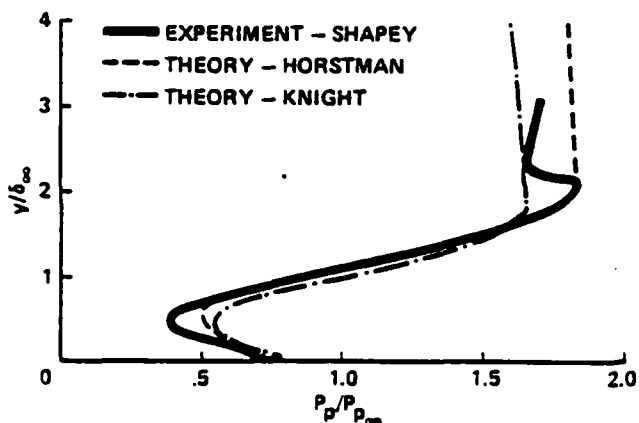
Fig. 10   Pitot Pressure at Station 8
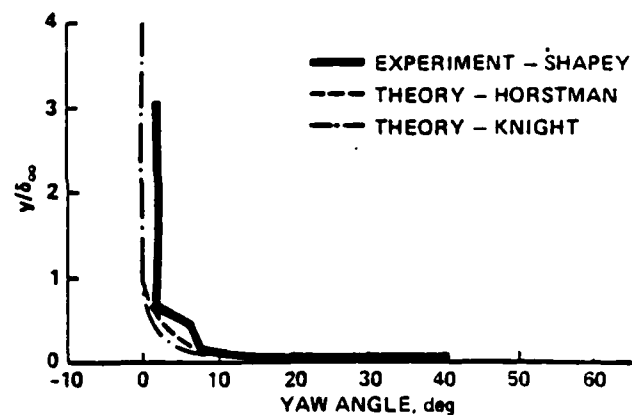

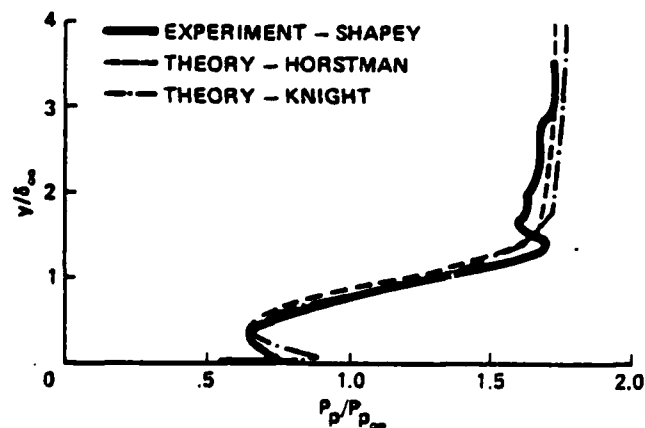Fig. 8   Pitot Pressure at Station 7

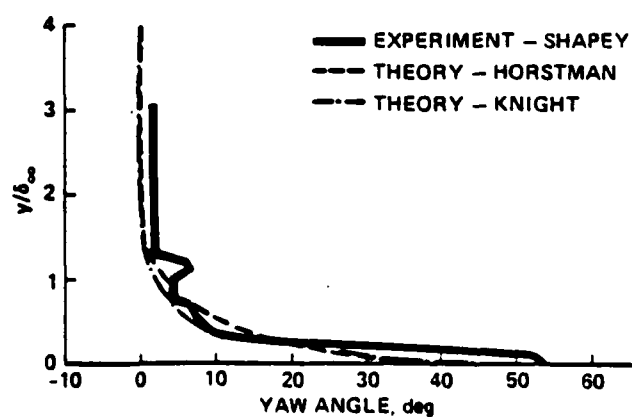Fig. 11   Yaw Angle at Station 3

Fig. 9   Pitot Pressure at Station 11

Fig. 12   Yaw Angle at Station 4
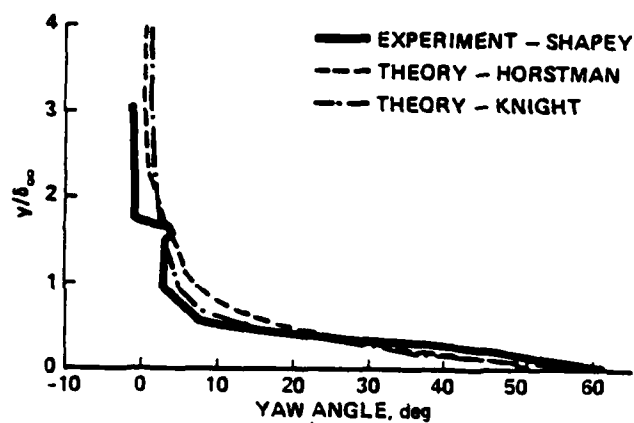
Fig. 13 Yaw Angle at Station 5
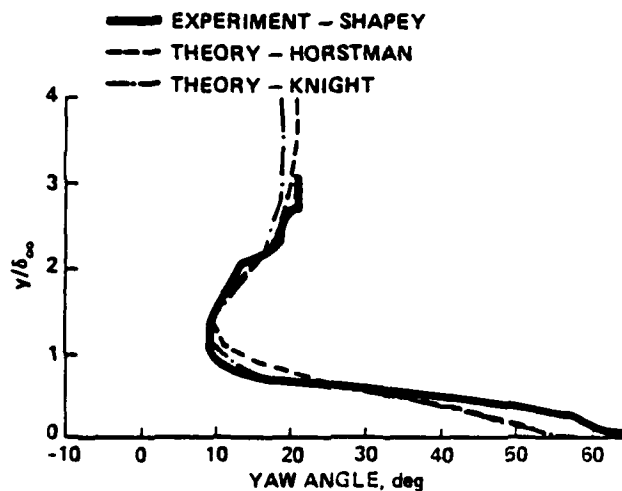
Fig. 16 Yaw Angle at Station 7
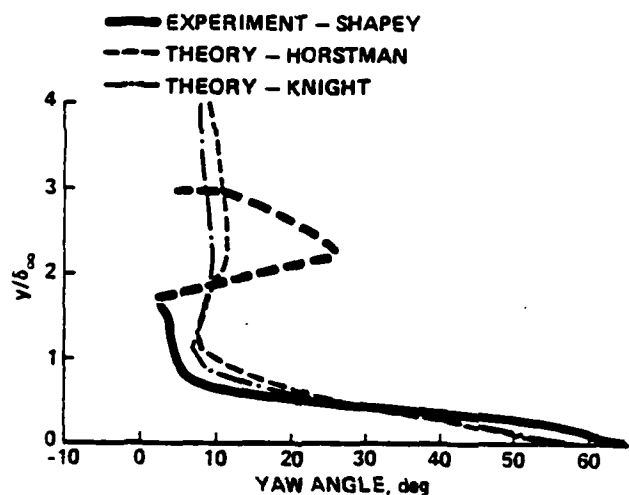
Fig. 14 Yaw Angle at Station 6
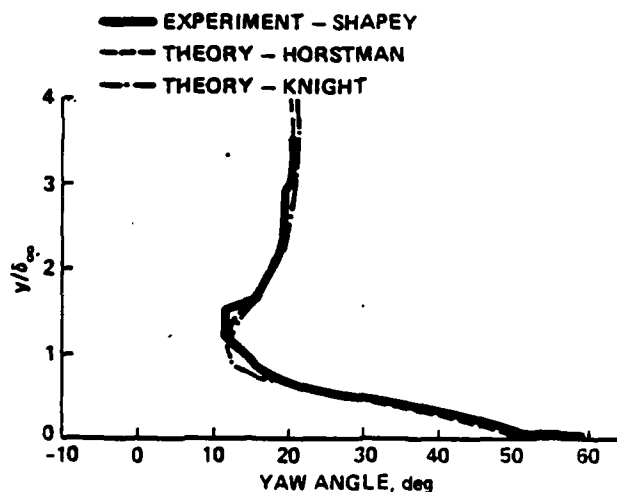
Fig. 17 Yaw Angle at Station 11
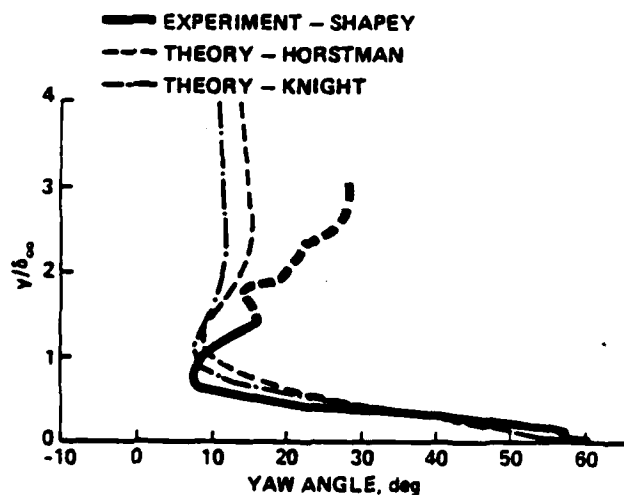
Fig. 15 Yaw Angle at Station 10
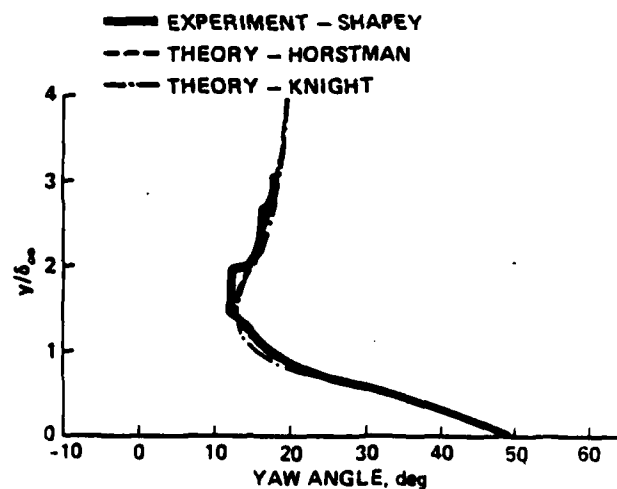
Fig. 18 Yaw Angle at Station 8
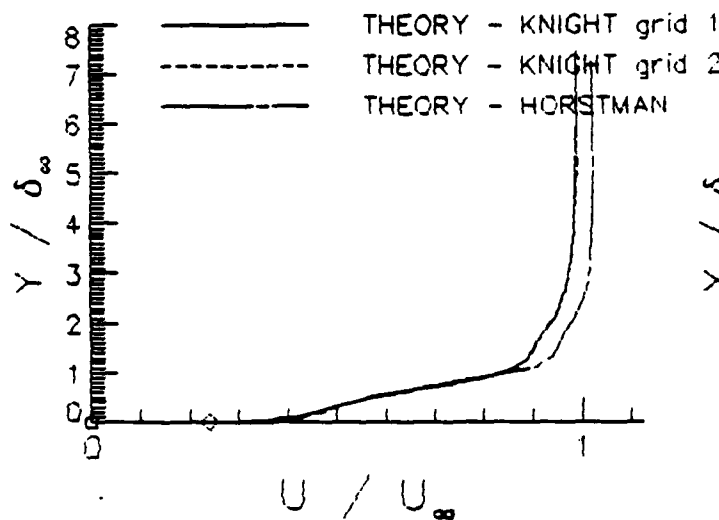
Fig. 19 Computed Velocity in x-direction at $x = 11\delta_\infty$, $z - z_{fin} = 6\delta_\infty$
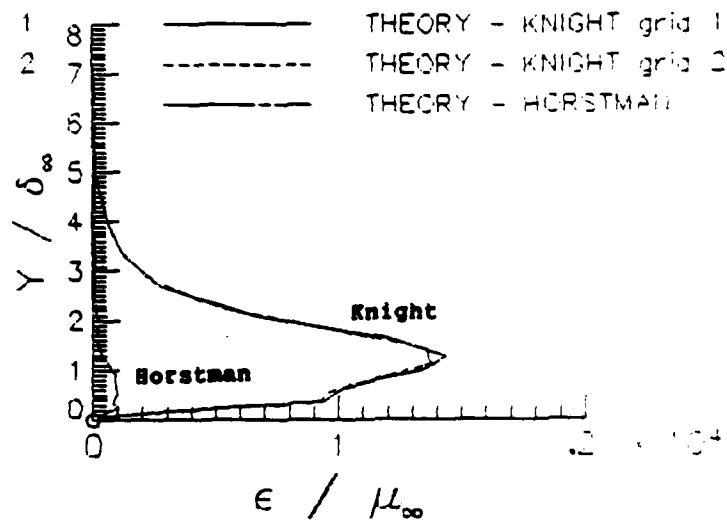
Fig. 22 Computed Turbulent Eddy Viscosity at $x = 11\delta_\infty$, $z - z_{fin} = 6\delta_\infty$
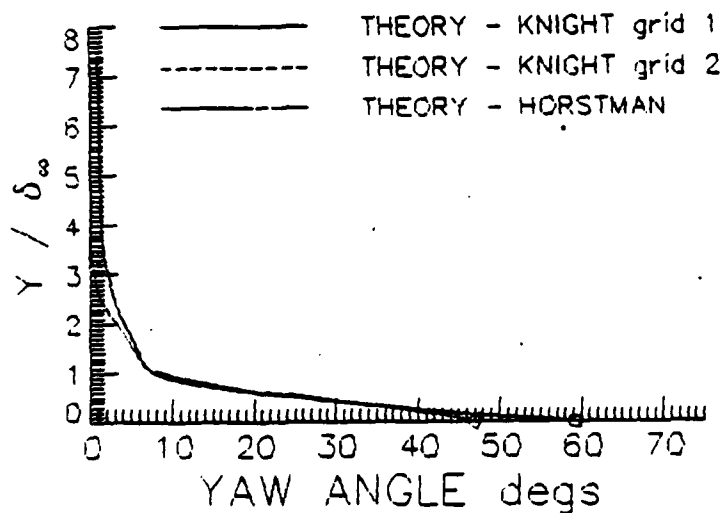
Fig. 20 Computed Yaw Angle at $x = 11\delta_\infty$, $z - z_{fin} = 6\delta_\infty$
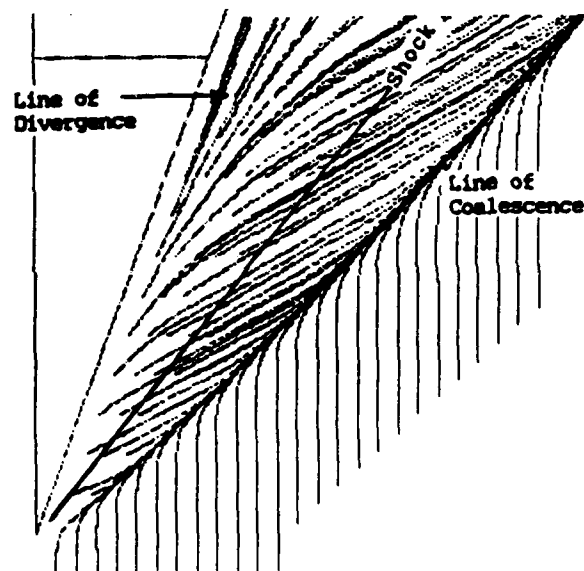
Fig. 23 Computed Surface Streamlines (Baldwin-Lomax)
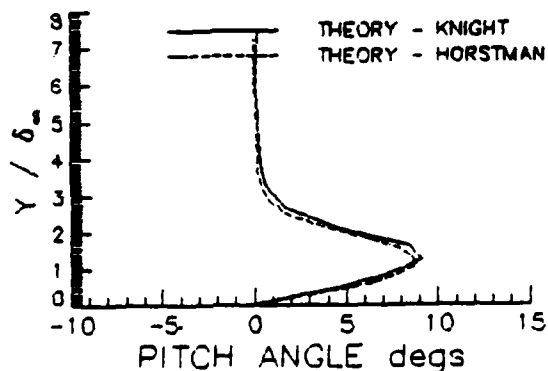
Fig. 21 Computed Pitch Angle at $x = 11\delta_\infty$, $z - z_{fin} = 6\delta_\infty$
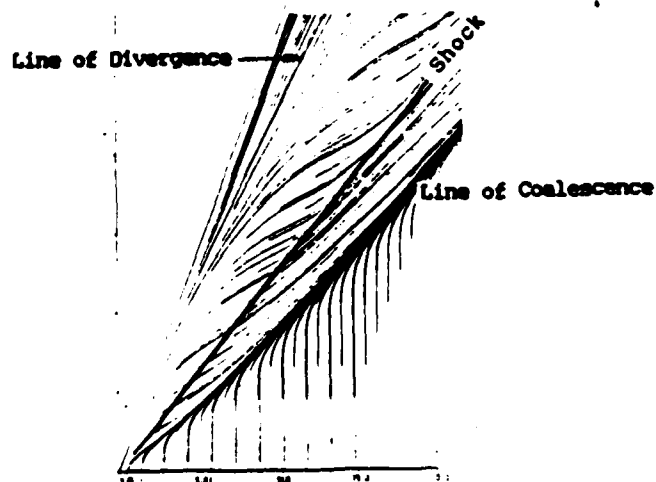
Fig. 24 Computed Surface Streamlines (Jones-Launder)

12

a) Top View

Line of Coalescence
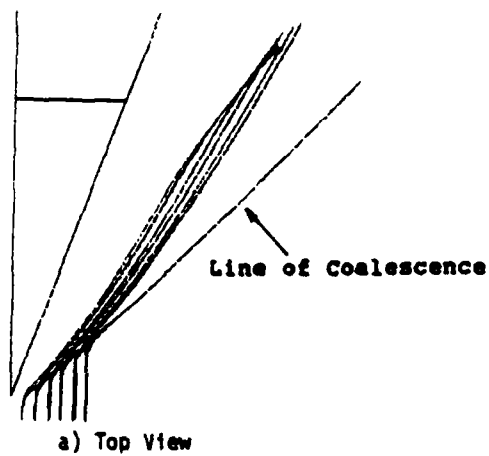
Fig. 25 Computed Mean Streamlines Originating Upstream at y = 0 and y = 0.0048δ (Vertical Scale Enlarged by Factor of 3)

b) Front View

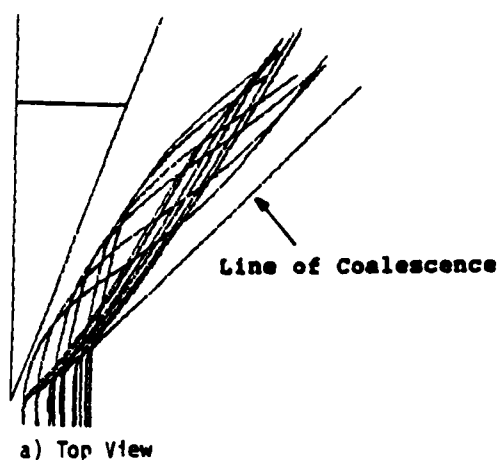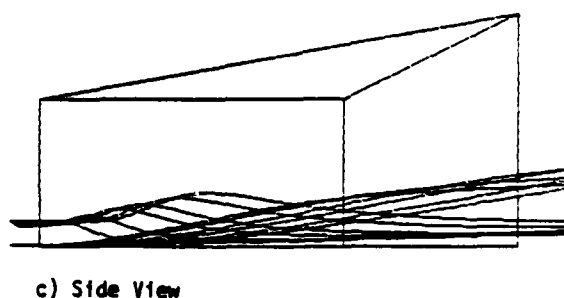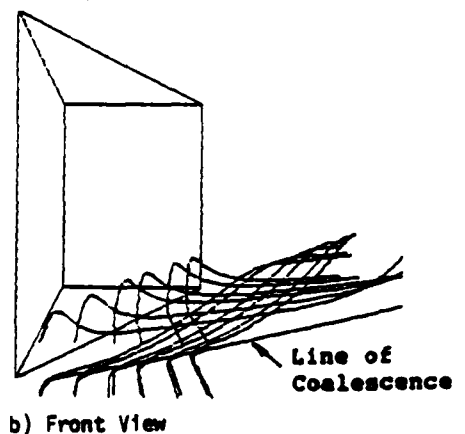Line of Coalescence

c) Side View

a) Top View

Line of Coalescence
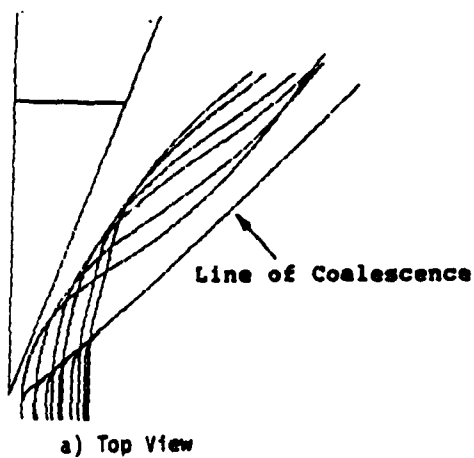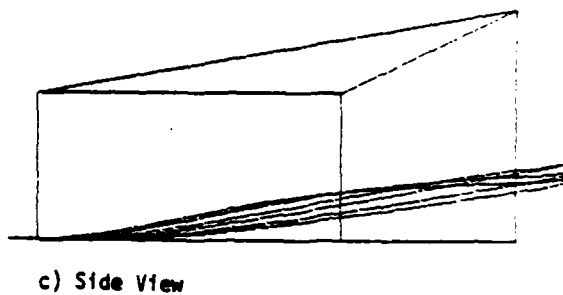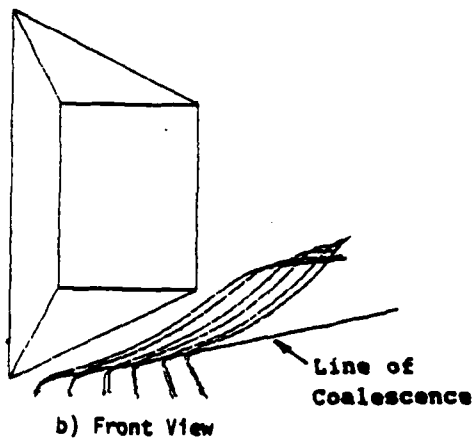
Fig. 26 Computed Mean Streamlines Originating Upstream at y = 0 and y = 0.52δ (Vertical Scale Enlarged by Factor of 3)
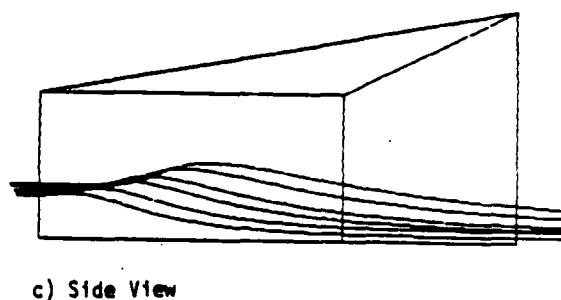
b) Front View

Line of Coalescence

c) Side View

13

a) Top View

Line of Coalescence

b) Front View

Line of
Coalescence

c) Side View
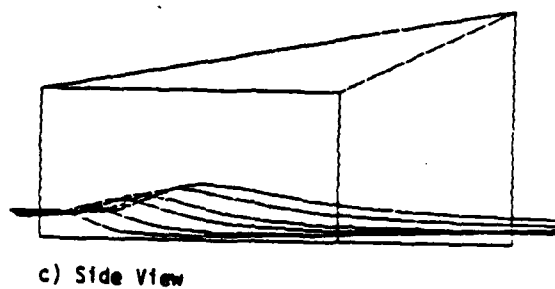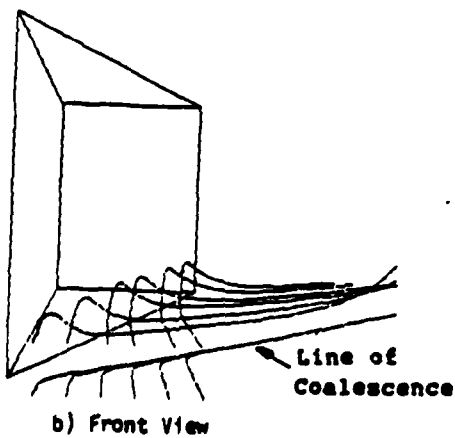
Fig. 27 Computed Mean Streamlines Originating Upstream at $y = 0$, $0.0048\delta_\infty$ and $0.52\delta_\infty$ (Vertical Scale Enlarged by Factor of 3)

a) Top View

Line of Coalescence

b) Front View

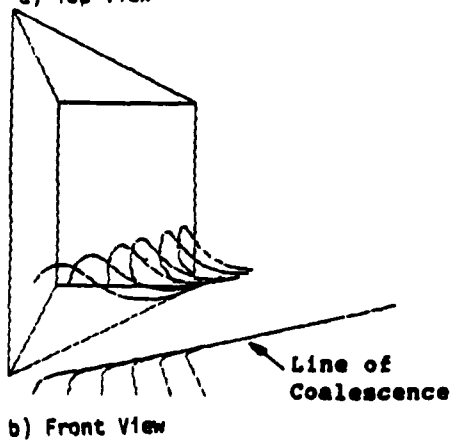Line of
Coalescence

c) Side View
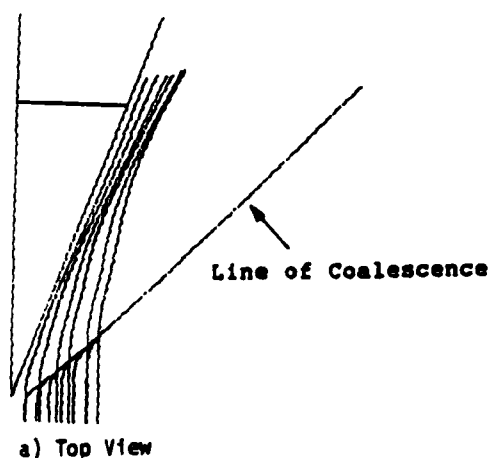
Fig. 28 Computed Mean Streamlines Originating Upstream at $y = 0$ and $y = 1.1\delta_\infty$
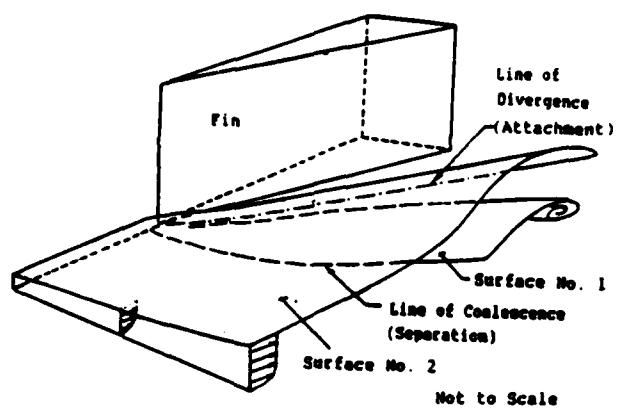
(Vertical Scale Enlarged by a Factor of 3)

14

Fig. 29 Mean Flowfield Structure

15

END

11-86

DTIC